Structures and Redox Regulations of Metal Complexes Having Bioactive Nitrogen Heteroaromatics

January, 2013

Yuji Inui

Department of Material and Life Science
Division of Advanced Science and Biotechnology
Graduate School of Engineering
Osaka University

Structures and Redox Regulations of Metal Complexes Having Bioactive Nitrogen Heteroaromatics

January, 2013

Yuji Inui

Department of Material and Life Science
Division of Advanced Science and Biotechnology
Graduate School of Engineering
Osaka University

Contents

General Introduction		**1**
Chapter 1:	Formation of "Naked" Guanine-Quartets Using 9-Isopropylguanine: Structures, Formation Thermodynamics, and Temperature-Dependent Structural Change of Supramolecular Assemblies with a Ni(II)-Porphyrin	**14**
Chapter 2:	Regulation of Redox Potential of a Pterin Derivative Bound to a Ruthenium(II) Complex by Intermolecular Hydrogen Bonding with Nucleobases	**42**
Chapter 3:	A Tetranuclear Iridium(III) Complex Having a Flavin Analogue as Bridging Ligands in Different Coordination Modes and Exchangeable Anion Encapsulation in a Supramolecular Cage	**64**
Chapter 4:	A Triangular Prismatic Hexanuclear Iridium(III) Complex Bridged by Flavin Analogues Showing Reversible Six-Electron Redox Processes	**77**
Concluding Remarks		**95**
List of Publications		**97**
Acknowledgement		**98**

General Introduction

Self-organization is one of the important processes in nature, and regulates structures and reactivity of active sites of enzymes in biological systems.[1] In higher-order structures, self-organization usually occurs through the combination of a number of non-covalent interactions which include electrostatic interactions, van der Waals' force, hydrophobic interaction, π-π interaction, cation-π interaction, CH-π interaction, and intermolecular hydrogen bonding. Although non-covalent interactions are considered as the driving force to form self-assembled structures,[2] the weak interactions are individually undetectable in bio-macromolecules due to numerous similar functional groups in the complicated structures. However, studies on non-covalent interactions have been significantly improved by virtue of the development of analytical techniques.[3] Especially, X-ray structural analysis of protein structures has great impact on understanding dynamics of biological reactions due to detailed descriptions of non-covalent interactions in the vicinities of active sites of enzymes as well as other bio-macromolecules.[4]

In biological systems, *N*-heteroaromatics have been found to act as building blocks to make functional assemblies: Protons of *N*-heteroaromatics can bind to other heteroaromatics by hydrogen bonding and also by π-π interactions of π-conjugated rings with other aromatic moieties. In addition, lone pairs of the heteroatoms, especially that of imidazole of histidine, are available for the coordination to metal ions as can be seen in the active sites of metalloenzymes. Among the *N*-heteroaromatics, flavins, pterins, and other redox-active heteroaromatic coenzymes have been known to play important roles in biological redox reactions, including electron transfer and substrate oxidation reactions. Those coenzymes are fixed at appropriate positions by non-covalent interactions, which can regulate the reactivity of the coenzymes for gaining appropriate redox potentials.

Many metal complexes having bioactive heteroaromatics as ligands have been prepared to obtain insights into the influences of metal ions.[5,6] For instance, metal complexes of heteroaromatic coenzymes like pterins and flavins have been investigated to elucidate their structures and redox properties on the basis of the fact that those heteroaromatics often exist in the vicinity of metal ions *in vivo*.[7] In order to gain further understanding of biological reactions performed by the coenzymes, non-covalent interactions of external molecules with metal complexes having bioactive heteroaromatics have been studied. However, since non-covalent interactions are found in the complicated higher-order structures, it has been difficult to identify the influence of the individual interaction in the active sites.

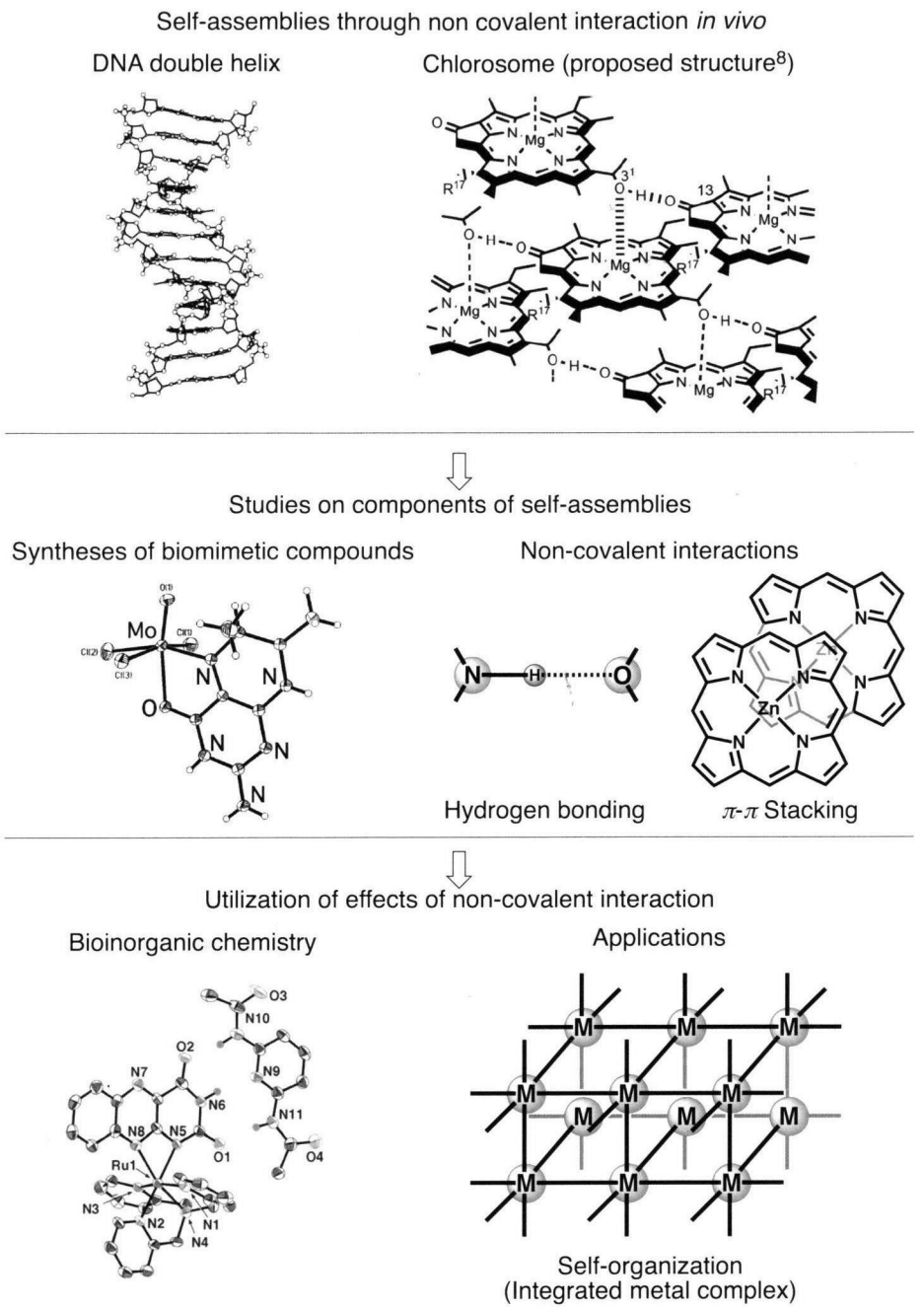

Figure 1. Schematic description of the background of this thesis.

The concept of self-organization has been applied to bioinspired materials and supramolecular chemistry.[9] Supramolecular chemistry is one of the well-established fields to deal with self-organization of molecules *via* non-covalent interactions.[10,11] And also, integration of metal complexes to construct unique supramolecular structures has been controlled by self-organization through intermolecular non-covalent

interactions.[12,13,14] Regulated supramolecular structures are expected to provide useful functions such as unique reaction fields,[15] gas absorption,[16] magnetic properties,[17] and electronic or ionic conduction,[18] which individual monomers can never achieve.

So far, multi-nuclear metal complexes, including metal-organic frameworks (MOFs) or supramolecular metal complexes, have been prepared to explore new functions of metal complexes as mentioned above.[19] Most of the integrated metal complexes are formed *via* self-organization of metal ions and bridging ligands and main concerns of the research have been their crystal structures and properties. The properties of the bridging ligands have not been emphasized and utilized,[20] however, the redox-active bridging ligands will allow us to access new functionality of integrated metal complexes (Figure 1).

Bioactive Heteroaromatics

To achieve self-organization of metal complexes *via* non-covalent interactions, bioactive heteroaromatics should be useful due to their structures and properties: They can coordinate to metal ions, forming complexes by hydrogen bonding and by π-π interaction with other appropriate functional molecules. Among many kinds of heteroaromatics found in biological systems, nucleic acids, flavins and pterins exist in almost every living cell: Nucleic acids are building blocks of DNA, which is essential for genetic information, and flavins and pterins are indispensable for many kinds of redox reactions. Both flavins and pterins are biologically synthesized from the same origin, guanosine triphosphate (GTP). The skeleton of guanosines is a purine derivative, and skeletons of flavins and pterins are pteridine derivatives. In common features, they have pyrimidine rings. These heteroaromatics have several hydrogen bonding site and coordination bonding sites.

About Guanine

Guanine is one of nucleic acids and a heteroaromatic in *vivo*. Nucleic acids are well known components of the DNA double helix, which is formed by intermolecular hydrogen bonding between each complementary nucleobase pairs, *i.e.*, guanine and cytosine, adenine and thymine (Figure 2).[21] However, it is known that guanine is not necessarily combined with cytosine.

In the 1960s, Gellert and coworkers suggested the supramolecular structure made of four guanines linked by hydrogen bonding.[22] The supramolecular assembly is called G-quartet, which has a cavity at the center. In the edge of telomere DNA, the G-quartet structure induces the formation of G-quadruplex by the integration of G-quartet planes.[23] The G-quadruplex is related with apoptotic deletion of cells.[24] A number of

crystal structures of G-quadruplexes have been reported to demonstrate binding of template cations to four oxygen atoms of four guanine moieties.[25] In the presence of excess amount of template cations, the formation of G-quadruplex has been observed in solutions. The selectivity of template cations can be ordered as follows: $K^+ > Na^+$, $Rb^+ >> Cs^+ > Li^+$.[26,27]

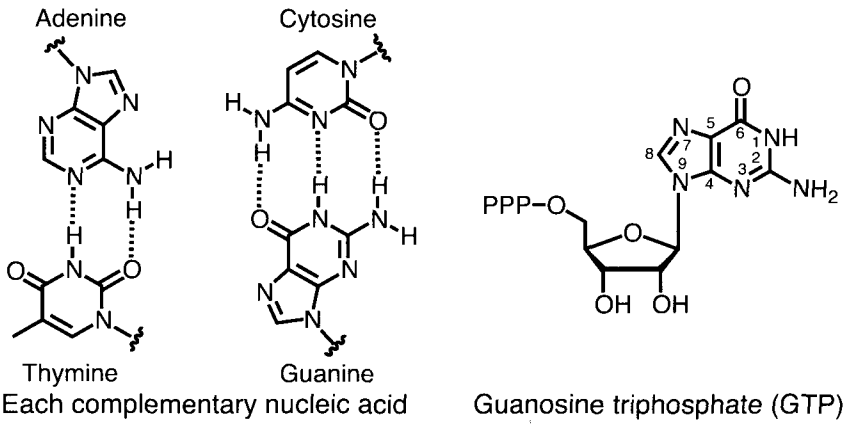

Figure 2. Hydrogen bonding between complementary base pairs, and schematic description of guanosine triphosphate (GTP) with numbering scheme of the guanine skeleton.

Studies on G-quadruplex have conducted in the field of biochemistry. Since G-rich oligonucleotide has usually been employed as a component of G-quadruplex, the analysis of G-quadruplex has always included complicated factors from peripheral groups. Therefore more fundamental information has been required.

This thesis will supply the fundamental data of the formation behavior of a single G-quartet based on thermodynamic analysis from the viewpoint of physical chemistry.

About Flavin

Flavins are redox-active heteroaromatic coenzymes. Flavins are prepared from guanosine triphosphate (GTP) by the biosynthetic pathway with GTP cyclohydrolase II, III, deaminase, reductase, lumazine synthase and riboflavin synthase.[28] Flavins can take various redox states *via* proton-coupled electron transfer (PCET) (Figure 3).[29] Thus, the most important role of flavins is electron transport as electron mediators in metabolisms. In xanthine oxidoreductase, flavins accept two electrons from iron-sulfur cluster, and donate two electrons and two protons to NAD^+ via PCET.[30] Flavins are also required for dioxygen activation for substrate oxidation. In the catalytic cycle of flavin monooxygenase (FMO), reduced flavins have high reactivity, being oxidized immediately by the nucleophilic attack of O_2.[31] The intermediate of dioxygen activation,

flavin hydroperoxide, has never been isolated due to the high reactivity.[32]

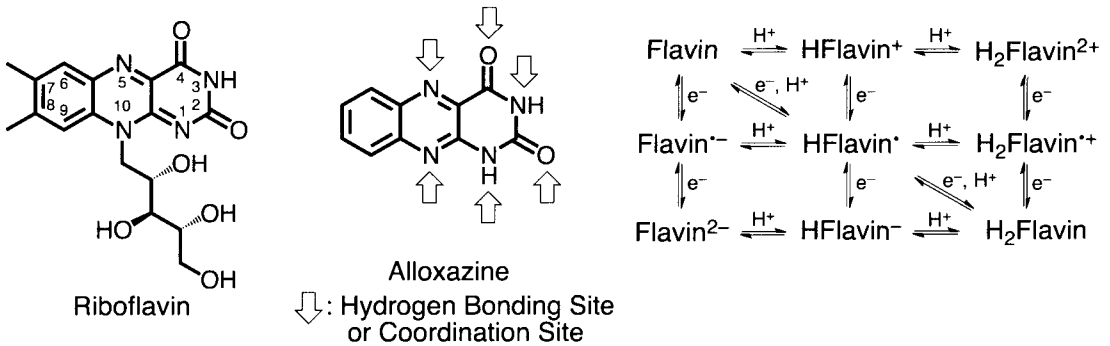

Figure 3. Schematic descriptions of riboflavin, alloxazine and various redox states of flavin.

Flavins *in vitro* show irreversible redox behaviors. Concerning the irreversibility, Rotello and coworkers have reported the influence of proton and hydrogen bonding on the redox process of flavins.[33] In parallel, since flavins can be often found near metal ions in reaction centers, Kaim and coworkers have conducted the study of the effects of metal ions using metal complexes having flavins as ligands.[34] As a result, reversibility of the redox processes of the flavin ligands has been improved by the coordination to metal ions and the redox potentials are shifted to the positive direction. Although flavins have been known to usually coordinate to metal ions at the 4- and 5-positions to form a five-membered chelate ring, the 1,10-coordination mode of alloxazine, which is a flavins analogue, to afford a four-membered chelate ring has been reported by Kojima and coworkers.[35]

About Pterin

Pterins, as well as flavins, are also redox-active heteroaromatic coenzymes. Pterins are also synthesized from guanosine triphosphate (GTP). The ring-opening reaction of GTP is catalyzed by GTP cyclohydrolase, and 7,8-dihydropterin triphosphate is produced. The synthesis of 5,6,7,8-tetrahydropterin requires several more steps with 6-pyruvoyl-tetrahydropterin synthase, sepiapterin reductase and $NADP^+$.[36] Pterin can manipulate four electrons and four protons, acting as cofactors of reductases and oxidases in the vicinity of metal ions in reaction centers (Figure 4).

Pterins are included in almost all molybdenum-containing enzymes except nitrogenase.[37] For example, in xanthine oxidoreductase, molybdopterin plays a role as an oxidase (xanthine oxidase, XO) and donates two electrons to an iron-sulfur cluster (Figure 5).[38]

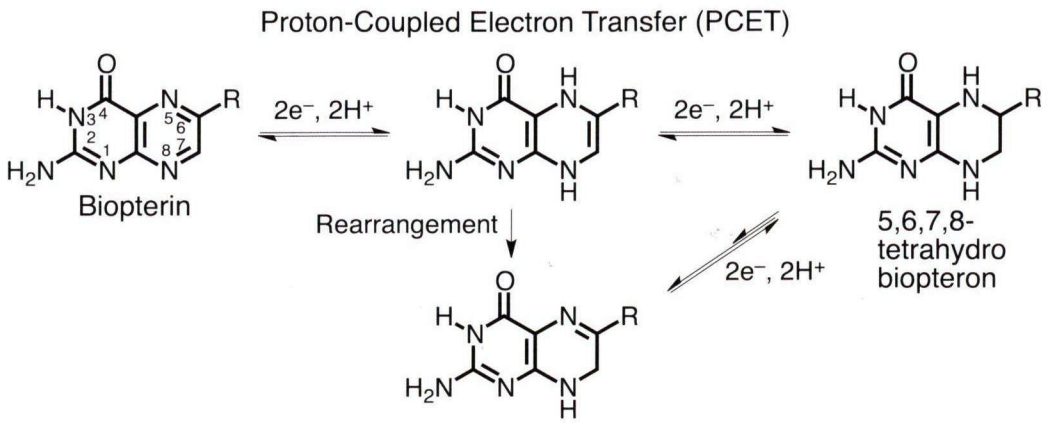

Figure 4. PCET scheme of biopterin.

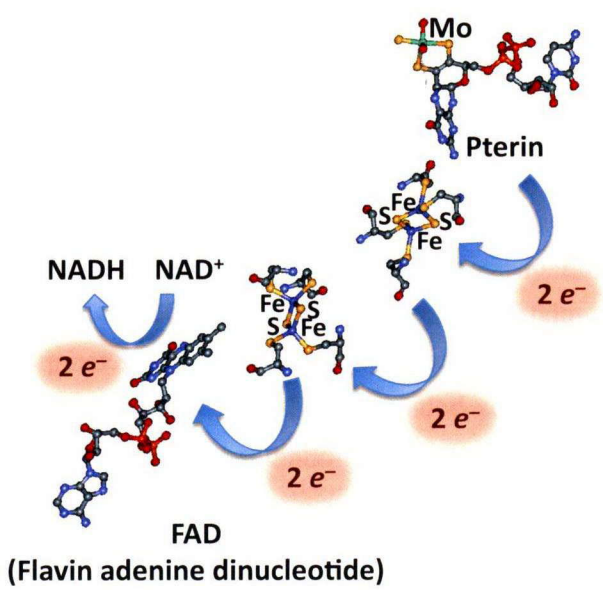

Figure 5. The electron flow in the reaction center of xanthine oxidoreductase.[38]

Pterin-metal complexes have been investigated to reveal that redox processes of the pterin ligands demonstrate improved reversibility by coordination to metal ions,[39] especially the second-row and third-row transition metal ions such as Ru(II) and Ir(III) ions. In addition, a Ru(II)-TPA complex having 6,7-dimethyl pterin has been demonstrated to exhibit a proton shift from 1-N to 8-N upon one-electron reduction of the pterin ligand.[40]

Although the redox behavior of pterin ligand has been clarified, the regulation of the redox potential of pterins by non-covalent interactions has yet to be explored. In

order to obtain information on the redox regulation of pterins by non-covalent interactions, formation of assemblies between pterin complexes and external molecules should be studied.

Metal units as platforms to form stable metal complexes with pterins or flavins

In this thesis, author employs two kinds of platforms as metal units to form integrated metal complexes and to elucidate redox regulation of coenzyme ligands. 1,2,3,4,5-penthamethylcyclopentadienyl (Cp*) is a useful ligand due to the formation of a stable octahedral structure, good solubility and excellent crystallinity of its complexes. An iridium(III) ion forms a low-spin $5d^6$ complex with an octahedral structure. One-electron reduction of an iridium(III) complex may afford an iridium(II) complex, however, the iridium(II) species should be unstable to afford iridium(I) and iridium(III) species *via* disproportionation. An iridium(I) complex should be in a low-spin d^8 electronic configuration to form a square-planar structure.[41] Actually, the two-electron reduction process of a iridium(III) ion occurs at low reduction potentials even if the ligands is selected carefully. The reduction potential of two-electron reduction of a iridium(III) center of $[IrCl(Cp^*)(bpy)]^+$ (bpy=2,2-bipyridine) reaches -1.55 V (vs. $Fc^{0/+}$).[42]

In the coordination chemistry of flavins and pterins, the $Ir^{III}Cp^*$ unit has been frequently used as a platform to form stable complexes because iridium(III) is a substitution-inert and redox-innocent (Figure 6). The characteristics of the $Ir^{III}Cp^*$ unit allows us to observe the redox behavior of flavins or pterins clearly without worrying the redox process of the metal center in a certain range of potential window.

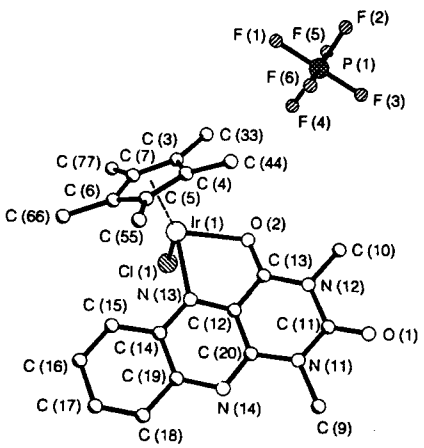

Figure 6. Crystal structure of an $Ir^{III}Cp^*$ complex having 1,3-dimethyl-alloxazine.[34]

In this thesis, the author uses the $Ir^{III}Cp^*$ unit to form integrated metal complexes having alloxazine with 3-dimensional structures on the basis of the octahedral coordination geometry of the Ir(III) ion. The research aims to discover novel functions of integrated metal complexes and to observe the redox behavior of alloxazines as bridging ligands in the integrated metal complexes.

As another platform, a ruthenium(II)-tris(2-pyridylmethyl)amine unit ($Ru^{II}TPA$) was employed.[43,44] Since TPA is a tetradentate chelating ligand, the $Ru^{II}TPA$ unit affords stable complexes with pterins or flavins acting as bidentate chelating ligands. The main purpose to use the $Ru^{II}TPA$ unit is the stabilization of the coordination bond due to the π-back donation from Ru^{II} center in a low-spin $4d^6$ electronic configuration to pterins or flavins ligands. Kojima and coworkers have synthesized, isolated and crystallized a $Ru^{II}TPA$-alloxazine complex with a novel coordination mode of alloxazine and observed the reversible redox behavior due to the high stability of the complex in solution.[35]

Contents of This PhD Thesis

In this thesis, the author focuses on non-covalent interactions that regulate structures and redox behavior of molecular and supramolecular assemblies.

In chapter 1, the crystal structures and the thermodynamics of formation of G-quartets are discussed with use of 9-isopropylguanine. The fundamental data of single G-quartet plane provides important information for the study of G-quadruplex on the basis of thermodynamic analysis of the quartet formation. The data set should be helpful to provide fundamental understanding on the G-quartet formation using the simple guanine derivative without complicated contribution of peripheral functional groups in the G-quadruplex. Further, the direct π-π interaction between a G-quartet and porphyrins in organic solvents has been detected by means of UV-vis and NMR spectroscopies, because the interaction between the G-quartet and external π-conjugated molecules is important for the development of anticancer and antitumor drugs. The author also describes the temperature-dependent structural change of supramolecular assemblies consisting of a Ni(II)-porphyrin and G-quartet.

In chapter 2, the regulation of the redox potential of a pterin ligand bound to the Ru(II)-TPA unit with nucleotide bases has been achieved by intermolecular hydrogen bonding. In addition, the structural change of the adduct of the Ru(II)-pterin complex and thymidine has been observed before and after the reduction of the pterin ligand. The regulation of the redox potential of the pterin ligand by intermolecular hydrogen bonding with nucleobases provides clear evidence for the influence of peripheral amino

acid residue to regulate the reactivity of pterins.

In chapter 3, the synthesis and the characterization of a novel tetranuclear iridium(III)-alloxazine complex with unprecedented coordination modes and self-reorganization have been described together with recovery of the tetranuclear structure in the course of crystallization. The tetranuclear complex has been revealed to interact with another tetranuclear iridium-alloxazine complex through four hydrogen bonds to form a supramolecular cage, in which two counter anions are included. The author also demonstrated exchange of the counter anions included in the cage by virtue of the self-reorganization.

In chapter 4, the synthesis and the characterization of a novel hexanuclear iridium(III) complex with three alloxazine anions as bridging ligands have been described together with the stability in solution and the multi-electron redox processes observed by cyclic voltammetry. The novel hexanuclear iridium-aloxazine complex has been demonstrated to act as an electron reservoir, which is reminiscent of iron-sulfur clusters in biological systems.

References

1 a) T. Misteli, *Nature*, 2008, **456**, 333; b) T. E. Kaiser, R. V. Intine and M. Dundr, *Science*, 2008, **322**, 1713; c) K. Oohora, A. Onoda and T. Hayashi, *Chem. Commun.*, 2012, **48**, 11714.

2 a) L. Meazza, J. A. Foster, K. Fucke, P. Metrangolo, G. Resnati and J. W. Steed, *Nature Chem.*, Published online 11 November 2012, doi:10.1038/nchem.1496; b) Y. Zhao, E. Tomšík, J. Wang, Z. Morávková, A. Zhigunov, J. Stejskal and M. Trchová, *Chem.–Asian J.*, Article first published online 8 November 2012, doi: 10.1002/asia.201200836. c) C. A. Hunter and J. K. M. Sanders, *J. Am. Chem. Soc.*, 1990, **12**, 5525.

3 M. R. Osés, D. G. de Oteyza, I. F. Torente, N. G. Lakunza, P. M. S. Weber, T. Kampen, K. Horn, A. Gourdon, A. Arnau and J. E. Ortega, *ChemPhysChem*, 2009. **10**, 896.

4 a) I. Efimov, S. K. Badyal, C. L. Metcalfe, I. Macdonald, A. Gumiero, E. L. Raven and P. C. E. Moody, *J. Am. Chem. Soc.*, 2011, **133**, 15376; b) G. I. Berglund, G. H. Carlsson, A. T. Smith, H. Szöke, A. Henriksen and J. Hajdu, *Nature*, 2002, **417**, 463.

5 a) H. Baker, P. Hambright, L. Wagner and L. Ross, *Inorg. Chem.*, 1973, **12**, 2200; b) H. Baker, P. Hambright and L. Wagner, *J. Am. Chem. Soc.*, 1973, **95**, 5942; c) P. Hambright and P. B. Chock, *J. Am. Chem. Soc.*, 1974, **96**, 3123; d) P. Hambright

and P. B. Chock, *Inorg. Chem.*, 1974, **13**, 3029; e) P. Hambright, M. K. Rishnamurthy and P. B. Chock, *J. Inorg. Nucl. Chem.*, 1975, **37**, 557; f) P. Hambright and P. B. Chock, *J. Inorg. Nucl. Chem.*, 1975, **37**, 2363.

6 a) D. M. Bryan, S. D. Pell, R. Kumar, M. J. Clarke, V. Rodriguez, M. Sherban and J. Charkoudian, *J. Am. Chem. Soc.*, 1988, **110**, 1498; b) D. M. Bryan, S. D. Pell, R. Kumar, M. J. Clarke, V. Rodriguez, M. Sherban and J. Charkoudian, *J. Am. Chem. Soc.*, 1988, **110**, 1498; c) M. J. Clarke, *Comments Inorg. Chem.*, 1984, **3**, 133; d) M. J. Clarke, *Rev. Inorg. Chem.*, 1980, **2**, 27.

7 W. Kaim. B. Schwederski, O. Heilmann and F. M. Hornung, *Coord. Chem. Rev.*, 1999, **182**, 323.

8 T.Miyatake and H. Tamiaki, *Coord. Chem. Rev.*, 2010, **254**, 2593.

9 J. M. Lehn, *Science*, 2002, **295**, 2400.

10 a) H. Rapaport, *Supramol. Chem.*, 2006, **18**, 445; b) M. A. Khalily, O. Ustahuseyin, R. Garifullin, R. Genc and M. O. Guler, *Chem. Commun.*, 2012, **48**, 11358; c) H. Ceylan, S. Kocabey, A. B. Tekinay and M. O. Guler, *Soft Matter*, 2012, **8**, 3929; d) H. Acar, R. Garifullin and M. O. Guler, *Langmuir*, 2011, **27**, 1079.

11 a) T. Emrick and J. M. Fréchet, *Curr. Opin. Colloid Interface Sci.*, 1999, **4**, 15; b) D. S. Lawrence, T. Jiang and M. Levett, *Chem. Rev.*, 1995, **95**, 2229; c) L. J. Prins, D. N. Reinhoudt and P. Timmerman, *Angew. Chem., Int. Ed.*, 2001, **40**, 2382; d) D. Philip and J. F. Stoddart, *Angew. Chem., Int. Ed.*, 1996, **35**, 1154; e) M. C. T. Fyfe and J. F. Stoddart, *Acc. Chem. Res.*, 1997, **30**, 393; f) G. M. Whitesides, E. E. Simanek, J. P. Mathias, C. T. Seto, D. N. Chin, M. Mammen and D. M. Gordon, *Acc. Chem. Res.*, 1995, **28**, 37.

12 a) D. Fujita, A. Takahashi, S. Sato and M. Fujita, *J. Am. Chem. Soc.*, 2011, **133**, 13317; b) T. Osuga, T. Murase and M. Fujita, *Angew. Chem., Int. Ed.*, 2012, **51**, 1.

13 a) M. D. Pluth, R. G. Bergman and K. N. Raymond, *Acc. Chem. Res.*, 2009, **42**, 1650; b) D. Fiedler, D. H. Leung, R. G. Bergman and K. N. Raymond, *Acc. Chem. Res.*, 2005, **38**, 349; c) M. D. Pluth and K. N. Raymond, *Chem. Soc. Rev.*, 2007, **36**, 161.

14 a) S. Leininger, B. Olenyuk and P. J. Stang, *Chem. Rev.*, 2000, **100**, 853; b) B. Hasenknopf, J. –M. Lehn, N. Boumediene, E. Leize and A. V. Dorsselaer, *Angew. Chem., Int. Ed.*, 1998, **37**, 3265.

15 a) M. Yoshizawa, Y. Takeyama, T. Okano and M. Fujita, *J. Am. Chem. Soc.*, 2003, **125**, 3243; b) M. Yoshizawa, N. Sato and M. Fujita, *Chem. Lett.*, 2005, **34**, 1392.

16 a) N. Yanai, K. Kitayama, Y. Hijikata, H. Sato, R. Matsuda, Y. Kubota, M. Takata, M. Mizuno, T. Uemura and S. Kitagawa, *Nature Mater.*, Published online 4 September 2011, doi: 10.1038/NMAT3104; b) K. Nakagawa, D. Tanaka, S. Horike,

S. Shimomura, M. Higuchi and S. Kitagawa, *Chem. Commun.*, 2010, **46**, 4258.

17 M. R. Godfrey, T. P. Newcomb, B. M. Hoffman and J. A. Ibers, *J. Am. Chem. Soc.*, 1990, **112**, 7260.

18 C. M. Drain, *Proc. Natl. Acad. Sci. U.S.A.*, 2002, **99**, 5178.

19 T. R. Cook, Y. R. Zheng and P. J. Stang, *Chem. Rev.*, 2012, *ASAP*, doi: 10.1021/cr3002824.

20 R. Chakrabarty, P. S. Mukherjee and P. J. Stang, *Chem. Rev.*, 2011, **111**, 6810.

21 J. D. Watson and F. H. C. Crick, *Nature*, 1953, **171**, 737.

22 M. Gellert, M. N. Lipsett and D. R. Davies, *Proc. Natl. Acad. Sci. U.S.A.*, 1962, **48**, 2013.

23 R. Jin, K. J. Breslauer, R. A. Jones and B. L. Gaffney, *Science*, 1990, **250**, 543.

24 a) D. Gomez, N. Aouali, A. L. Vallejo, L. Lacroix, F. M. Chanet, T. Lemarteleur, C. Douarre, K. Shin-ya, P. Mailliet, C. Trentesaux, H. Morjani, J. L. Mergny and J. F. Riou, *J. Biol. Chem.*, 2003, **278**, 50554; b) A. Nakajima, T. Tauchi, G. Sashida, M. Sumi, K. Abe, K. Yamamoto, J. H. Ohyashiki and K. Ohyashiki, *Leukemia*, 2003, **17**, 560.

25 J. T. Davis, *Angew. Chem., Int. Ed.*, 2004, **43**, 668.

26 C. C. Hardin, A. G. Perry and K. White, *Biopolymers*, 2001, **56**, 147.

27 T. J. Pinnavaia, C. L. Marshall, C. M. Mettler, C. L. Fisk, H. T. Miles and E. D. Becker, *J. Am. Chem. Soc.*, 1978, **100**, 3625.

28 a) M. Fischer and A. Bacher, *Arch. Biochem. Biophys.*, 2008, **474**, 252; b) L. Chatwell, T. Krojer, A. Fidler, W. Römisch, W. Eisenreich, A. Bacher, R. Huber and M. Fischer, *J. Mol. Biol.*, 2006, **359**, 1334.

29 a) P. Hemmerich, C. Veeger and H. C. S. Wood, *Angew. Chem., Int. Ed.*, 1965, **4**, 671; b) S. Fukuzumi and T. Kojima, *J. Biol. Inorg. Chem.*, 2008, **13**, 321; c) S. L. J. Tan and R. D. Webster, *J. Am. Chem. Soc.*, 2012, **134**, 5954.

30 J. Hunt and V. Massey, *J. Biol. Chem.*, 1994, **269**, 18904.

31 Y. Imada, H. Iida, S. Ono, Y. Masui and S. Murahashi, *Chem.–Asian J.*, 2006, **1-2**, 136.

32 a) C. Kemal, T. W. Chan and T. C. Bruice, *J. Am. Chem. Soc.* 1977, **99**, 7272; b) C. T. Walsh, *Acc. Chem. Res.*, 1980, **13**, 148; c) T. C. Bruice, *Acc. Chem. Res.*, 1980, **13**, 256; d) B. P. Branchaud and C. T. Walsh, *J. Am. Chem. Soc.*, 1985, **107**, 2153; e) M. Meyer, *J. Mol. Struct.*, 1997, **417**, 163; f) C. Canepa, R. D. Bach and O. Dmitrenko, *J. Org. Chem.*, 2002, **67**, 8653; g) R. D. Bach and O. Dmitrenko, *J. Am. Chem. Soc.*, 2004, **126**, 127; h) G. Ottolina, G. de Gonzalo and G. Carrea, *J. Mol. Struct.*, 2005, **757** 175; i) A. Mattevi, *Trends Biochem. Sci.*, 2006, **31**, 276

33 a) A. Niemz and V. M. Rotello, *Acc. Chem. Res.*, 1999, **32**, 44; b) E. Breinlinger, A.

Niemz and V. M. Rotello, *J. Am. Chem. Soc.*, 1995, **117**, 5379.

34 a) O. Heilmann, F. M. Hornung, J. Fiedler and W. Kaim, *J. Organomet. Chem.*, 1999, **589**, 2; b) O. Heilmann, F. M. Hornung, W. Kaim and J. Fiedler, *J. Chem. Soc., Faraday Trans.*, 1996, **92**, 4233.

35 a) S. Miyazaki, K. Ohkubo, T. Kojima and S. Fukuzumi, *Angew. Chem., Int. Ed.*, 2007, **46**, 905; b) S. Fukuzumi and T. Kojima, *J. Biol. Inorg. Chem.*, 2008, **13**, 321; c) S. Miyazaki, T. Kojima and S. Fukuzumi, *J. Am. Chem. Soc.*, 2008, **130**, 1556.

36 a) B. Thöny, G. Auerbach and N. Blau, *Biochem. J.*, 2000, **347**, 1; b) J. Kim, S. I. Park, C. Ahn, H. Kim and J. Yim, *J. Biol. Chem.*, 2009, **284**, 23426; c) J. V. Vivar, *Free Radical Biol. Med.*, 2009, **47**, 1108.

37 a) S. Leimkühler, M. M. Wuebbens and K. V. Rajagopalan, *Coord. Chem. Rev.*, 2011, **255**, 1129; b) Russ Hille, *Chem. Rev.*, 1996, **96**, 2757; c) C. C. Wei, B. R. Crane and D. J. Stuehr, *Chem. Rev.*, 2003, **103**, 2365.

38 a) U. Dietzel, J. Kuper, J. A. Doebler, A. Schulte, J. J. Truglio, S. Leimkühler and C. I. Kisher, *J. Biol. Chem.*, 2009, **284**, 8768; b) H. Ishikita, B. T. Eger, K. Okamoto, T. Nishino and E. F. Pai, *J. Am. Chem. Soc.*, 2012, **134**, 999; c) T. Nishino, K. Okamoto, B. T. Eger, E. F. Pi and T, Nishino, *FEBS J.*, 2008, **275**, 3278; d) R. Kappl, S. Sielker, K. Ranguelova, J. Wegner, K. Parschat, J. Hüttermann and S. Fetzner, *Biochemistry*, 2006, **45**, 14853.

39 a) D. H. Lee, N. N. Murthy, Y. Lin, N. S. Nasir and K. D. Karlin, *Inorg. Chem.*, 1997, **36**, 6328; b) H. L. Kaufmann, P. J. Carroll and S. J. N. Burgmayer, *Inorg. Chem.*, 1999, **38**, 2600; c) S. J. N. Burgmayer and H. L. Kaufmann, *Inorg. Chem.*, 1999, **38**, 2607; d) B. Fischer, H. Schmalle and E. Dubler, *Inorg. Chem.*, 1995, **34**, 5726.

40 a) S. Miyazaki, K. Ohkubo, T. Kojima and S. Fukuzumi, *Angew. Chem., Int. Ed.*, 2008, **47**, 9669; b) S. Miyazaki, T. Kojima, T. Sakamoto, T. Matsumoto, K. Ohkubo and S. Fukuzumi, *Inorg. Chem.*, 2008, **47**, 333; c) S. Miyazaki, T. Kojima, J. M. Mayer and S. Fukuzumi, *J. Am. Chem. Soc.*, 2009, **131**, 11615.

41 M. Ladwig and W. Kaim, *J. Organomet. Chem.*, 1992, **439**, 79.

42 W. Kaim, S. Berger, S. Greulich and R. Reinhardt, *J. Fiedler*, 1999, **582**, 153.

43 a) R. A. Ghiladi, E. E. Chufn, D. del Ro, E. I. Solomon, C. Krebs, B. H. Huynh, H. Huang, P. Monne-Loccoz, S. Kaderli, M. Honecker, A. D. Zuberbhler, L. Marzilli, R. J. Cotter and K. D. Karlin, *Inorg. Chem.*, 2007, **46**, 3889; b) H. R. Lucas, G. J. Meyer and K. D. Karlin, *J. Am. Chem. Soc.*, 2009, **131**, 13924; c) H. R. Lucas, G. J. Meyer and K. D. Karlin, *J. Am. Chem. Soc.*, 2010, **132**, 12927; d) R. L. Shook, S. M. Peterson, J. Greaves, C. Moore, A. L. Rheingold and A. S. Borovik, *J. Am. Chem. Soc.*, 2011, **133**, 5810; e) N. L. Poul, B. Douziech, J. Zeitouny, G. Thiabaud, H.

Colas, F. Conan, N. Cosquer, I. Jabin, C. Lagrost, P. Hapiot, O. Reinaud and Y. L. Mest, *J. Am. Chem. Soc.*, 2009, **131**, 17800.

44 a) T. Kojima, T. Morimoto, T. Sakamoto, S. Miyazaki and S. Fukuzumi, *Chem. –Eur. J.*, 2008, **14**, 8904; b) T. Kojima, K. Hayashi, S. Iizuka, F. Tani, Y. Naruta, M. Kawano, Y. Ohashi, Y. Hirai, K. Ohkubo, Y. Matsuda and S. Fukuzumi, *Chem.–Eur. J.*, 2007, **13**, 8212; c) T. Kojima, D. M. Weber and C. T. Choma, *Acta Cryst.*, 2005, **E61**, m226; d) T. Kojima, S. Miyazaki, K. Hayashi, Y. Shimazaki, F. Tani, Y. Naruta and Y. Matsuda, *Chem.–Eur. J.*, 2004, **10**, 6402.

Chapter 1

Formation of "Naked" Guanine-Quartets Using 9-Isopropylguanine: Structures, Formation Thermodynamics, and Temperature-Dependent Structural Change of Supramolecular Assemblies with a Ni(II)-Porphyrin

Abstract

Formation of guanine quartets with 9-isopropylguanine (^{i}PG) is discussed in organic solvents. Crystal structures of the ^{i}PG quartets were determined by X-ray crystallography with template cations (Na^+ and Ca^{2+}) and the structure without a template cation was also obtained by virtue of the stabilization by intermolecular hydrogen bonding with water molecules of crystallization. In the presence of Na^+ and Ca^{2+}, ΔH and ΔS values in the formation of ^{i}PG-4-Na^+ and ^{i}PG-4-Ca^{2+} complexes were determined to be ΔH = –8.4 kcal mol^{-1} and ΔS = +50 cal mol^{-1} K^{-1} for Na^+ and ΔH = –12.9 kcal mol^{-1} and ΔS = +34 cal mol^{-1} K^{-1} for Ca^{2+} on the basis of van't Hoff plots attained from the results of temperature-dependent UV-vis spectroscopic measurements. The G-quartet, ^{i}PG-4-Na^+, forms 1:1 or 2:1 complexes with octaethylporphinatonickel(II) (NiOEP) depending on temperature, whereas the corresponding free-base porphyrin (H_2OEP) exhibits negligible interactions with the G-quartet. The formation constants were determined from the titration curve in methanol/chloroform as 1:1 or 2:1 complexes of ^{i}PG-4-Na^+ with NiOEP.

Introduction

Since Gellert and coworkers suggested the guanine tetrad structure linked by intermolecular hydrogen bonding in 1962,[1] the characteristic guanine-quartet (hereafter referred to as G-4) structure has attracted great attention of researchers in many different areas.[2-8] Especially, integrated G-4 structures which exist at the edge of DNA chain, called guanine quadruplexes (hereafter denoted as G-quadruplex), have been reported in large numbers.[9-15] So far, many kinds of G-quadruplexes included in higher-order structures have been crystallized with various template cations.[16,17] In parallel, studies on interaction of molecules to show certain selectivity for the part of the G-quadruplex have been conducted.[18–27] The main purpose of those studies has been the acquirement of an anticancer effect. The effect is based on inhibition of telomerase binding to the G-quadruplex moiety of DNA by protecting the moiety with the molecules. G-quadruplexes have also been utilized to develop functional biomaterials: The cavity of G-quadruplex can include guest ions, which can be applied to ion-conducting material and so on.[28,29]

Study on solution behaviors of guanine and its derivatives in organic solvents should be important for elucidating the dynamics of the G-4 structure formation by intermolecular hydrogen bonding in detail. However, the formation dynamics of a discrete G-4 structure has yet to be well investigated. The lack of the thermodynamic data on the formation of a discrete and single-layer G-4 structure has hampered the discussion on the detail of the G-4 formation, including the driving force of the formation. In fact, G-quadruplex structures involve too many complicated factors including noncovalent intermolecular interactions[30] provided by many functional groups such as sugar and phosphate moieties, which cover the part of G-4 cores.[31,32] Therefore, interactions of external molecules with a G-quadruplex have been observed as interactions with the peripheral groups, not direct interactions with the G-4 units. In addition, the conformational regulation of the peripheral moieties has been considered to be difficult for formation of supramolecular assemblies of guanine derivatives linked only by intermolecular hydrogen bonding in solutions.[33-35] Thus, G-4 formation with use of a guanine derivative without complicated peripheral groups is indispensable to clarify intrinsic thermodynamics of the complementary hydrogen bonding and interaction of G with a template cation in a discrete and single-layer G-4 structure.

In this work, 9-isopropylguanine (^{i}PG)[36] having the isopropyl group at the 9-N position was used to form the G-4 structure (Figure 1). The introduction of the small isopropyl group allowed us not only to improve the solubility into organic solvents and but also to accommodate the crystallization of "naked" G-4 supramolecules, without

any steric protection of the G-4 core by such as deoxyribose-phosphate moieties in guanosine derivatives reported so far. The strategy presented herein makes it possible for the first time to discuss on the intrinsic characteristics of the G-4 structure and on detailed thermodynamics of the G-4 formation to elucidate the role of the template cations. Based on the observations, the author would clarify the switching of the driving force of the G-4 formation from desolvation of the guanine molecule in the absence of template metal ions to electrostatic attractive interactions between ^{i}PG and metal ions in the presence of the template cations.

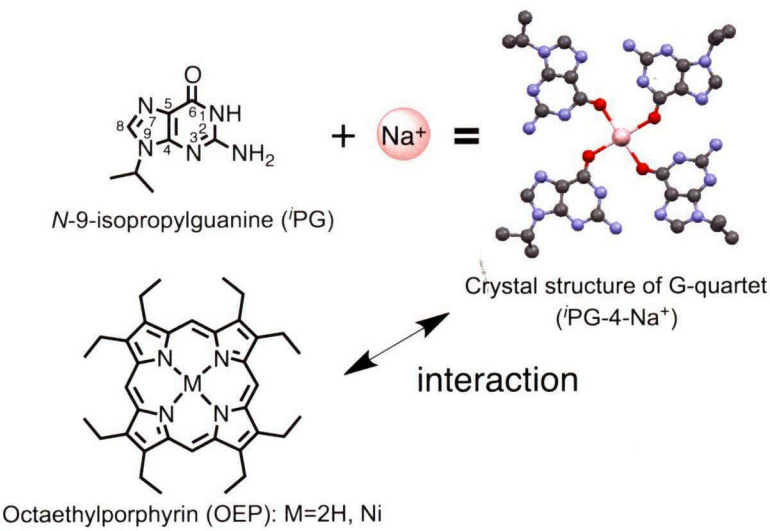

Figure 1. Schematic descriptions of *N*-9-isopropylguanine (^{i}PG), octaethylporphyrin (OEP) and the crystal structure of the G-quartet (^{i}PG-4-Na^{+}).

As mentioned above, intermolecular interaction between G-quadruplex[2,37] and an external molecule has been considered to play an important role in anticancer strategies based on protecting the part of G-quadruplex from telomerase.[23-26] So far, several adducts of G-quadruplexes and external molecules have been reported to clarify their crystal structures, binding modes of the external molecules and the binding selectivity for the G-quadruplex moiety in G-rich oligonucleotides.[19-21,38] When porphyrin derivatives are used as external molecules, the intermolecular interactions between G-quadruplex and porphyrins have been observed in various topologies such as the intercalation of porphyrins into G-quadruplex,[18,22] side binding,[31] and end-stacking of porphyrins around the G-quadruplex,[27,32] depending on substituents connected to G-quadruplexes. These different binding modes need to be clarified for the development of telomerase inhibition. However, the direct interaction between a G-quartet moiety in

G-quadruplex and porphyrins has not been always clearly elucidated in solutions due to additional complicated interactions with peripheral groups of G-quadruplex.[30] Thus, study on the direct interaction between the G-quartet without peripheral groups and porphyrin is expected to supply fundamental information on the complex formation between G-quadruplex and porphyrin.

The author presents the direct observation of the interactions between the naked ^{i}PG-4-Na^{+} and porphyrins as an external molecule by the UV-Vis and ^{1}H NMR spectroscopic measurements. Octaethylporphyrin (H_2OEP) having ethyl groups at the pyrrole β-positions and octaethylporphinatonickel(II) (NiOEP) were used as external molecules. The square planar geometry of NiOEP is reasonable for π-π interaction with the G-quartet plane, and the use of diamagnetic NiOEP makes possible to detect the interaction with the G-quartet by ^{1}H NMR measurements.

Results and discussion

1.1. Quartet formation of a guanine derivative with an isopropyl group: Crystal structures of "naked" G-quartets and thermodynamics of G-quartet formation

1.1.1. Crystal structures of G-quartets

In all cases, crystallization of G-4 assemblies was conducted in methanol solutions with vapor diffusion of diethyl ether. Crystal structures of the G-4 assemblies made of ^{i}PG are shown in Figure 2 to 4. Even in the absence of a template cation, it was clearly demonstrated that ^{i}PG could form the quartet (^{i}PG-4) structure in the crystal with the aid of two water molecules (Figure 2(a)). As observed in the G-quadruplex, the G-4 assembly was formed by the complementary intermolecular hydrogen bonding between the 6-O and 1-NH groups and that between the 2-NH_2 group and the 7-nitrogen atom. Intermolecular hydrogen bonding was observed among the water molecule of crystallization and the oxygen atoms at the 6-position in ^{i}PG showing the interatomic distance (O1•••O3(W) and O2•••O3(W), 2.85 and 3.03 Å, respectively). This hydrogen bonding could assist the G-4 formation to compensate the lack of the stabilization by template cations. In the packing structure, the ^{i}PG-4 planes overlap partially due to CH/π and π-π interactions (Figure 2(b)). The integration of the ^{i}PG-4 planes by stacking as seen in the G-quadruplex could not be observed, because the two hydrogen atoms of the water molecule of crystallization can direct only to one ^{i}PG-4 plane and the water molecule cannot link two ^{i}PG-4 planes. Although a G-4 structure without template cations has been reported,[39,40] no report has appeared on "naked" G-4 structures without steric protection by large substituents attached to the guanine scaffold.

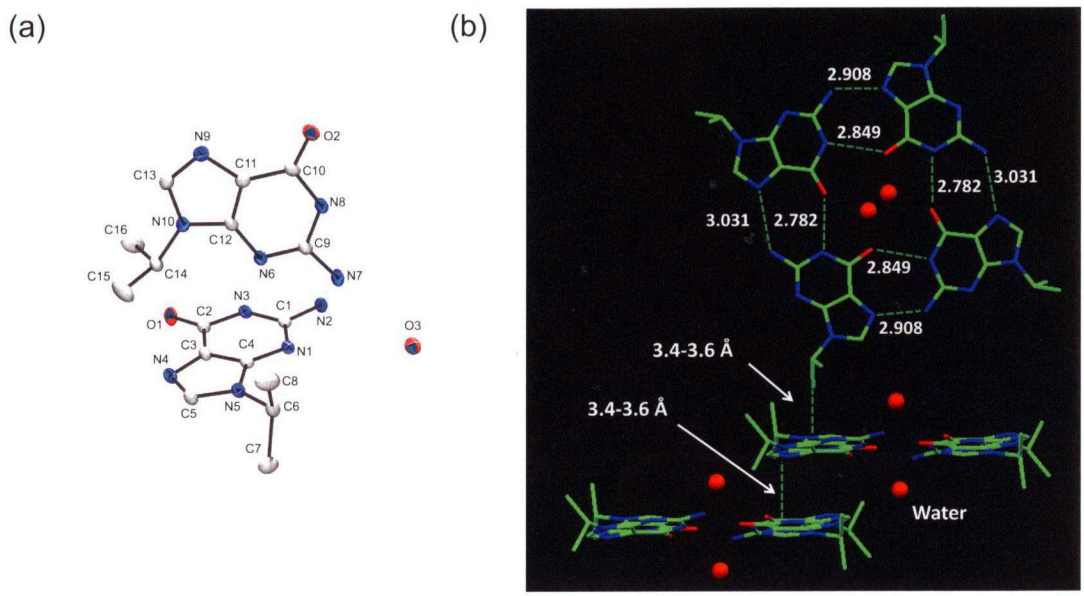

Figure 2. (a) Crystal structure of the asymmetric unit of ^{i}PG-4 without template cations. (b) A view of crystal packing. Interatomic distances (Å), representing intermolecular CH/π and π-π interactions and hydrogen bonding, are given in the figure.

In the presence of sodium cation derived from $Na[B(C_6H_5)_4]$ ($NaBPh_4$), the crystal structure of ^{i}PG clearly demonstrated the formation of the G-4 dimer. The Na^+ ion resided nearly in the mean plane of the ^{i}PG-4 assembly. Two of the G-4 assemblies formed a dimer by the electrostatic interaction between Na^+ and 6-O of guanine in the other ^{i}PG-4 plane, showing the interatomic distance of Na•••O4' to be 2.729(4) Å (Figure 3). One diethyl ether molecule was found to bind to the Na^+ ion with the interatomic distance of 2.609(7) Å to cap the dimeric structure, preventing further stacking with the ^{i}PG-4 assemblies. In the dimeric unit in the crystal, π-π interactions are operating with the closest interatomic distance of 3.422(8) Å.

The author also examined the formation of the ^{i}PG-4 structures in the presence of calcium ion derived from $CaCl_2$. In this case, a ^{i}PG-4 structure was formed and the Ca^{2+} ion also resided in the mean plane of the ^{i}PG-4 structure. Two chloride counter anions interacted with the calcium ion with the Ca^{2+}•••Cl^- distance of 2.6980(4) Å both above and below the mean plane of the ^{i}PG-4 bound to Ca^{2+} (^{i}PG-4-Ca^{2+}) (Figure 4). The packing structure is similar to that of the water-assisted ^{i}PG-4 assembly: As well as in the case of the water-assisted ^{i}PG-4, two of the ^{i}PG-4-Ca^{2+} assemblies stack *via* CH/π and π-π interactions to form a dimeric motif in the crystal.

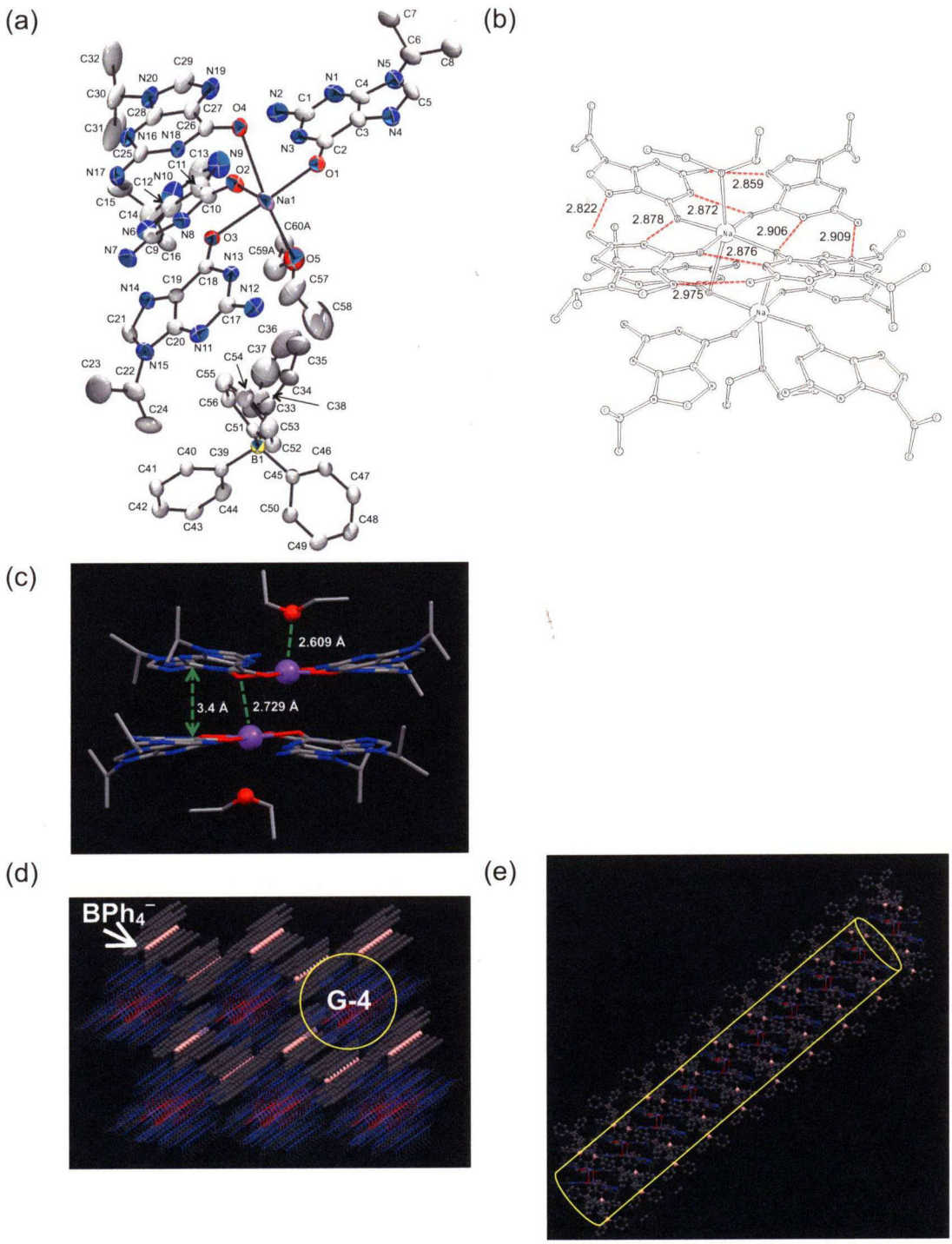

Figure 3. (a) Crystal structure of the asymmetric unit of ^{i}PG-4-Na^{+}. (b) Interatomic distances for intermolecular hydrogen bonding in the quartet (Å). (c) Axial interactions to Na^{+}. (In (b) and (c), BPh_4^- was omitted for clarity.) (d) and (e) Views of crystal packing of ^{i}PG-4–Na^{+} (the diethyl ether molecules were omitted clarity).

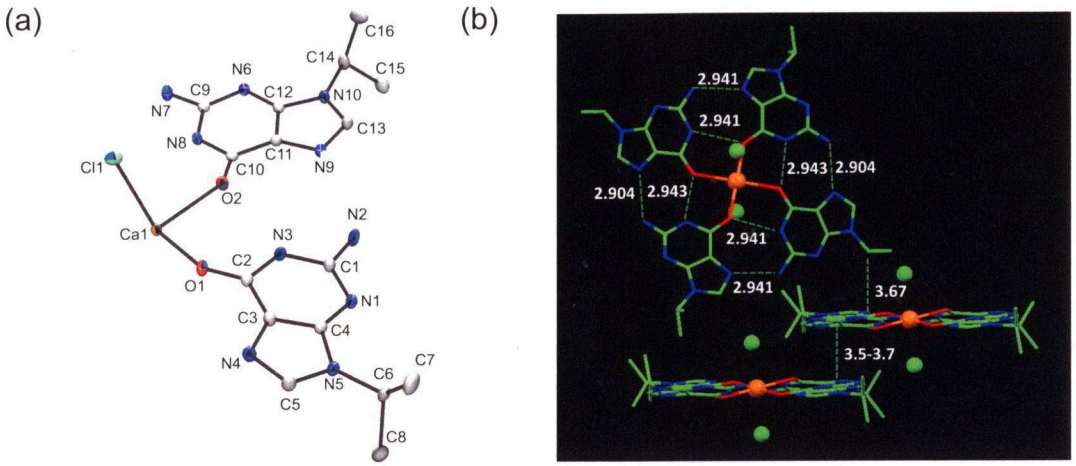

Figure 4. (a) Crystal structure of the asymmetric unit of ^{i}PG-4-Ca^{2+}. (b) A view of crystal packing structure. Interatomic distances (Å), representing intermolecular CH/π and π-π interactions and hydrogen bonding, are given in the figure.

Table 1. Summary of the interatomic distances related to template cations, those of 3-*N*H•••4-O as intermolecular hydrogen bonding in ^{i}PG-4 structures, and interplane distances between two G-4 assemblies.

^{i}PG-4		^{i}PG-4-Na^{+}		^{i}PG-4-Ca^{+}	
Water•••O (Å)		**Cation•••O (Å)**			
O3•••O1	2.852(1)	Na1•••O1	2.257(4)	Ca1•••O1	2.3212(9)
		Na1•••O2	2.300(3)		
O3•••O2	3.030(1)	Na1•••O3	2.320(4)	Ca1•••O2	3.3232(9)
		Na1•••O4	2.357(3)		
N*H*•••O (Å)					
N8•••O1	2.849(2)	N18•••O1	2.876(5)	N8•••O1	2.941(2)
		N3•••O2	2.878(6)		
N3•••O2	2.782(1)	N8•••O3	2.872(4)	N3•••O2	2.943(1)
		N13•••O4	2.906(5)		
G-4 plane•••G-4 plane (Å)					
3.597		3.626		3.652	
Selected bonds					
		Na1•••O4'	2.729(4)	Ca1•••Cl1	2.6980(4)
		Na1•••O5	2.609(7)		

Each distance between the cation and 6-O of guanine in the corresponding ^{i}PG-4 plane and that between 3-*N*H and 6-O for the hydrogen bonding to form the ^{i}PG-4

structure were slightly different among three kinds of ^{i}PG-4 structures. However, the distances fall in the normal range of those reported in G-quadruplexes, i.e., 2.3 Å and 2.9 Å, respectively,[41] as summarized in Table 1. Thus, the G-4 formation can be assisted by electrostatic interactions of 6-O in guanine with a cationic entity or water molecules having polarized O-H bonds, regardless of the steric protection by bulky peripheral substituents.

All the X-ray crystallographic data are summarized in Table 2.

Table 2. X-ray crystallographic data for supramolecular structures of 9-isopropylguanine (^{i}PG) (^{i}PG_R, ribbon-type assembly; ^{i}PG-4-water, a quartet of ^{i}PG with water; ^{i}PG-4-Na^{+}, a quartet of ^{i}PG with Na^{+}; ^{i}PG-4-Ca^{2+}, a quartet of ^{i}PG with Ca^{2+}).

File name	^{i}PG_R	^{i}PG-4-water	^{i}PG-4-Na^{+}	^{i}PG-4-Ca^{2+}
formula	$C_{17}H_{23}Cl_3N_{10}O_2$	$C_{16}H_{22}N_{10}O_3$	$C_{60}H_{69}BN_{20}NaO_5$	$C_{16}H_{22}Ca_{0.5}ClN_{10}O_2$
fw	505.80	402.44	1184.15	441.93
crystal system	orthorhombic	monoclinic	monoclinic	monoclinic
space group	*Pbca*	$P2_1/n$	$C2/c$	$P2_1/n$
T (K)	120(2)	120(2)	120(2)	90(2)
a (Å)	15.6275(12)	8.9487(6)	35.482(4)	8.9942(5)
b (Å)	14.9143(11)	16.7979(11)	10.0503(11)	17.9689(11)
c (Å)	20.2340(15)	13.0420(8)	35.888(4)	12.8636(8)
β (deg)		97.5930(10)	108.3960(10)	99.8840(10)
V (Å^3)	4716.0(6)	1943.3(2)	12144(2)	2048.1(2)
Z	8	4	8	4
no. of reflections measured	25346	10876	33535	11513
no. of observations	5420	4410	13705	4614
no. of parameters refined	293	266	779	272
$R1^{a}$	0.0353	0.0423	0.1217	0.0304
$R_W{}^{b}$	0.0941 ($I > 2.0\sigma(I)$)^{c}	0.1119 ($I > 2.0\sigma(I)$)^{d}	0.3335 ($I > 2.0\sigma(I)$)^{e}	0.0753 ($I > 2.0\sigma(I)$)^{f}
GOF	1.030	1.061	1.069	1.050
CCDC no.	898242	898243	898245	898244

^{a} $R1 = \Sigma \, ||Fo| - |Fc|| \, / \, \Sigma \, |Fo|$. ^{b} $Rw = [\, \Sigma \, (w \, (F_0^2 - F_c^2)^2) \, / \, \Sigma \, w(F_0^2)^2]^{1/2}$. ^{c} $w = 1 \, / \, [\sigma^2(F_0^2) + (0.0474P)^2 + 3.9739P]$, where $P = (\mathrm{Max}(F_0^2, 0) + 2F_c^2) \, / \, 3$, ^{d} $w = 1 \, / \, [\sigma^2(F_0^2) + (0.0535P)^2 + 1.2778P]$, where $P = (\mathrm{Max}(F_0^2, 0) + 2F_c^2) \, / \, 3$, ^{e} $w = 1 \, / \, [\sigma^2(F_0^2) + (0.1754P)^2 + 43.3385P]$, where $P = (\mathrm{Max}(F_0^2, 0) + 2F_c^2) \, / \, 3$, ^{f} $w = 1 \, / \, [\sigma^2(F_0^2) + (0.0348P)^2 + 1.1119P]$, where $P = (\mathrm{Max}(F_0^2, 0) + 2F_c^2) \, / \, 3$.

1.1.2. Discussion of G-quartet formation in organic solvents

Observations of the ^{i}PG-4 structure formation in organic solvents were carried out using ESI-MS, UV-vis and ^{1}H NMR measurements. Since ^{i}PG is capable of forming a variety of supramolecular structures by virtue of intermolecular hydrogen bonding, including a ribbon structure as shown in Figure 5. Thus, the regulation of the supramolecular structure should be carried out under strictly optimized conditions in organic solvents to form the G-4 structure selectively.

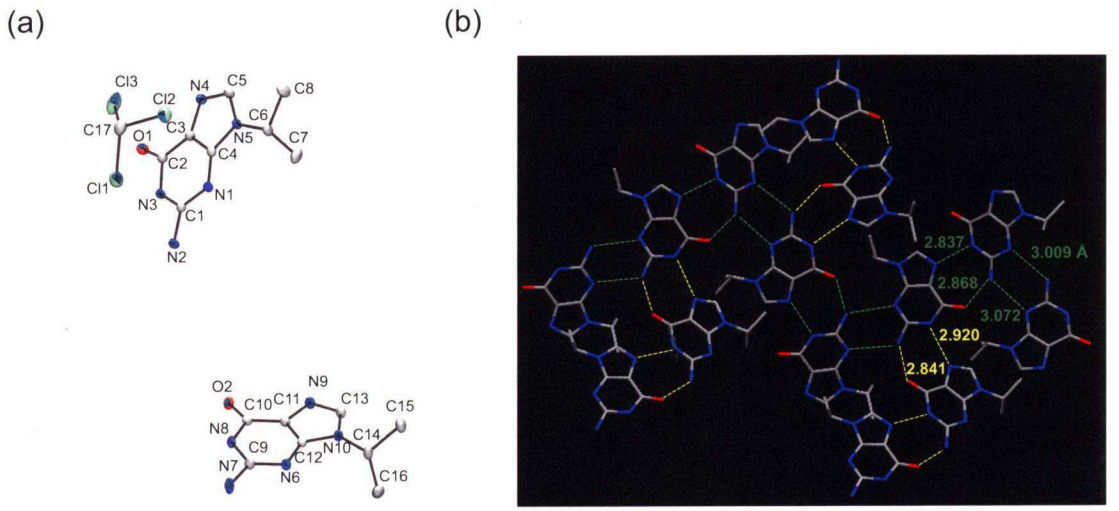

Figure 5. (a) Crystal structure of the asymmetric unit of ^{i}PG-ribbon. (b) A view of crystal packing to clarify the ribbon-type supramolecular structure. Interatomic distances (Å) representing intermolecular hydrogen bonding are given in the figure.

In general, following issues have been considered: (1) The proton of N1*H* fixed into a G-4 assembly by intermolecular hydrogen bonding does not undergo exchange with deuterium of solvents, and (2) noncovalent intermolecular interactions including hydrogen bonding and electrostatic interaction in G-4 become stronger at low temperature, and then the G-4 structure is stabilized by the decrease of enthalpy beyond the decrease of entropy.[42] In the presence of Na^{+}, the proton signal of N1*H* of ^{i}PG forming the ^{i}PG-4 assembly can be detected around 12 ppm in the mixed solvent of CH_3OH and $CDCl_3$. The signal became clearer as cooling down to 253 K (Figure 6(a)). On the other hand, in the absence of Na^{+}, the ^{i}PG-4 structure could not be formed even cooling down to 253 K. Instead, the chemical shift of the proton of N1*H* of ^{i}PG without forming the ^{i}PG-4 structure (δ = 10.5 ppm) could be observed clearly at low temperature. In addition, as cooling, the signal of N1*H* showed downfield shift due to

intermolecular hydrogen bonding probably between the guanine derivative and methanol (Figure 6(b)). This result indicates that, in the absence of electrostatic interaction with template cations, the solvation of the ^{i}PG molecule by methanol exerts stronger effect in the methanol solution of ^{i}PG rather than intermolecular hydrogen bonding to form the ^{i}PG-4 structure. This result suggests that the gain of the enthalpy by Na^{+}•••O interaction can compensate the instability caused by desolvation.

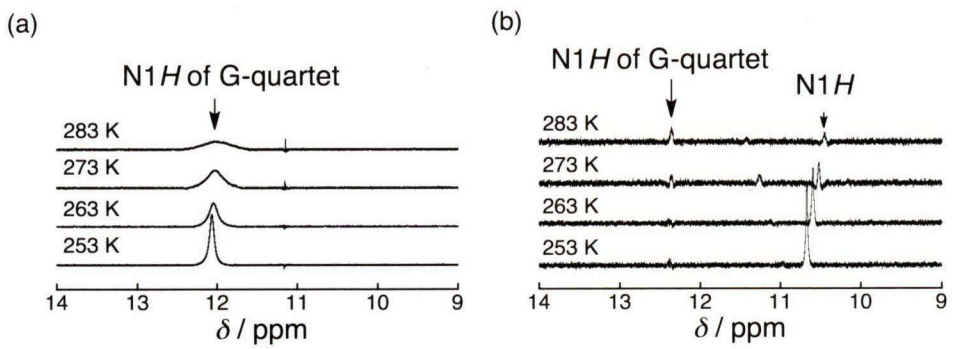

Figure 6. Temperature dependent ^{1}H NMR studies of ^{i}PG with $NaBPh_4$.; Conditions: (a) ^{i}PG (19 mM) and $NaBPh_4$ (5.4 mM) in $CDCl_3$ and CH_3OH (600 μl (30:1 v/v)); (b) ^{i}PG (3.6 mM) in $CDCl_3$ and CH_3OH (600 μl (5:1 v/v)).

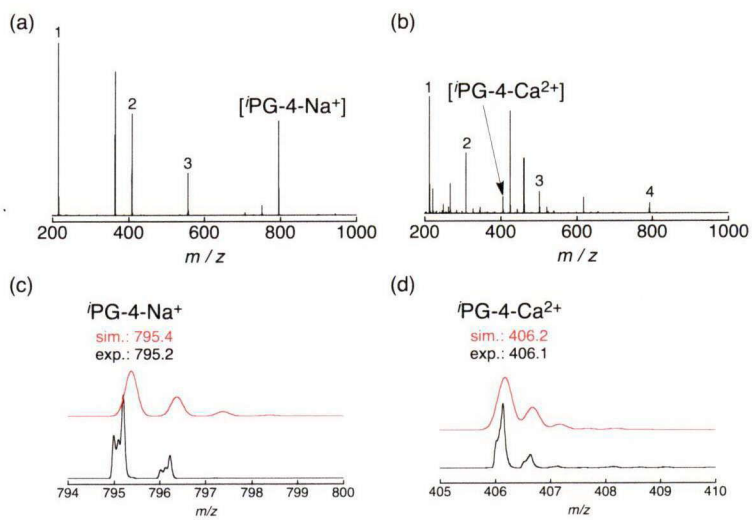

Figure 7. ESI-MS spectra of self-assembled species of ^{i}PG with (a) $NaBPh_4$ and (b) $CaCl_2$; in methanol at room temperature under N_2. Conditions: (a) ^{i}PG (15 mM), $NaBPh_4$ (6.8 mM); (b) ^{i}PG (18 mM), $CaCl_2$ (8.4 mM). Peaks: (a) 1: ^{i}PG-Na^{+} (m/z = 216.0). 2: ^{i}PG-2-Na^{+} (m/z = 409.1). 3: ^{i}PG-$NaBPh_4$-Na^{+} (m/z = 558.1). (b) 1: ^{i}PG-2-Ca^{2+} (m/z = 213.0). 2: ^{i}PG-3-Ca^{2+} (m/z = 309.6). 3: ^{i}PG-5-Ca^{2+} (m/z = 502.7). 4: ^{i}PG-8-Ca^{2+} (m/z = 792.3).

ESI-MS measurements of ^{i}PG in the presence of template cations allowed us to detect the formation of the ^{i}PG-4 structure clearly even in the methanol solution. Upon addition of $NaBPh_4$ to provide Na^+ as a template cation, a peak cluster was observed at m/z = 795.2 (calcd., 795.4), assignable to that derived from ^{i}PG-4-Na^+ (Figure 7(a) and (c)). In the presence of Ca^{2+}, a peak cluster assigned to [^{i}PG-4-Ca^{2+}]$^{2+}$ was observed at m/z = 406.1 (calcd., 406.2; see Figure 7(b) and (d)), also confirming its formation.

Further scrutiny was given to the formation of ^{i}PG-4 in the presence of the template cations in CH_3OH-$CHCl_3$ mixed solution by UV-vis absorption spectroscopy. The absorption spectra of ^{i}PG showed red shifts in the course of addition of $NaBPh_4$ or $CaCl_2$ (Figure 8(a) and Figure 9(a)). The shift was assigned to form G-4-cation complexes: A Job's plot for ^{i}PG and $NaBPh_4$ gave the maximum at 0.2 mole fraction, indicating the 4:1 complexation of ^{i}PG with sodium ion (Figure 8(c)). In the presence of excess amount of Na^+, however, the presence of a 1:1 complex of ^{i}PG with Na^+ was observed by ESI-MS spectrometry (Figure 10).

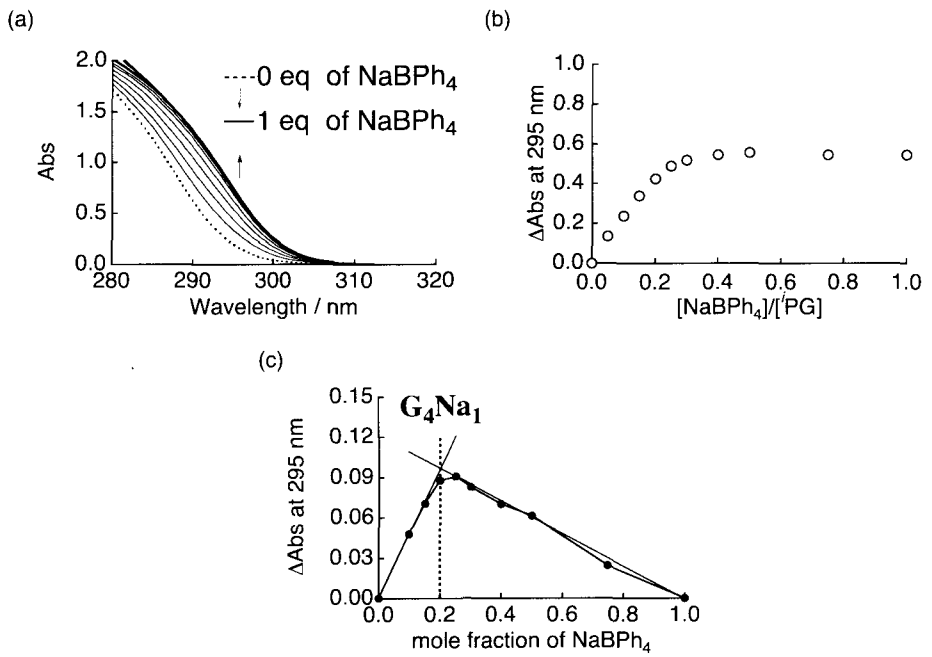

Figure 8. UV-vis spectral change by adding (a) $NaBPh_4$, (b) titration curve at 295 nm and (c) Job's plot of the ^{i}PG-Na^+ complex: Conditions: (a) ^{i}PG (207 μM) in CH_3OH and $CHCl_3$ (1:74 v/v), the additional $NaBPh_4$ (15.5 mM) in CH_3OH and $CHCl_3$ (1:9 v/v); (b) The total mole concentration was adjusted to 41.3 μM in CH_3OH and $CHCl_3$ (1:374 v/v), ^{i}PG (0.62 mM) in CH_3OH and $CHCl_3$ (1:24 v/v), $NaBPh_4$ (0.62 mM) in CH_3OH and $CHCl_3$ (1:24 v/v); All the measurements were carried out at room temperature.

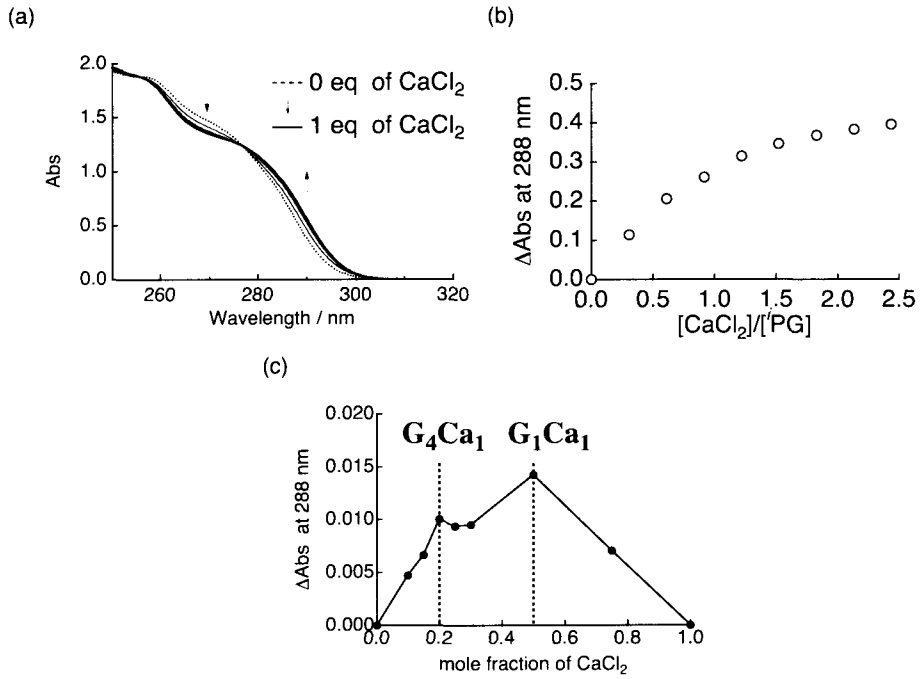

Figure 9. UV-vis spectral change by adding (a) $CaCl_2$ to ^{i}PG, (b) titration curve at 295 nm and (c) job's plot of the ^{i}PG-cation complexes: Conditions: (a)(b) ^{i}PG (146 μM) in CH_3OH and $CHCl_3$ (1:74 v/v), the additional $CaCl_2$ (66.9 mM) in CH_3OH and $CHCl_3$ (1:19 v/v); (c) The total mole concentration was adjusted to 32.9 μM in CH_3OH and $CHCl_3$ (1:374 v/v), ^{i}PG (0.49 mM) in CH_3OH and $CHCl_3$ (1:24 v/v), $CaCl_2$ (0.48 mM) in CH_3OH and $CHCl_3$ (1:24 v/v); All the measurements were carried out at RT.

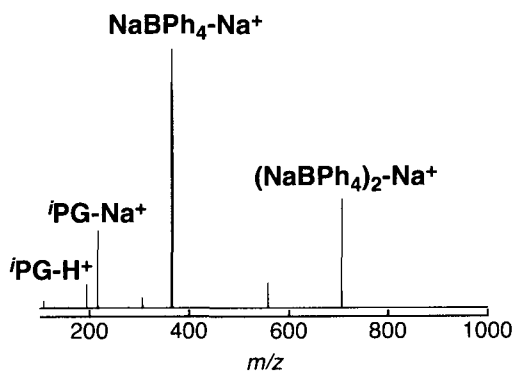

Figure 10. ESI-MS spectrum of ^{i}PG in the presence of excess amounts of $NaBPh_4$ in methanol.

In contrast, the Job's plot for ^{i}PG and $CaCl_2$ afforded two maximums at 0.2 and 0.5, indicating that ^{i}PG-4-Ca^{2+} is formed at lower concentration of Ca^{2+}, however, a 1:1

complex (^{i}PG-Ca^{2+}) became dominant at higher concentrations of Ca^{2+} (Figure 9(c)). It should be noted that the Ca^{2+} ion binds to guanine more tightly than the Na^{+} ion due to the higher cationic charge, even though the Cl^{-} anion may interact with the Ca^{2+} ion in solution to reduce the Lewis acidity.

In the range under 0.5 mole fraction in the Job's plots, allosteric effects could not be observed clearly on the sequential process relating to the formation of ^{i}PG-4-cation complexes in both cases of Na^{+} and Ca^{2+} (Figure 8(b) and inset of Figure 9(b)). This indicates that the intermolecular hydrogen bonding to form the G-4 structure is much weaker than the electrostatic interaction between the 6-O oxygen of guanine and the template cation. Therefore, in the presence of a template cation, the main driving force of the G-4 formation is the interaction of the guanine 6-O oxygen with the template cation.

1.1.3. Thermodynamics of the formation of G-quartet analyzed by van't Hoff plots

As mentioned above, the electrostatic interaction among the template cation and the 6-O oxygen of guanine is much stronger than the intermolecular hydrogen bonding to form the G-4 structure. In addition, the contribution of equilibrium of G-4 formation by the metal-free guanine molecules should be negligible. Furthermore, as observed in variable-temperature NMR measurements (Figure 6), ^{i}PG molecules can form a ^{i}PG-4 structure in CH_3OH-$CDCl_3$ at temperatures above 253 K, however, below 253 K, the formation is negligible. Therefore, in order to simplify the equilibrium of G-4 formation in the presence of a template cation, spectroscopic titration to determine the equilibrium constants of the ^{i}PG-4 formation was conducted at temperatures below 253 K. Under such conditions, the equilibrium can be elucidated as shown in Scheme 1.

$$^{i}\mathrm{PG} \underset{-\mathrm{Na^+}}{\overset{K_1\ +\mathrm{Na^+}}{\rightleftharpoons}} {}^{i}\mathrm{PG\text{-}Na^+} \underset{-{}^{i}\mathrm{PG}}{\overset{K_2\ +{}^{i}\mathrm{PG}}{\rightleftharpoons}} {}^{i}\mathrm{PG_2\text{-}Na^+} \underset{-{}^{i}\mathrm{PG}}{\overset{K_3\ +{}^{i}\mathrm{PG}}{\rightleftharpoons}} {}^{i}\mathrm{PG_3\text{-}Na^+} \underset{-{}^{i}\mathrm{PG}}{\overset{K_4\ +{}^{i}\mathrm{PG}}{\rightleftharpoons}} {}^{i}\mathrm{PG_4\text{-}Na^+}$$

Scheme 1. The equilibrium of G-quartet formation with a template cation.

Spectroscopic titration to determine the equilibrium constant of the ^{i}PG-4-Na^{+} formation was carried out at 253 K or lower and under 0.5 of the equivalence of $NaBPh_4$ relative to ^{i}PG, i.e., under 0.333 of the mole fraction of $NaBPh_4$ for ^{i}PG. At temperatures below 253 K, the plot of UV-vis absorbance changes at 295 nm by adding $NaBPh_4$ exhibited no sigmoidal change, suggesting the absence of the allosteric effect (Figure 8(b)). The analysis of the spectral change at each temperature was made to

determine an apparent equilibrium constant based on the following equation.

$$K = K_1K_2K_3K_4 = \frac{[^i\text{PG-4-Na}^+]}{[^i\text{PG}]^4[\text{Na}^+]} \qquad (1)$$

In the case of $CaCl_2$, the treatments were the same as described above for $NaBPh_4$, using $[Ca^{2+}]$ in eq. (1) in place of $[Na^+]$.

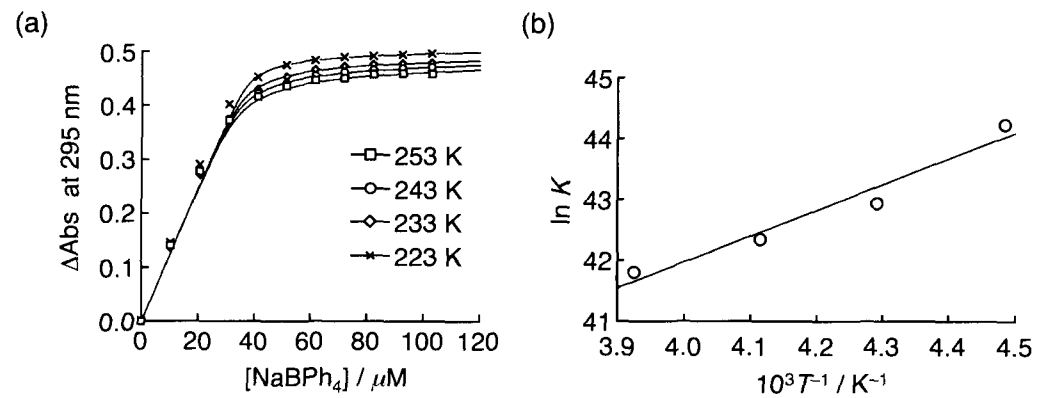

Figure 11. (a) Absorbance change of ^{i}PG at 295 nm upon addition of $NaBPh_4$ at various temperatures in the course of the formation of ^{i}PG-4-Na^+; (b) a van't Hoff plot for the equilibrium constants. Conditions: ^{i}PG (215 μM) in CH_3OH and $CHCl_3$ (1:74 v/v), the additional $NaBPh_4$ (15.5 mM) in CH_3OH and $CHCl_3$ (1:9 v/v).

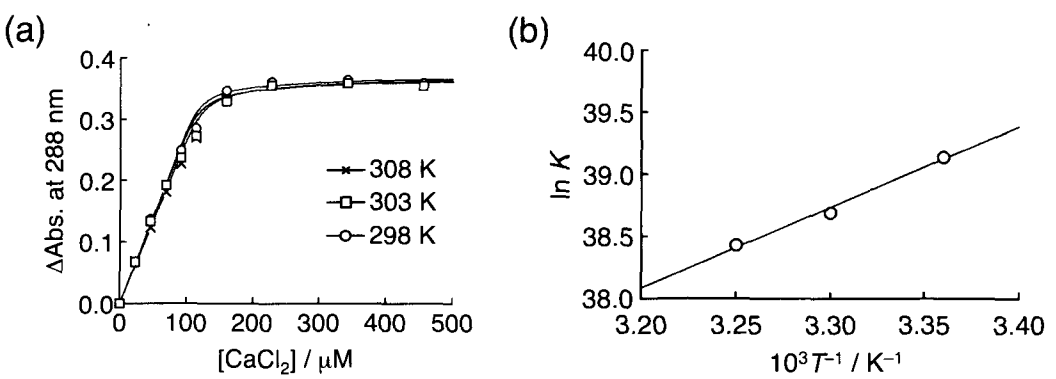

Figure 12. (a) Absorbance change of ^{i}PG at 288 nm upon addition of $CaCl_2$ at various temperature in the course of the formation of ^{i}PG-4-Ca^{2+}; (b) a van't Hoff plot for the equilibrium constants. Conditions: ^{i}PG (218 μM) in CH_3OH and $CHCl_3$ (1:74 v/v), the additional $CaCl_2$ (34.3 mM) in CH_3OH and $CHCl_3$ (1:9 v/v).

Equilibrium constants (K, M^{-4}) of the formation of ^{i}PG-4-Na^{+} and ^{i}PG-4-Ca^{2+} at various temperatures are summarized in Table 3. The enthalpy and entropy changes (ΔH and ΔS, respectively) in the formation of ^{i}PG-4-Na^{+} were determined to be –8.4 kcal mol^{-1} and +50 cal mol^{-1} K^{-1}, respectively, on the basis of a van't Hoff plot (ln K *vs.* $1/T$) as depicted in Figure 11(b). Similarly, the ΔH and ΔS values of the ^{i}PG-4-Ca^{2+} formation were also determined to be –12.9 kcal mol^{-1} and +34 cal mol^{-1} K^{-1}, respectively (Figure 12). The results indicate that the more positive Ca^{2+} ion binds more tightly to the ^{i}PG-4 assembly to stabilize the quartet structure than the Na^{+} ion does.

Table 3. Equilibrium constants at each temperature and the enthalpy and entropy of the formation of ^{i}PG-4-Na^{+} and ^{i}PG-4-Ca^{2+}.

^{i}PG-4-Na^{+}			
T (K)	K (M^{-4}) [a]	ΔH [b] (kcal mol^{-1})	ΔS [c] (cal mol^{-1} K^{-1})
253	1.4×10^{18}	-8.4	+50
243	2.5×10^{18}		
233	4.7×10^{18}		
223	1.6×10^{19}		
^{i}PG-4-Ca^{2+}			
T (K)	K (M^{-4}) [a]	ΔH [b] (kcal mol^{-1})	ΔS [c] (cal mol^{-1} K^{-1})
308	4.9×10^{16}	-12.9	+34
303	6.3×10^{16}		
298	1.0×10^{17}		

[a] Each equilibrium constant was obtained by temperature-dependent UV-vis measurements.[43] [b,c] Each value was estimated by the slope and the intercept of the van't Hoff plot; $\ln K = -\Delta H/RT + \Delta S/R$.

The enthalpy change can be elucidated as the summation of the stabilization by the coulombic interaction between ^{i}PG and sodium ion, intermolecular hydrogen bonding between each ^{i}PG and the desolvation of methanol from ^{i}PG. As noted at the end of the former section, since the intermolecular hydrogen bonding cannot become the main driving force to form ^{i}PG-4, the enthalpy change should be derived from the attractive electrostatic interaction between ^{i}PG and the template-cation. In addition, although the formation of ^{i}PG-4-Na^{+} and ^{i}PG-4-Ca^{2+} should be unfavorable in terms of entropy changes, the entropy loss can be compensated by the desolvation of methanol from ^{i}PG as well as Na^{+}. The degree of contributions to the entropy change from the desolvation of ^{i}PG and the template cations, however, remains unclear due to the lack of the

thermodynamic parameters for the ^{i}PG-4 formation in the absence of a template cation.

1.2. Temperature-dependent formation behavior of supramolecular assemblies between a G-quartet and a Ni(II)-porphyrin complex

1.2.1. Detection of interactions between porphyrins and a G-quartet

The UV-Vis measurements in $CH_3OH/CHCl_3$ (1:40 v/v) were examined to observe intermolecular interactions between the G-quartet and the porphyrin molecules. The ^{i}PG-4-Na^+ solution, prepared with ^{i}PG and $NaBPh_4$ (4:1 mol/mol), was added to the solution containing H_2OEP or NiOEP. The absorption spectra were recorded after stirring for 20 min at 293 K at every addition of a portion of the ^{i}PG-4-Na^+ solution.

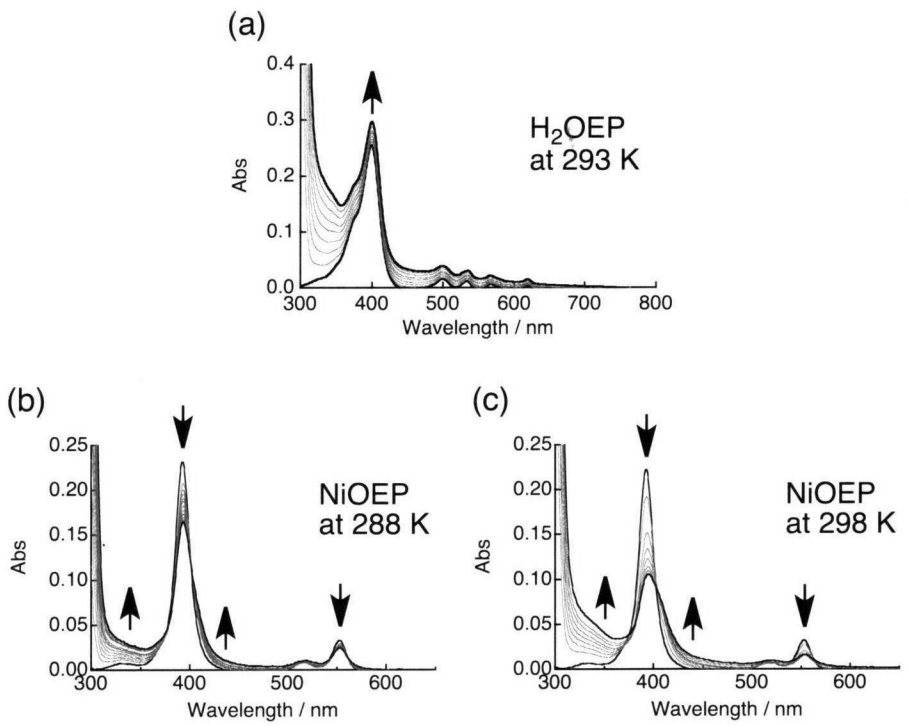

Figure 13. UV-Vis spectral changes of (a) H_2OEP (1.6 μM) by adding ^{i}PG-4-Na^+ (0 to 1.6 mM) at 293 K in $CHCl_3/CH_3OH$, (b) NiOEP (1.4 μM) by adding ^{i}PG-4-Na^+ (0 to 0.26 mM) at 288 K in $CHCl_3/CH_3OH$ and (c) NiOEP (1.4 μM) by adding ^{i}PG-4-Na^+ (0 to 0.46 mM) at 298 K in $CHCl_3/CH_3OH$: ^{i}PG-4-Na^+ solutions were made from ^{i}PG and $NaBPh_4$ (4:1 mol/mol) in $CH_3OH/CHCl_3$ (1:40 v/v).

When H_2OEP was employed as an external molecule, the author could observe spectral change as shown in Figure 13(a). Although continuous spectral change was

observed during the addition of ^{i}PG-4-Na^{+} (~1000 eq) to the H_2OEP solution, the change showed neither isosbestic points nor the saturation behavior. This spectral change was merely caused by the raise of the baseline due to the significant amount of ^{i}PG-4-Na^{+} (Figure 14(a) and (b)). Thus, the interaction of H_2OEP with the quartet should be negligible under the experimental conditions.

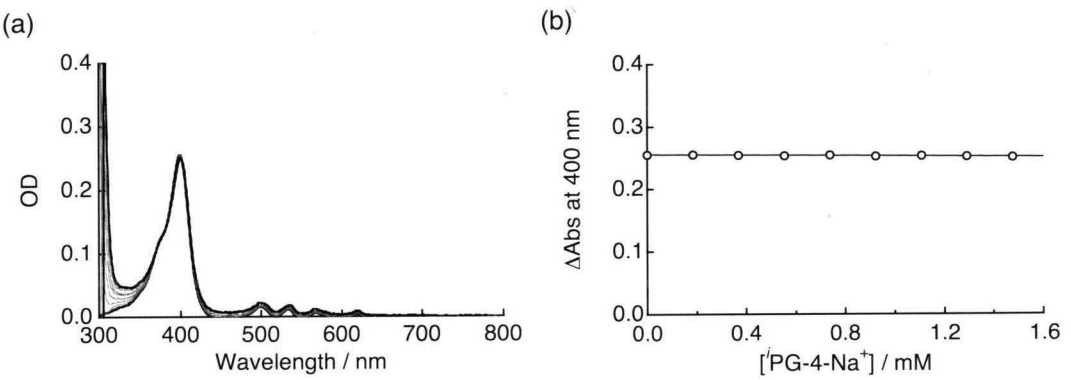

Figure 14. (a) Spectral change in the course of the addition of ^{i}PG-4-Na^{+} to the solution of H_2OEP (1.6 μM). The baseline was adjusted by subtracting the absorbance of ^{i}PG-4-Na^{+} at each concentration. (b) A plot of absorbance at 400 nm relative to [^{i}PG-4-Na^{+}] in the corrected absorption spectra depicted in (a).

In sharp contrast to the case of H_2OEP, UV-Vis spectral changes with several isosbestic points were observed by adding the ^{i}PG-4-Na^{+} solution to that containing NiOEP at each temperature (283 K to 298 K), as shown in Figure 13(b) and (c). The absorption of NiOEP showed the decrease of the Soret (393 nm) and Q (519, 553 nm) bands with slight red shifts (~2 nm).[44] The decrease of the Soret band of porphyrin has been observed for a porphyrin forming an adduct by intermolecular interactions and the red shift can be attributed to the formation of a J-type π-π stacking assembly between ^{i}PG-4-Na^{+} and NiOEP.[45] The difference from H_2OEP may stem from the stronger π-π interaction due to the more rigid planar structure of NiOEP.[46] Additionally, there should be an electrostatic interaction between the positively charged ^{i}PG-4-Na^{+} complex and NiOEP bearing -2 charges on the porphyrin ligand, whereas H_2OEP is a neutral compound. As the consequence, the J-type π-π stacked assembly between ^{i}PG-4-Na^{+} and NiOEP is more stabilized than that of H_2OEP.

To confirm that the UV-Vis spectral change was derived from the intermolecular interaction between ^{i}PG-4-Na^{+} and NiOEP, following experiments were carried out. When the solution of NiOEP was added to the ^{i}PG solution (0.21 mM) without $NaBPh_4$,

no change was observed the absorption of NiOEP (Figure 15(a)). This result indicates that NiOEP does not interact apparently with ^{i}PG molecules in the absence of Na^{+} as a template of the quartet structure.[47] In addition, the absorption spectrum of NiOEP did not change by the addition of only $NaBPh_4$ (Figure 15(b)). These results indicate that NiOEP interacts only with ^{i}PG-4-Na^{+} formed in the presence of Na^{+}.

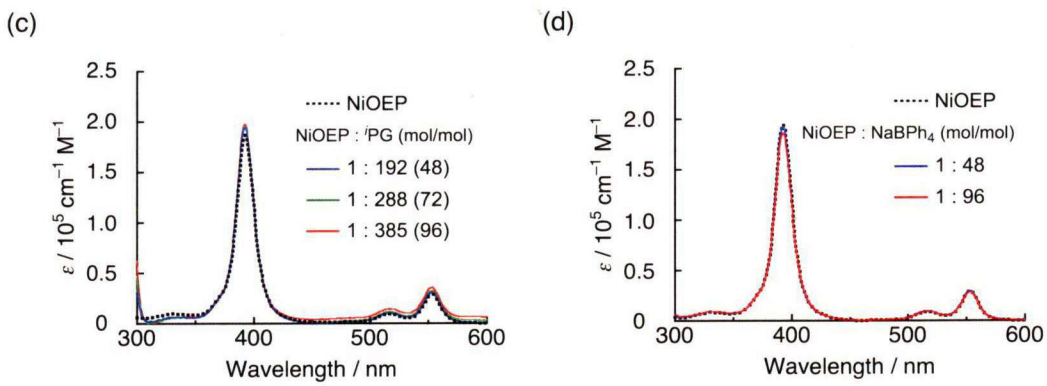

Figure 15. (a) Absorption spectral change of NiOEP in the presence of ^{i}PG (0.21 mM) at room temperature in $CH_3OH/CHCl_3$. (b) Absorption spectra of NiOEP upon addition of $NaBPh_4$ (0–106 μM) to NiOEP solution (1.1 μM) at room temperature in $CH_3OH/CHCl_3$. In (b), the number in parentheses shows the mole ratio as ^{i}PG-4-Na^{+} ([^{i}PG]/(4[NiOEP]))

ESI-MS measurements were made for the ^{i}PG-4-Na^{+} solution containing ^{i}PG and $NaBPh_4$ (4:1 mol/mol), to which excess amount of NiOEP was added. A peak cluster was detected at 1385.7, as shown in Figure 16, corresponding to the calculated *m/z* value of the 1:1 complex of ^{i}PG-4-Na^{+} with NiOEP, [^{i}PG-4-Na^{+}•••NiOEP]. This result

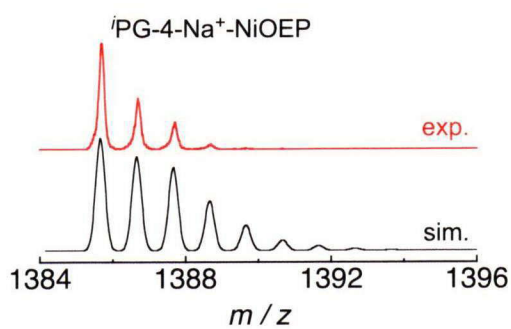

Figure 16. A peak cluster observed in the ESI-MS spectrum of ^{i}PG-4-Na^{+} and NiOEP solution in the mixed solvent of $CH_3OH/CHCl_3$ (red line) and a simulation spectrum for the 1:1 complex, [^{i}PG-4-Na^{+}•••NiOEP] (black line).

provides a direct evidence to support the complexation between ^{i}PG-4-Na^{+} and NiOEP in solution.

The intermolecular interaction between the G-quartet and NiOEP can be also observed directly by ^{1}H NMR measurements in the mixed solvent of $CH_3OH/CDCl_3$ (1:60 v/v) (Figure 17). In the absence of ^{i}PG-4-Na^{+}, the chemical shift of the signal due to the proton at the *meso*-position of NiOEP was observed at 9.77 ppm at 283 K. On the other hand, in the presence of ^{i}PG-4-Na^{+}, the *meso*-proton signal showed a slight upfield shift (9.76 ppm) compared to that of NiOEP at 283 K (Figure 17(a)). Together with the results of the UV-Vis and ESI-MS measurements mentioned above, the upfield shift indicates the shielding of the *meso*-proton of NiOEP over aromatic rings of ^{i}PG due to the π-π interaction between the G-quartet plane and NiOEP. Similarly, the methylene proton signal of NiOEP (q: δ = 3.93 ppm, J = 7.6 Hz, without ^{i}PG-4-Na^{+}) exhibited upfield shifts (q: δ = 3.91 ppm, J = 7.6 Hz) in the presence of ^{i}PG-4-Na^{+} (Figure 17(b)).

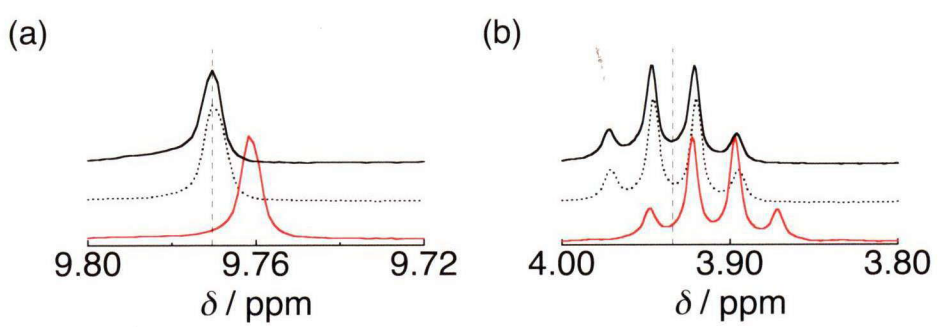

Figure 17. ^{1}H NMR signal due to (a) the *meso*-proton of NiOEP and (b) the ethyl-proton of NiOEP with ^{i}PG-4-Na^{+} (red line), with only $NaBPh_4$ (dotted line) and without additive(black line). Conditions: ^{i}PG (9.9 mM), $NaBPh_4$ (2.5 mM) and NiOEP (1.3 mM) at 283 K in $CH_3OH/CDCl_3$ (1:60 v/v). ^{i}PG-4-Na^{+} means the mixture of ^{i}PG (9.9 mM) and $NaBPh_4$ (2.5 mM).

1.2.2. Temperature-dependent structures of assemblies of ^{i}PG-4-Na^{+} with NiOEP

Scrutiny was given to the thermodynamics of the complex formation between ^{i}PG-4-Na^{+} and NiOEP by variable-temperature UV-Vis titration. At 288 K, the titration curves for the absorbance changes at 393 nm are shown in Figure 18(a). A plot of inverse of the absorbance of NiOEP at 393 nm relative to 1/[^{i}PG-4-Na^{+}] is depicted in Figure 18(b) (the titration curve at 283 K are shown in Figure 20). The plot suggests that the adduct is a 1:1 complex of the G-quartet and NiOEP (see eq (3) in experimental section).[48] When the adduct is assumed as a 1:1 complex, the formation constant is estimated to be 1.4×10^{4} M^{-1} by the fitting curve (see eq (2) in experimental section).[48]

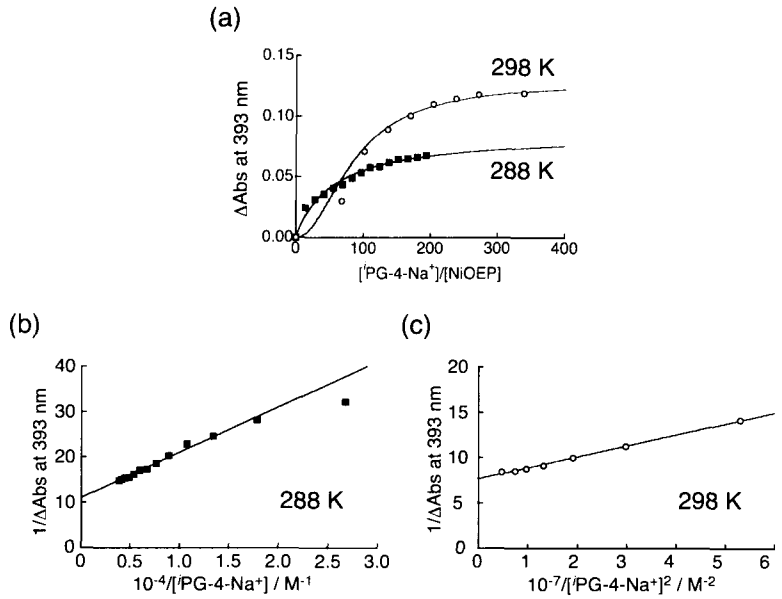

Figure 18. Analysis of the UV-Vis spectral change due to the adduct formation in $CHCl_3/CH_3OH$: Fitting curves of the absorbance change during the addition of ^{i}PG-4-Na^+ to NiOEP (a) at 393 nm and (b) a plot of 1/ΔAbs at 393 nm against $1/[^{i}\text{PG-4-Na}^+]$ at 288 K and (c) a plot of 1/ΔAbs at 393 nm against $1/[^{i}\text{PG-4-Na}^+]^2$ at 298 K.

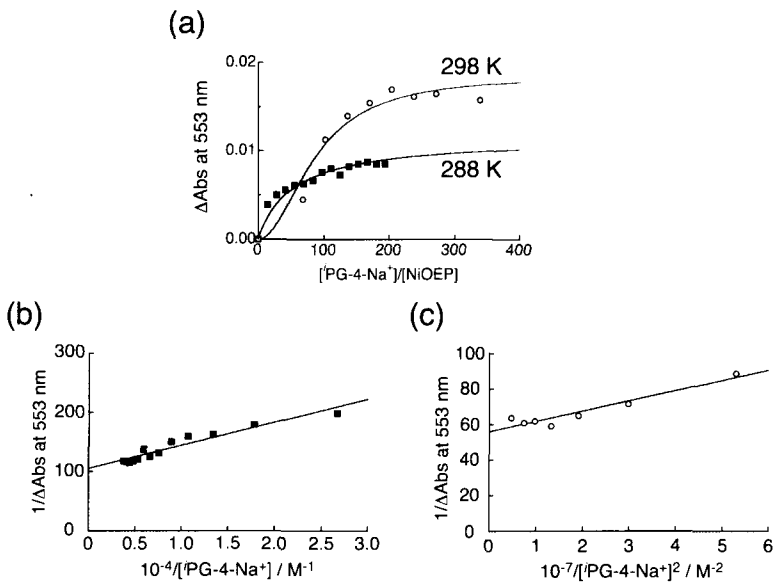

Figure 19. Analysis of the UV-Vis spectral change at 553 nm for the adduct formation: Fitting curves of the absorption change of the adduct of ^{i}PG-4-Na^+ with NiOEP (a) at 288 K (■) and at 298 K (○), (b) Plot of $1/(A_0\text{-}A)$ *vs.* $[^{i}\text{PG-4-Na}^+]^{-1}$ at 288 K, and (c) Plot of $1/(A_0\text{-}A)$ *vs.* $[^{i}\text{PG-4-Na}^+]^{-2}$ at 298 K in $CHCl_3/CH_3OH$.

The titration curve based on the absorbance at 553 nm afforded the same formation constant at 288 and 298 K (Figure 19).

In contrast to the results at 288K, the titration curves showed sigmoidal shapes at 298 K as shown in Figure 18(a) for 393 nm and Figure 19(a) for 553 nm, respectively. In addition, the linear plot of the inverse of the absorption of NiOEP relative to $1/[^{i}PG\text{-}4\text{-}Na^{+}]^{2}$ suggests the formation of a 2:1 complex of $^{i}PG\text{-}4\text{-}Na^{+}$ and NiOEP (see eq (5) in experimental section). These sigmoidal behavior and 2:1 complexation were also observed at 293 K (Figure 20). The formation constant of the 2:1 complex was estimated to be 7.6×10^{7} M^{-2} by the fitting curve (see eq (4) in experimental section). In this case, NiOEP is assumed to be sandwiched between two $^{i}PG\text{-}4\text{-}Na^{+}$ planes as described in Scheme 2. The proposed structure of the 2:1 complex is supported by (1) the observation of the peak cluster assignable to the 1:1 complex, [$^{i}PG\text{-}4\text{-}Na^{+}$•••NiOEP], as a fragment in the ESI-MS spectrum (Figure 16), (2) no peak cluster assignable to a doubled G-quartet ($[^{i}PG\text{-}4\text{-}Na^{+}]_{2}^{2+}$), and (3) the observation of the upfield shift of the *meso*-proton signal in the ^{1}H NMR spectrum (Figure 17).

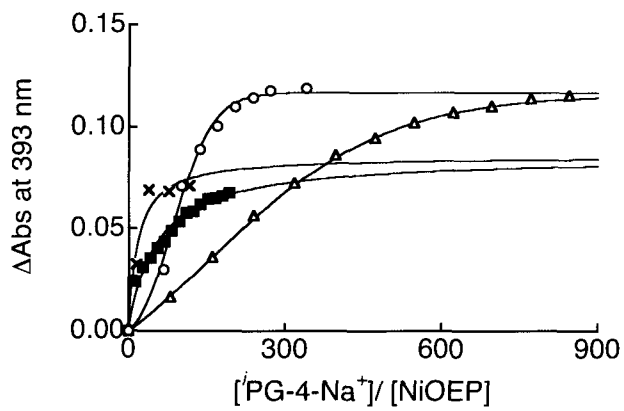

Figure 20. Titration curves for temperature-dependent UV-Vis measurements on the adduct formation of $^{i}PG\text{-}4\text{-}Na^{+}$ and NiOEP. Conditions: $^{i}PG\text{-}4\text{-}Na^{+}$ prepared by ^{i}PG and $NaBPh_4$ (4:1 mol/mol) was added to the NiOEP (1.4 μM) at 283 K (–×–), 288K (–■–) and 298 K (–○–) in the mixed solvent of CH3OH/CHCl3. At 293 K (–△–), NiOEP (1.6 μM) solution was prepared and then the absorbance at 393 nm of NiOEP was normalized by the ratio of the concentration of NiOEP (Abs. (393 nm) × 1.4/1.6).

Since the adduct exhibits the 2:1 structure at higher temperature, the formation of the supramolecular assemblies depending on temperature should be an entropy-controlled process, which is enhanced at higher temperatures probably due to the desolvation. Actually, the formation constant of the 1:1 complex decreases with

raising temperature. At some temperature in the range from 288 K to 293 K, the adduct formation is switched from the 1:1 complex to the 2:1 complex, and then the formation constant becomes larger (4.6×10^{6} M^{-2} (293 K) to 7.6×10^{7} M^{-2} (298 K)) as temperature is raised (Figure 20).

Summary

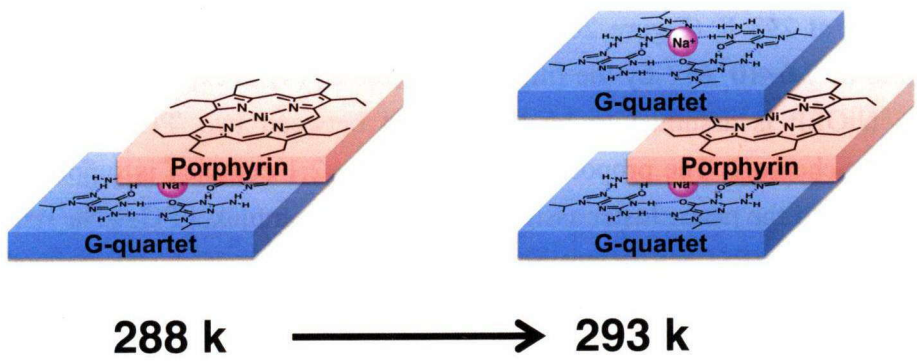

Scheme 2. The schematic description of the adducts.

In this study, the author determined crystal structures of "naked" G-4 assemblies without bulky substituents using ^{i}PG as a building block. In the crystal structure of ^{i}PG-4-H_2O, the quartet structure is stabilized by intermolecular hydrogen bonding among the 6-O oxygen of ^{i}PG in the quartet and the water molecules of crystallization. In the structures of ^{i}PG-4-Na^{+} and ^{i}PG-4-Ca^{2+}, the template cations such as Na^{+} and Ca^{2+} reside at the centre of the quartets. It should be noted that the ^{i}PG-4 structure can be obtained without the presence of the template cations and bulky peripheral substituents to protect the hydrogen-bonded supramolecular G-tetramer.

The author also discussed the thermodynamics of the ^{i}PG-4 formation in CH_3OH and CH_3OH-$CH(D)Cl_3$ solutions on the basis of spectroscopic measurements. Concerning the ^{i}PG-4 formation, it is clarified that the electrostatic interactions between the template cations and the 6-O oxygen of ^{i}PG contribute more dominantly to the stabilization than the multiple intermolecular hydrogen bonding among the guanine molecules in the ^{i}PG-4 structure. In the absence of the template cations, the ^{i}PG-4 formation is governed by entropy change due to the desolvation of methanol from ^{i}PG. In sharp contrast, in the presence of template cations, the charge of the cations, i.e., the Lewis acidity of the cations, is important to stabilize the ^{i}PG-4 assemblies by virtue of the electrostatic attractive interaction between the template cations and the electrostatically negative 6-O oxygen of ^{i}PG. This is clearly reflected on the more

negative ΔH values of the ^{i}PG-4-Ca^{2+} formation than that of the ^{i}PG-4-Na^{+} formation. Thus, the dicationic Ca^{2+} ion is more favorable to stabilize the ^{i}PG-4 structure thermodynamically than the monocationic Na^{+} ion.

In addition, the author has described the direct interaction between the less sterically-hindered G-quartet and the porphyrin complex observed by UV-Vis, ^{1}H NMR, and ESI-MS measurements. The structure of supramolecular assembly depends on the temperature: The 1:1 complex of the G-quartet and the porphyrin is formed at 288 K or lower, whereas the 2:1 complex at 293 K or upper (*note*; the G-quartet structure is unstable over 313 K).

The results obtained in this work provide solid thermodynamic basis of the driving force of the G-quartet formation without any bulky substituents on the guanine scaffold. This work will also contribute to the manipulation of G-quartet structures toward their further application to construction of supramolecular materials.

Experimental section

Materials and methods. $CHCl_3$, (Wako Pure Chemical Industries) were purified by distilled with CaH_2. CH_3OH (Wako Pure Chemical Industries) were dried using Mg and I_2. $CDCl_3$ was purchased from Cambridge Isotope Laboratories, Inc.. Other chemicals and solvents were purchased from Wako Pure Chemical Industries and Tokyo Chemical Industries. These reagents were used as received. 9-isopropylguanine was synthesized according to the literature method (see the reference, 36, in the text). Octaethylporphinatonickel(II) (NiOEP) was also synthesized by a literature method (see the references 44 and 46).

Apparatus. ^{1}H NMR spectra were measured on a JNM-EX270 spectrometer (JEOL). UV–vis absorption spectra were recorded on a SHIMAZU UV2450. ESI-MS measurements were recorded on an Applied Biosystems QStar Pulsar i (ESI-TOF; positive mode) spectrometer.

^{1}H NMR measurements. A mixed solvent of $CDCl_3/CH_3OH$ was used for measurements and chemical shifts were determined relative to an internal standard (TMS). Variable-temperature NMR measurements were made on a sample containing 9-isopropylguanine and each template cation after incubating for over 3 minutes at certain temperature.

UV-vis titration to determine thermodynamic parameters. UV-vis spectroscopic titrations of ^{i}PG upon addition of template cations were conducted in mixed solvents of $CHCl_3/CH_3OH$. Sodium tetraphenylborate and calcium dichloride were used as the sources of the template cations. In order to determine K value (expressed by eq (1) in

the text), absorbance at an appropriate wavelength (295 nm for ^{i}PG–4–Na^{+} and 288 nm for ^{i}PG–4–Ca^{2+}) was monitored. Thermodynamic parameters were determined using van't Hoff plot (Table 3).

UV-Vis titration to determine the equilibrium constant. UV-Vis spectroscopic titrations of H_2OEP and NiOEP upon addition of ^{i}PG-4-Na^{+} were conducted in mixed solvents of $CHCl_3/CH_3OH$ after stirring for 20 min at every addition of ^{i}PG-4-Na^{+} at each temperature. Sodium tetraphenylborate was used as the sources of the template cation and the ^{i}PG-4-Na^{+} solution was prepared from the mixture of ^{i}PG/$NaBPh_4$ (4:1 mol/mol) in $CH_3OH/CHCl_3$ (1:40 v/v). H_2OEP and NiOEP solutions were prepared in $CHCl_3$ for every measurement. In order to determine K values (see below), absorbance at 393 nm due to the Soret band of NiOEP was monitored. The UV-Vis spectra of ^{i}PG (0.21 mM) in $CH_3OH/CHCl_3$ were monitored with addition of NiOEP solution in $CHCl_3$ due to the low solubility of ^{i}PG in $CHCl_3$. The UV-Vis spectrum of NiOEP upon addition of $NaBPh_4$ was monitored by adding $NaBPh_4$ solution (0–106 μM) in $CH_3OH/CHCl_3$ to the solution of NiOEP (1.1 μM) in $CHCl_3$. Their absorption coefficients were used for the comparison (Figure 14).

Analysis of titration curves of the adduct formation. Data obtained from temperature-dependent UV-Vis measurements were analyzed by curve fitting for plots of $[^{i}\text{PG-4-Na}^{+}]^{-n}$ *vs.* $1/(A_0\text{-}A)$ (n=1 or 2) to determine formation constants of complexes between ^{i}PG-4-Na^{+} and NiOEP. Concerning the formation of the 1:1 complex, the author assumed the following equilibrium:

$$^{i}\text{PG-4-Na}^{+} + \text{NiOEP} \overset{K}{\rightleftharpoons} {}^{i}\text{PG-4-Na}^{+}\text{-NiOEP}$$

Curve-fitting was made to estimate the formation constants of the 1:1 complex on the basis of following equation (2) for the plots in Figure 18(a) and Figure 19(a) at 288 K and equation (3) for the plots in Figure 18(b) and Figure 19(b):

$$\Delta A = \Delta\varepsilon \frac{[\text{G4}]_{\text{add}} + [\text{Por}]_0 + 1/K - \sqrt{([\text{G4}]_{\text{add}} + [\text{Por}]_0 + 1/K)^2 - 4[\text{G4}]_{\text{add}}[\text{Por}]_0}}{2} \qquad (2)$$

$$\frac{1}{\Delta A} = \left(\frac{1}{\Delta\varepsilon K[\text{G4}]_{\text{add}}} + \frac{1}{\Delta\varepsilon}\right)\left(\frac{1}{[\text{Por}]_0}\right) \qquad (3)$$

As for the formation constant of the 2:1 complex between ^{i}PG-4-Na^{+} and NiOEP, the author assumed the following equilibrium:

$$^{i}\text{PG-4-Na}^{+} + \text{NiOEP} \overset{K_1}{\rightleftharpoons} {}^{i}\text{PG-4-Na}^{+}\text{-NiOEP} \overset{K_2\ {}^{i}\text{PG-4-Na}^{+}}{\rightleftharpoons} ({}^{i}\text{PG-4-Na}^{+})_2\text{-NiOEP}$$

The calculation of the formation constant for the 2:1 complex was made on the basis of following equation (4) for the plots in Figure 18(a) and Figure 19(a) at 298 K and equation (5) for the plots in Figure 18(c) and Figure 19(c):

$$[\text{G4}]_{\text{add}} = 2(\Delta A/\Delta\varepsilon) + \sqrt{\frac{(\Delta A/\Delta\varepsilon)}{K([\text{Por}]_0 - (\Delta A/\Delta\varepsilon))}} \qquad (4)$$

$$(K = K_1K_2)$$

$$\frac{1}{\Delta A} = \left(\frac{1}{\Delta\varepsilon K[\text{G4}]_{\text{add}}^2} + \frac{1}{\Delta\varepsilon}\right)\left(\frac{1}{[\text{Por}]_0}\right) \qquad (5)$$

X-ray crystallography. Single crystals of ^{i}PG-4 assemblies made of ^{i}PG with water molecules of crystallization and template cations were attained by recrystallization from methanol with vapor diffusion of diethyl ether. The crystallization of the G-ribbon type was carried out in the mixed solvent of methanol and chloroform with vapor diffusion of diethyl ether. All measurements were performed on a Bruker SMART APEX II ULTRA CCD diffractometer at 120 K or 90 K with graphite-monochromated Mo Kα radiation (λ = 0.71073 Å). The structures were solved by direct methods and expanded using Fourier techniques. Non-hydrogen atoms were refined anisotropically including solvents except disordered molecules (ether in the crystal structure of the G-4 with sodium tetraphenylborate). Refinements were carried out by full-matrix least squares techniques on F^2 with scattering factors[49] and including anomalous dispersion effects.[50] All calculations were performed using the Yadokari-XG crystallographic software package,[51] and structure refinements were made by using *SHELXL 97*.[52]

References

1 M. Gellert, M. N. Lipsett and D. R. Davies, *Proc. Natl. Acad. Sci., U.S.A.*, 1962, **48**, 2013.

2 J. T. Davis, *Angew. Chem., Int. Ed.*, 2004, **43**, 668.

3 J. R. Williamson, *Curr. Opin. Struct. Biol.*, 1993, **3**, 357.

4 D. E. Gilbert and J. Feigon, *Curr. Opin. Struct. Biol.*, 1999, **9**, 305.

5 M. A. Keniry, *Biopolymers*, 2001, **56**, 123.

6 R. H. Shafer and I. Smirnov, *Biopolymers*, 2001, **56**, 209.

7 G. Fang and T. R. Cech, *Biochemistry*, 1993, **32**, 11646.

8 H. Arthanari and P. H. Bolton, *Chem. Biol.*, 2001, **8**, 221.

9 J. McCallum, S. Amare and R. Nolan, *Nucleosides, Nucleotides and Nucleo Acids*, 2010, **29**, 801.

10 D. J. E. Yue, K. W. Lim and A. T. Phan, *J. Am. Chem. Soc.*, 2011, **133**, 11462.

11 G. N. Parkinson, M. P. H. Lee and S. Neidle, *Nature*, 2002, **417**, 876.

12 S. Haider, G. N. Perkinson and S. Neidle, *J. Mol. Biol.*, 2002, **320**, 189.

13 Y. Xu, Y. Suzuki, T. Lönnberg and M. Komiyama, *J. Am. Chem. Soc.*, 2009, **131**, 2871.

14 Y. Wang and D. J. Patel, *Biochemistry*, 1992, **31**, 8112.

15 K. Y. Wang, S. Swaminathan and P. H. Bolton, *Biochemistry*, 1994, **33**, 7517.

16 S. L. Forman, J. C. Fettinger, S. Pieraccini, G. Gottarelli and J. T. Davis, *J. Am. Chem. Soc.*, 2000, **122**, 4060.

17 T. J. Pinnavaia, C. L. Marshall, C. M. Mettler, C. L. Fisk, H. T. Miles and E. D. Becker, *J. Am. Chem. Soc.*, 1978, **100**, 3625.

18 K. Saito, H. Tai, H. Hemmi, N. Kobayashi and Y. Yamamoto, *Inorg. Chem.*, 2012, **51**, 8168.

19 H. Yaku, T. Fujimoto, T. Murashima, D. Miyoshi and N. Sugimoto, *Chem. Commun.*, 2012, **48**, 6203.

20 G. W. Collie, R. Promontorio, S. M. Hampel, M. Micco, S. Neidle and G. N. Parkinson, *J. Am. Chem. Soc.*, 2012, **134**, 2723.

21 J. E. Reed, A. A. Arnal, S. Neidle and R. Vilar, *J. Am. Chem. Soc.*, 2006, **128**, 5992.

22 I. Haq, J. O. Trent, B. Z. Chowdhry and T. C. Jenkins, *J. Am. Chem. Soc.*, 1999, **121**, 1768.

23 J. Dai, M. Carver, L. H. Hurley and D. Yang, *J. Am. Chem. Soc.*, 2011, **133**, 17673.

24 C. L. Grand, H. Han, R. M, Muñoz, S. Weitman, D. D. V. Hoff, L. H. Hurley and D. J. Bearss, *Mol. Cancer Ther.*, 2002, **1**, 565.

25 D. F. Shi, R. T. Wheelhouse, D. Sun and L. H. Hurley, *J. Med. Chem.*, 2001, **44**, 4509.

26 E. Izbicka, R. T. Wheelhouse, E. Raymond, K. K. Davidson, R. A. Lawrence, D. Sun, B. E. Windle, L. H. Hurley and D. D. V. Hoff, *Cancer Res.*, 1999, **59**, 639.

27 S. E. Evans, M. A. Mendez, K. B. Turner, L. R. Keating, R. T. Grimes, S. Melchoir and V. A. Szalai, *J. Biol. Inorg. Chem.*, 2007, **12**, 1235.

28 V. A. Szalai and H. H. Thorp, *J. Am. Chem. Soc.*, 2000, **122**, 4524.

29 R. Freeman, X. Liu and I. Willner, *J. Am. Chem. Soc.*, 2011, **133**, 11597.

30 C. C. Hardin, A. G. Perry and K. White, *Biopolymers*, 2001, **56**, 147.

31 G. N. Parkinson, R. Ghosh and S. Neidle, *Biochemistry*, 2007, **46**, 2390.

32 J. Pan and S. Zhang, *J. Biol. Inorg. Chem.*, 2009, **14**, 401.

33 J. Lim and O. Š. Miljanić, *Cryst. Eng. Comm.*, 2011, **13**, 5309.

34 M. Meyer and J. Sühnel, *J. Phys. Chem. A*, 2003, **107**, 1025.

35 T. Giorgi, F. Grepioni, I. Manet, P. Mariani, S. Masiero, E. Mezzina, S. Prieraccini, L. Saturni, G. P. Spada and G. Gottarelli, *Chem.–Eur. J.*, 2002, **8**, 2143.

36 S. Fletcher, V. M. Shahani, A. J. Lough and P. T. Gunning, *Tetrahedron*, 2010, **66**, 4621.

37 J. T. Davis and G. P. Spada, *Chem. Soc. Rev.*, 2007, **36**, 296.

38 T. Nakamura, K. Iida, M. Tera, K. Shin-ya, H. Seimiya and K. Nagasawa, *ChemBioChem*, 2012, **13**, 774.

39 J. L. Sessler, M. Sathiosatham, K. Doerr, V. Lynch and K. A. Abboud, *Angew. Chem., Int. Ed.*, 2000, **39**, 1300.

40 T. N. Pham, S. Masiero, G. Gottarelli and S. P. Brown, *J. Am. Chem. Soc.*, 2005, **127**, 16018.

41 K. Phillips, Z. Dauter, A. I. H. Murchie, D. M. J. Lilley and B. Luisi, *J. Mol. Biol.*, 1997, **273**, 171.

42 A. J. Dingley, R. D. Peterson, S. Grzesiek and J. Feigon, *J. Am. Chem. Soc.*, 2005, **127**, 14466.

43 Each equilibrium constant was estimated by the following formula:

$$[\text{Cation}]_{\text{add}} = \frac{\Delta A}{\varepsilon K}\left(\left(\frac{\varepsilon}{\varepsilon[^{1}\text{PG}]_{0} - 4\Delta A}\right)^{4} + K\right) \qquad (\varepsilon = \varepsilon_{^{1}\text{PG}_4} - 4\varepsilon_{^{1}\text{PG}_1})$$

44 N. Hayashi, M. Sato, K. Miyabashi, M. Miyake and H. Higuchi, *Sci. Technol. Adv. Mater*, 2006, **7**, 237.

45 R. F. Khairutdinov and N. Serpone, *J. Phys. Chem. B*, 1999, **103**, 761.

46 D. L. Cullen and E. F. Meyer, Jr., *J. Am. Chem. Soc.*, 1974, **96**, 2095.

47 In the absence of Na^+, no quartet structure was formed under the present conditions, where [^{i}PG] = (0.21 mM).

48 For details of the curve fitting to estimate the formation constants of the complexes between the G-quartet and NiOEP are described in ESI.

49 D. C. Creagh and W. J. McAuley, *International Tables for X-ray Crystallography*, A. J. C. Wilson, Ed. Kluwer Academic Publisher, Boston, 1992, vol. **C**, Table 4.2.6.8 and 6.1.1.4.

50 J. A. Ibers and W. C. Hamilton, *Acta Cryst.*, 1964, **17**, 781.

51 *Yadokari-XG 2009*: Crystal Structure Analysis Package; modified by T. Nemoto, 2009, based on version 2007.5.12 (written by K. Wakita, C. Kabuto, S. Akine, T. Nemoto, E. Kwon). Release of software (Yadokari-XG 2009) for crystal structure analyses: *J. Cryst. Soc. Jpn.*, 2009, **51**, 218.

52 G. M. Sheldrick, *Acta Cryst.*, 2008, **A64**, 112.

Chapter 2

Regulation of Redox Potential of a Pterin Derivative Bound to a Ruthenium(II) Complex by Intermolecular Hydrogen Bonding with Nucleobases

Abstract

A Ru(II)-bound pterin forms a stable hydrogen-bonding adduct with a guanine derivative through three-point recognition: The hydrogen bonding allowed us to observe a large positive shift of the reduction potential of the pterin ligand up to +320 mV. In the case of a thymine derivative, the mode of hydrogen bonding is altered upon reduction of the pterin ligand from a two-point mode to a single-point mode. This is the first example to demonstrate the regulation of redox potentials of a pterin coenzyme by non-covalent interaction.

Introduction

Pterins are redox-active heteroaromatic coenzymes involved in a variety of redox-related reactions in biological systems to perform proton-coupled electron transfers (PCET).[1] They are originated from guanosine triphosphate[2] and fixed in the vicinity of metal ions by non-covalent interactions including hydrogen bonding and π-π interactions to form active sites of metalloenzymes.[3] In order to realize a required functionality in a certain enzyme, redox potential of the pterin cofactor needs to be appropriately regulated. For example, in the active site of heme-containing induced nitric oxide synthase (iNOS), tetrahydrobiopterin (H_4B) has π-π interaction with the indole ring of tryptophan 457 in the vicinity of the heme cofactor, resulting in the stabilization of the radical intermediate of H_4B to facilitate electron transfer from H_4B to an Fe-O_2 complex.[4,5] Since the pterin cofactors are involved in extensive hydrogen-bonding network in the active sites of pterin-dependent enzymes,[6] hydrogen bonding should be an important factor to regulate the redox potential. Any clear evidence, however, has yet to be provided to support that hydrogen-bonding interaction exerted to the pterins is the critical factor for the regulation of their redox behavior. This is due to the fact that the direct determination of the redox potentials of pterins is generally difficult in biological systems,[7] and thus, the lack of sufficient dataset of redox potentials of pterins has precluded the detailed discussion on the reactivity control of pterin-dependent enzymes by non-covalent interactions, which regulate the redox potentials of pterins in active sites of pterin-dependent enzymes.

Transition metal complexes of pterin and their derivatives have been synthesized and characterized to demonstrate mainly their structures and redox behaviors.[8-11] Among the complexes, Ru^{II} complexes have been revealed to be useful for evaluating the redox potentials of the pterin ligand and for elucidating the PCET processes.[12,13] The author has employed a Ru^{II}-TPA unit (TPA = tris(2-pyridylmethyl)amine) as a platform to obtain Ru^{II}-pterin complexes, which have exhibited reversible redox waves for the pterin ligands to afford fairly stable radical species, which were spectroscopically well-characterized.[13] Herein, the author would like to demonstrate the first observation of redox potential control of pterin cofactors by hydrogen bonding on the Ru^{II}-TPA platform. The author adopted the Ru^{II}-bound 6,7-dimethylpterin anion (dmp^-) of complex **1** (Figure 1) and ribonucleoside derivatives of guanosine, adenosine, and cytidine, and a deoxyribonucleoside derivative of thymidine, as hydrogen-bonding receptors (Figure 1).

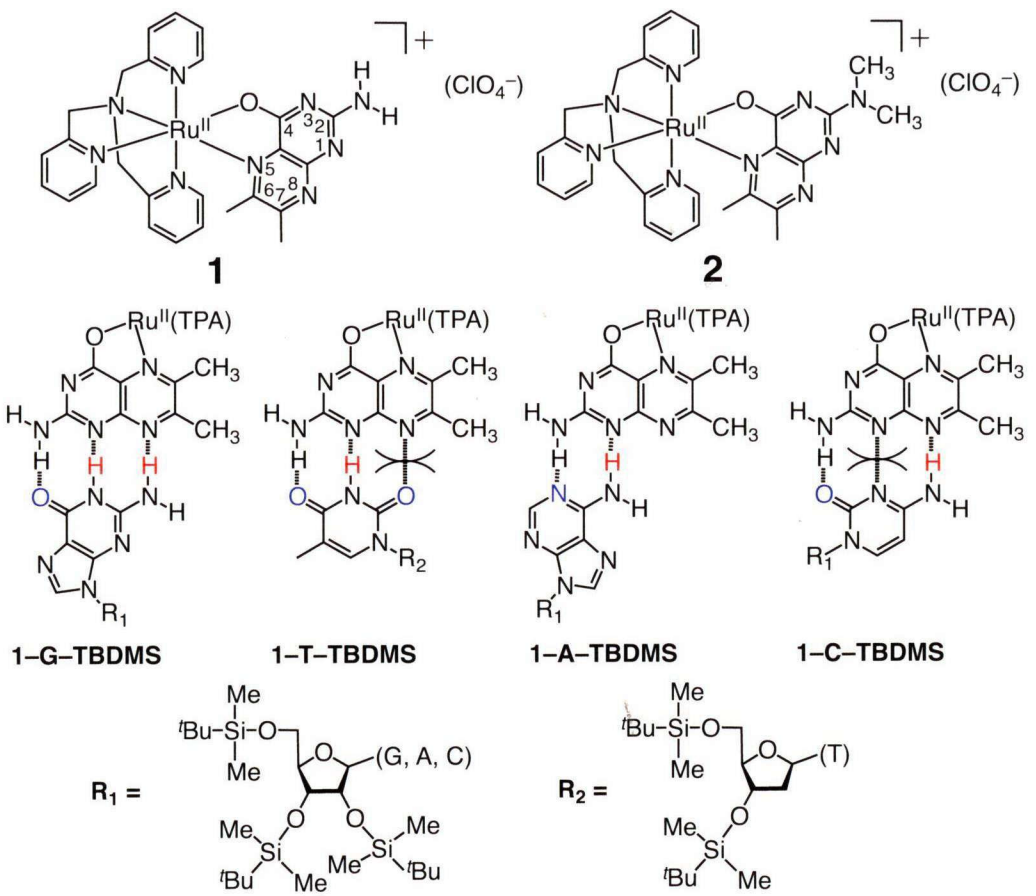

Figure 1. Structures of Ru-pterin-TPA complexes (**1** and **2**) (upper) and Schematic description of plausible structures of hydrogen-bonding adducts between **1** and the nucleosides (middle). R denotes the sugar moiety in the corresponding nucleosides (lower).

Results and discussion

The author performed spectroscopic titration experiments of nucleoside derivatives into the solution of **1** in a mixed solvent of acetonitrile and chloroform to determine the binding constants.[14] In the ^{1}H NMR spectrum of **1** in $CDCl_3/CD_3CN$/ (4:1 v/v), a singlet peak assigned to the 7-methyl group of the dmp^- ligand was observed at 2.83 ppm and the signal showed a gradual upfield shift in the course of the addition of G-TBDMS as shown in Figure 2.[15] Curve fitting of the change of the chemical shift relative to the concentration of G-TBDMS, as depicted in Figure 3(a), allowed us to determine the binding constant to be 1.0×10^3 M^{-1}. The addition of T-TBDMS caused a slight upfield shift of the 7-methyl signal of the dmp^- ligand and the binding constant was estimated to be $\sim 1 \times 10^2$ M^{-1} (Figure 3(b)). Concerning A-TBDMS and C-TBDMS, no significant

change was observed even in the presence of *ca.* 50-fold excess amount of the nucleosides. These results indicate that the guanine part of G-TBDMS binds to the pterin ligand most strongly among the four nucleosides.

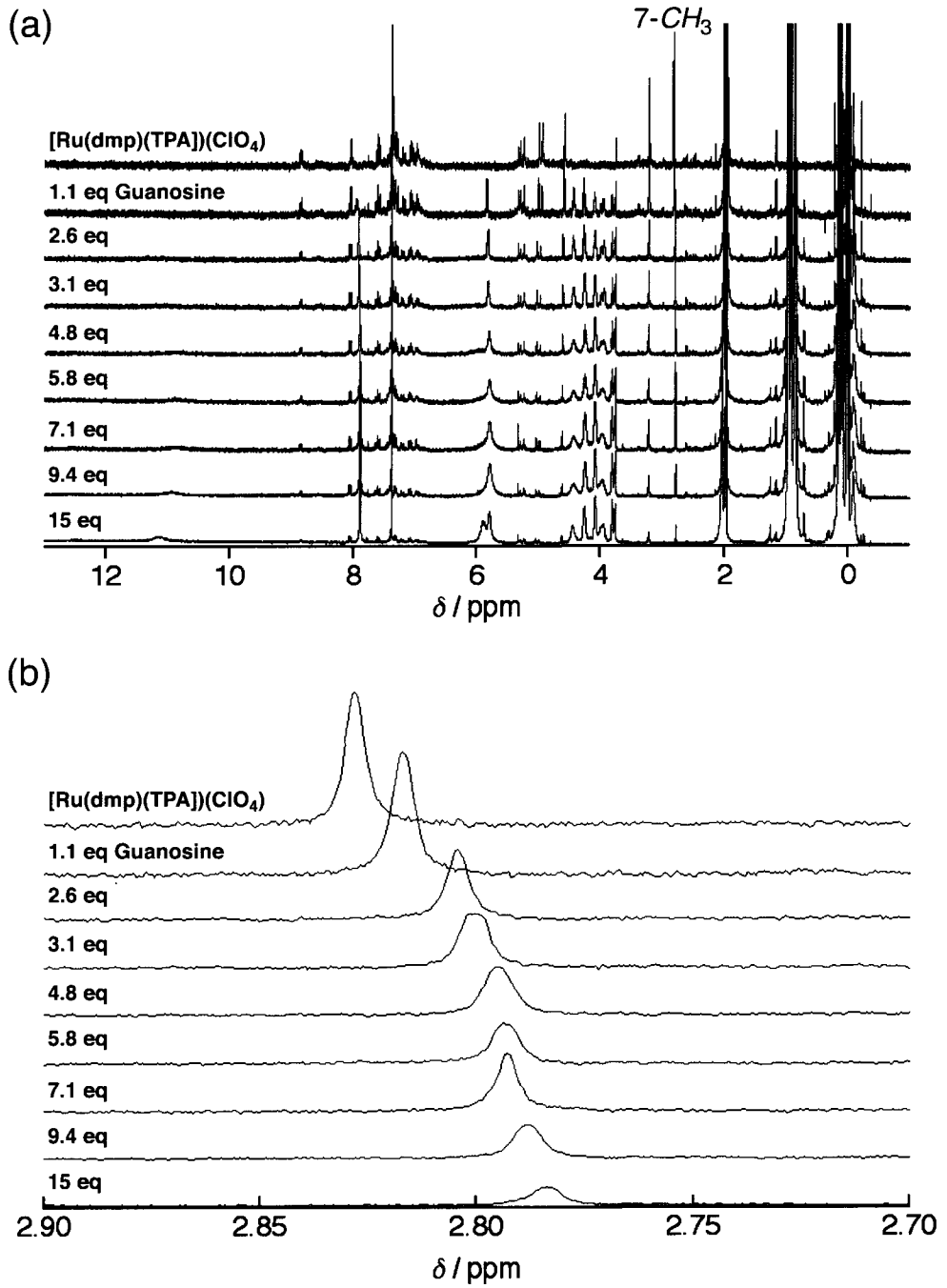

Figure 2. (a) ^{1}H NMR spectral change of **1** (1.0 mM) during the addition of G-TBDMS at 293 K in $CDCl_3/CD_3CN$ (4:1 v/v); (b) expanded plots of the region involving the signal due to 7-CH_3 of **1**.

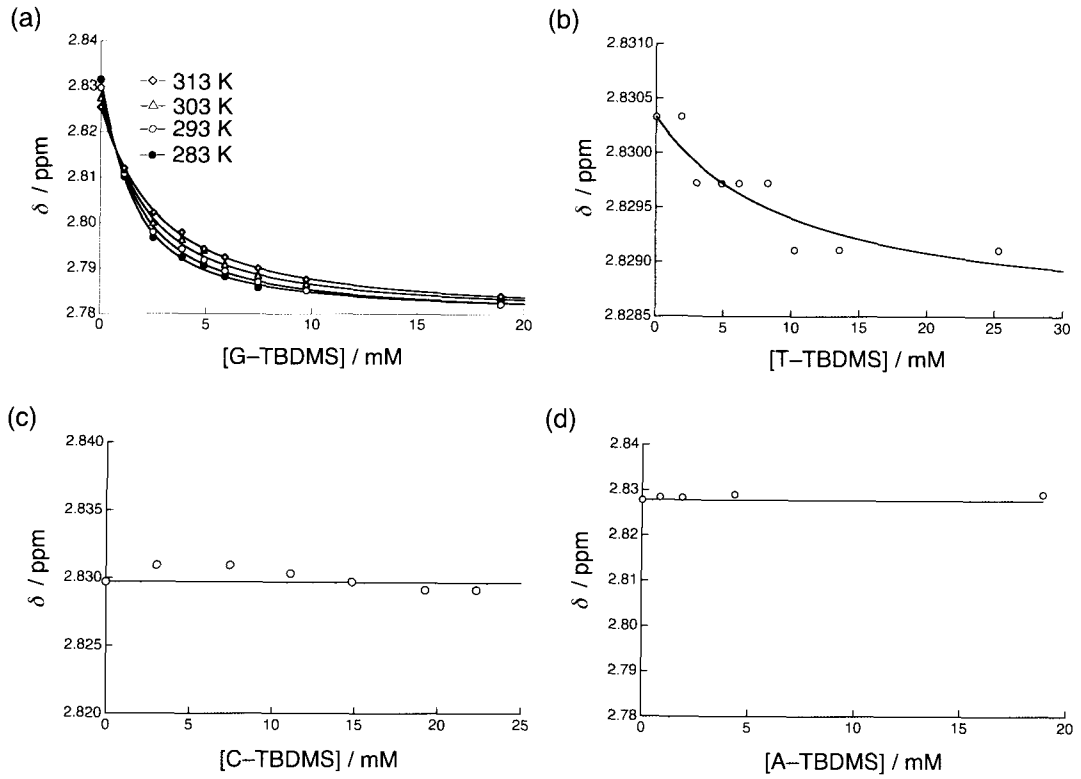

Figure 3. Chemical shift changes of the signal due to 7-CH_3 of **1** during the addition of (a) G-TBDMS ([**1**] = 1.1 mM), (b) T-TBDMS ([**1**] = 1.2 mM), (c) C-TBDMS ([**1**] = 0.66 mM), (d) A-TBDMS ([**1**] = 0.98 mM) in $CDCl_3/CD_3CN$ (4:1 v/v).

For the combination of the dmp^- ligand in **1** with the guanine, it is possible to form an adduct with three-point complementary hydrogen bonding as depicted in Figure 4. The possibility has been clarified by the determination of the crystal structure of the hydrogen bonding complex of 2-(isobutyrylamide)-6,7-dimethylpterin (Figure 5) with 9-isopropylguanine, as shown in Figure 4, which clearly demonstrates a three-point hydrogen bonding between them.[16] On the basis of the crystal structure depicted in Figure 4, in the complementary hydrogen bonding pair between complex **1** and the guanine part of G-TBDMS, the dmp^- ligand accepts two protons at the 1-N and 8-N positions, one of which is donated from the 2-amino group and the other from the 1-NH of the guanine part of G-TBDMS, and donates one proton of the 2-amino group of the dmp^- ligand to the carbonyl oxygen at the 6-position of the guanine part. All the X-ray crystallographic data are summarized in Table 1. Selected bond lengths (Å) and angles (deg) of 2-(isobutyrylamide)-6,7-dimethylpterin and the adduct are listed in Tables 2 and 3, respectively. Interatomic distances (Å) for hydrogen bonding in the adduct are also summarized in Table 4.

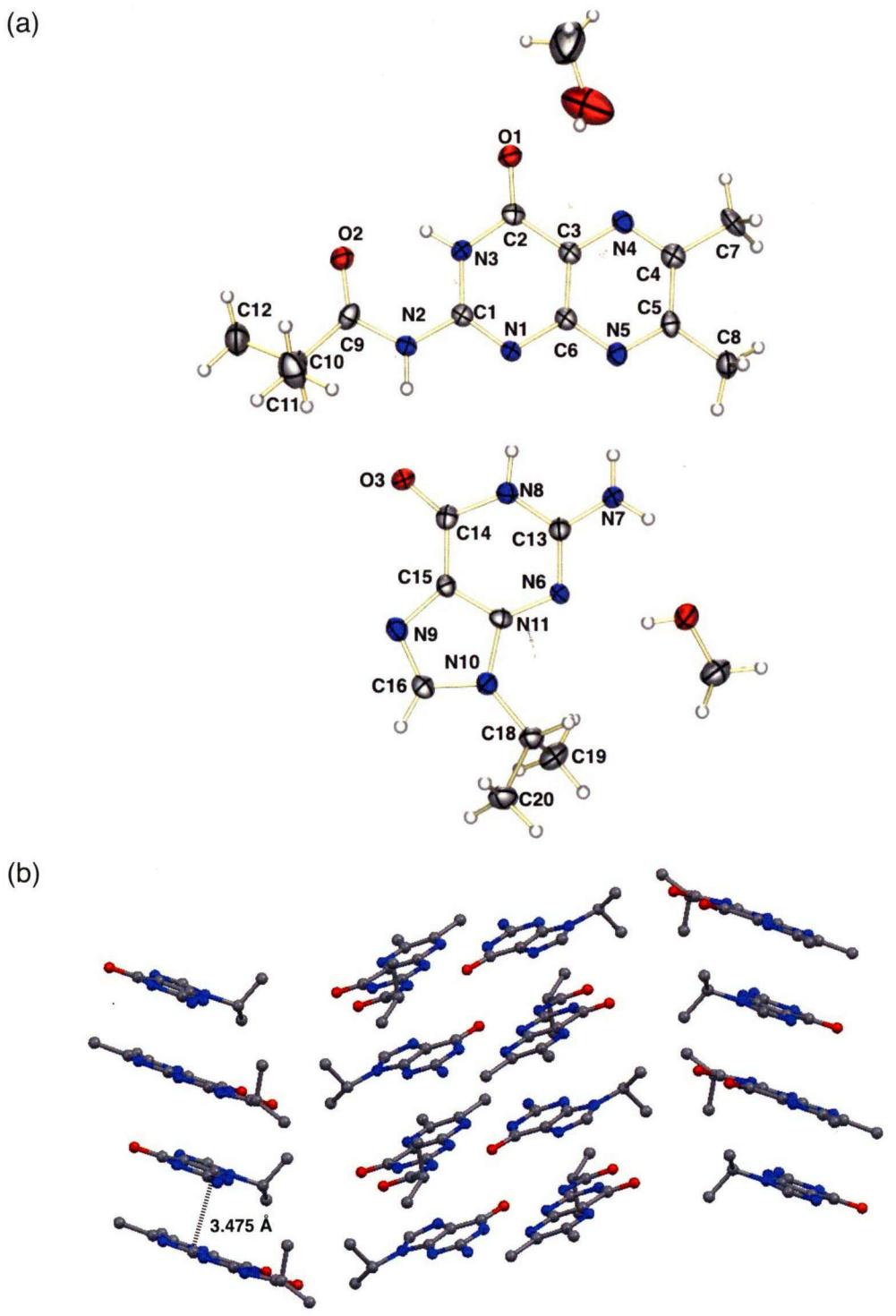

Figure 4. (a) An ORTEP drawing of the adduct made of 2-(isobutyrylamide)-6,7-dimethylpterin and 9-isopropylguanine with three-points hydrogen bonding with 50% probability thermal ellipsoids: N2•••O3 2.767 Å, N1•••N8 2.957Å, N5•••N7 2.988 Å. (b) a view of the crystal packing.

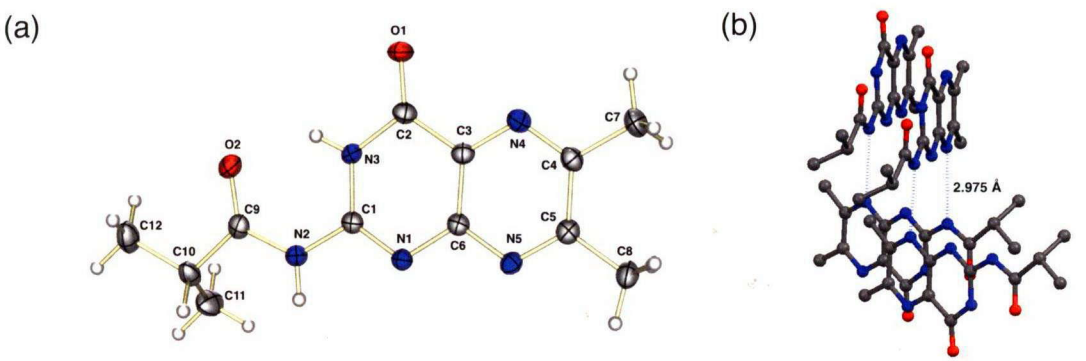

Figure 5. The crystal structure of 2-(isobutyrylamide)-6,7-dimethylpterin: (a) An ORTEP drawing of the molecular structure; (b) intermolecular hydrogen bonding.

Table 1. X-ray crystallographic data for 2-(isobutyrylamide)-6,7-dimethylpterin and the adduct made of 2-(isobutyrylamide)-6,7-dimethylpterin and 9-isopropylguanine.

	2-(isobutyrylamide)-6,7-dimethylpterin	The adduct
formula	$C_{12}H_{15}N_5O_2$	$C_{22}H_{34}N_{10}O_5$
fw	261.29	518.59
crystal system	orthorhombic	monoclinic
space group	$P2_12_12_1$	$P2_1/a$
T (K)	120	120
a (Å)	7.2428(15)	7.681(3)
b (Å)	9.5601(19)	28.221(12)
c (Å)	17.720(4)	11.958(5)
β (deg)		104.335(6)
V (Å^3)	1226.9(4)	2511.38(18)
Z	4	4
no. of reflections measured	6934	11976
no. of observations	2773	4472
no. of parameters refined	184	344
$R1$[a]	0.0363	0.0725
R_W[b]	0.0790 ($I > 2.0\sigma(I)$)[c]	0.1723 ($I > 2.0\sigma(I)$)[d]
GOF	1.021	0.998
CCDC no.	851578	849641

[a] $R1 = \Sigma \, ||Fo| - |Fc|| \, / \, \Sigma \, |Fo|$. [b] $Rw = [\, \Sigma \, (w \, (F_0^2 - F_c^2)^2) \, / \, \Sigma \, w(F_0^2)^2]^{1/2}$. [c] $w = 1 \, / \, [\sigma^2(F_0^2) + (0.0301P)^2 + 0.4853P]$, where $P = (\mathrm{Max}(F_0^2, 0) + 2F_c^2) \, / \, 3$, [d] $w = 1 \, / \, [\sigma^2(F_0^2) + (0.0996P)^2 + 0.00P]$, where $P = (\mathrm{Max}(F_0^2, 0) + 2F_c^2) \, / \, 3$.

Table 2. Selected bond lengths (Å) and angles (deg) of 2-(isobutyrylamide)-6,7-dimethylpterin

N1 – C1	1.298(2)	N1 – C1 – N2	117.3(1)
N1 – C6	1.373(2)	N1 – C6 – N5	115.4(1)
C1 – N2	1.380(2)	C1 – N2 – C9	126.7(1)
C1 – N3	1.360(2)	N2 – C9 – O2	121.8(2)
N2 – C9	1.384(2)	N3 – C2 – O1	120.6(1)
N3 – C2	1.395(2)	O1 – C2 – C3	127.3(2)
C2 – C3	1.468(2)	C2 – C3 – N4	118.6(1)
C2 – O1	1.211(2)		
C3 – C6	1.394(2)		
N4 – C4	1.323(2)		
C5 – N5	1.326(2)		
N5 – C6	1.352(2)		

Table 3. Selected bond lengths (Å) and angles (deg) of the adduct of 2-(isobutyrylamide)-6,7-dimethyl- pterin and 9-isopropylguanine.

N1 – C1	1.299(5)	N1 – C1 – N2	117.4(3)
N1 – C6	1.382(4)	N1 – C6 – N5	116.7(3)
C1 – N2	1.385(5)	C1 – N2 – C9	126.8(4)
C1 – N3	1.352(5)	N2 – C9 – O2	122.9(4)
N2 – C9	1.375(5)	N3 – C2 – O1	120.6(4)
N3 – C2	1.380(5)	O1 – C2 – C3	126.6(4)
C2 – C3	1.468(6)	C2 – C3 – N4	117.8(4)
C2 – O1	1.223(5)	N6 – C13 – N7	119.9(4)
C3 – C6	1.389(5)	N6 – C17 – N10	124.5(4)
N4 – C4	1.313(5)	N7 – C13 – N8	117.0(4)
C5 – N5	1.328(5)	N8 – C14 – O3	120.0(4)
N5 – C6	1.344(5)	C13 – N6 – C17	111.9(3)
C9 – O2	1.291(5)	C13 – N8 – C14	125.8(3)
N6 – C13	1.330(5)	N9 – C15 – C14	130.4(4)
N7 – C13	1.333(5)		
N8 – C13	1.364(5)		
N8 – C14	1.399(5)		
N9 – C15	1.391(5)		
N9 – C16	1.305(5)		
C14 – O3	1.239(5)		
C14 – C15	1.418(5)		
C15 – C17	1.366(5)		

Table 4. Interatomic distances (Å) for hydrogen bonding in the adduct consist of 2-(isobutyrylamide)-6,7-dimethylpterin and 9-isopropylguanine.

Intermolecular hydrogen bonding	
N1•••HN8	2.957(4)
N2H•••O3	2.767(4)
N5•••HN7	2.988(5)
O4H•••N6	2.786(4)
N7H•••O4	2.949(5)
O1•••HO5	2.894(6)

Intramolecular hydrogen bonding	
N3H•••O2	2.621(4)

The binding constant of G-TBDMS exhibited a linear correlation with T^{-1} to allow us to determine the enthalpy change ($\Delta H°$) upon the formation of the hydrogen-bonding complex to be –4.5 kcal mol^{-1} from the slope and the entropy change to be –1.9 cal mol^{-1} K^{-1} (Figure 6). These values are comparable to those values obtained for the formation of three-point hydrogen bonding adducts of flavin derivatives with 2,6-bisamidepyridines.[17]

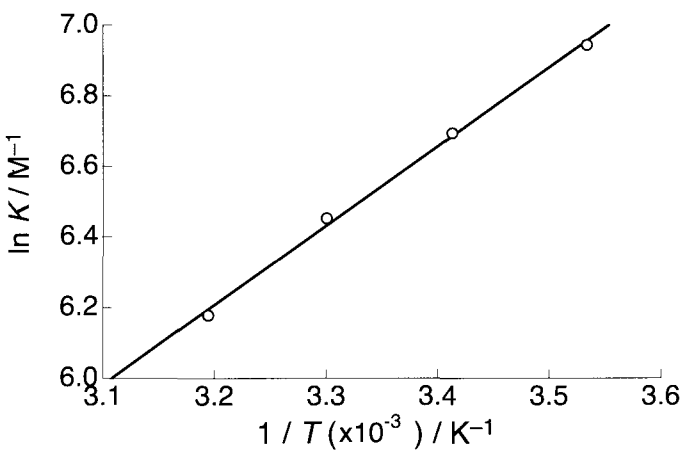

Figure 6. A van't Hoff plot for the binding constants of G-TBDMS with **1** in $CDCl_3/CD_3CN$ (4:1 v/v).

As for the thymidine derivative, a two-point hydrogen bonding should be available with the 1-N and 2-NH_2 sites of the dmp^- ligand as depicted in Figure 1. However, the lone pair of one of the two carbonyl oxygen atoms of the thymine part causes

electrostatic repulsion with that of the 8-N nitrogen of the dmp^- ligand. DFT calculations suggested that, in the formation of a hydrogen-bonding adduct, the thymine plane should be tilted with a dihedral angle of 9° relative to the pterin mean plane to avoid the repulsion as shown in Figure 13. This may cause partial loss of stabilization of the hydrogen-bonding adduct to afford a small binding constant as mentioned above. Since the most basic site in the dmp^- ligand has been proved to be the N-1 position,[13c] the hydrogen bonding to the 1-N position is favorable for the dmp^- ligand. From this viewpoint, G, T, and A should be favored because of their possibility to form at least two-point hydrogen bonding with the dmp^- ligand. However, the electrostatic repulsion between the lone pairs of 1-N of dmp^- and 3-N of the cytosine may avoid the close contact of the pterin ligand to the cytosine moiety of C-TBDMS. As can be seen in Figure 1, the adenine moiety of A-TBDMS is assumed to form two-point complementary hydrogen boning at the 6-amino group and the 1-N atom with the 1-N and the 2-amino group of the pterin ligand, respectively, however, its binding constant is too low to be determined. The author assume that the acidity of the 6-amino group of the adenine moiety is too weak to form a stable hydrogen-bonding adduct in a polar medium containing acetonitrile.[18]

The author examined the importance of the 2-amino group of the dmp^- ligand to form hydrogen bonding with the nucleobases by using complex **2** (Figure 1) bearing $dmdmp^-$ (Hdmdmp = *N*,*N*-dimethyl-6,7-dimethylpterin),[13] which has the *N*,*N*-dimethylamino group in place of the amino group at the 2-position, as a ligand. The singlet signal assigned to the 7-methyl group of the $dmdmp^-$ ligand of **2**, which was initially observed at 2.82 ppm, did not show any shift by addition of G-TBDMS, because the steric hindrance caused by the *N*,*N*-dimethylamino group of the $dmdmp^-$ ligand inhibited the hydrogen bonding with nucleobases even for G-TBDMS. This difference between **1** and **2** clearly indicates the importance of the 2-amino group of the dmp^- ligand in the formation of hydrogen-bonding complexes with nucleobases.

Cyclic voltammetry (CV) and differential pulse voltammetry (DPV) were applied to determine the redox potentials of **1** with or without nucleoside derivatives in CH_3CN in the presence of 0.1 M of tetra(*n*-butyl)ammonium hexafluorophosphate ($TBAPF_6$) as an electrolyte at room temperature under Ar. In the absence of the nucleosides, the complex **1** showed a reversible redox wave at –1.63 V vs SCE due to the $dmp^-/dmp^{\bullet 2-}$ couple to produce $[Ru^{II}(dmp^{\bullet 2-})(TPA)]$ (the dotted line on Figure 7).[13] Upon addition of 7.7-fold excess amount of G-TBDMS, the redox wave in the CV trace showed a large positive shift and lost the reversibility (Figure 8(a)). The DPV measurement allowed us to determine the reduction potential of the dmp^- ligand to be –1.31 V vs SCE (ΔE_{red} = +0.32 V) (the solid line in Figure 7) in the hydrogen-bonding complex.

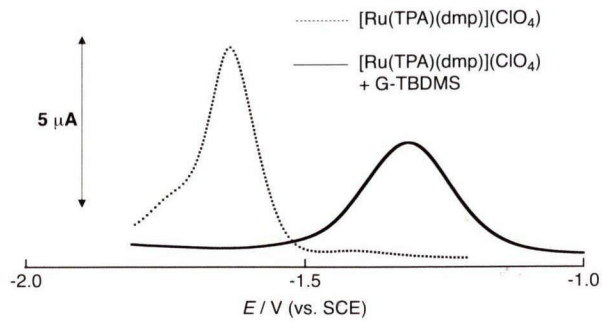

Figure 7. DPV traces for **1** (0.94 mM) in the absence (dotted line) and the presence (solid line) of 7.2 mM of G-TBDMS in CH_3CN in the presence of 0.1 M of $TBAPF_6$ as an electrolyte under Ar at room temperature.

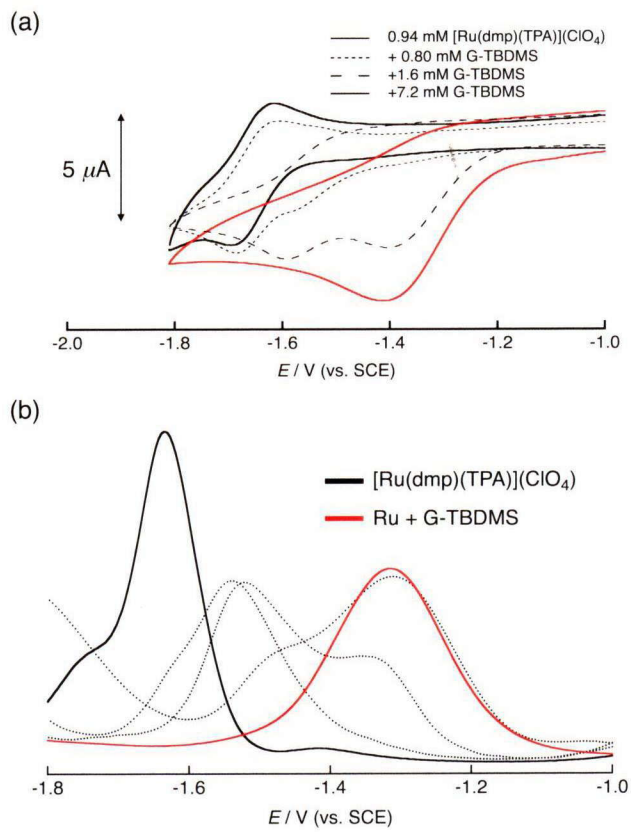

Figure 8. (a) CV traces for **1** (0.94 mM) in the absence (black solid line) and the presence of 0.80 mM (dotted line), 1.6 mM (black broken line) and 7.2 mM (red solid line) of G-TBDMS in CH_3CN in the presence of 0.1 M of $TBAPF_6$ as an electrolyte under Ar at room temperature. (b) DPV traces for **1** in the absence (black solid line) and the presence of 0.51, 1.4 and 2.4 eq (dotted lines) and 7.7 eq (red solid line) of G-TBDMS in CH_3CN in the presence of 0.1 M of $TBAPF_6$ as an electrolyte under Ar at room temperature.

In the case of T-TBDMS, the addition of the nucleoside to the solution of **1** gave an anodic shift of the redox wave due to the $dmp^{-}/dmp^{\bullet 2-}$ couple from –1.63 V to –1.42 V vs SCE (ΔE_{red} = +0.21 V) (Figure 9). This suggests that the thymine moiety of T-TBDMS also strongly interacts with the reduced form of the dmp^{-} ligand ($dmp^{\bullet 2-}$), even though it does not bind so strongly to the dmp^{-} ligand.

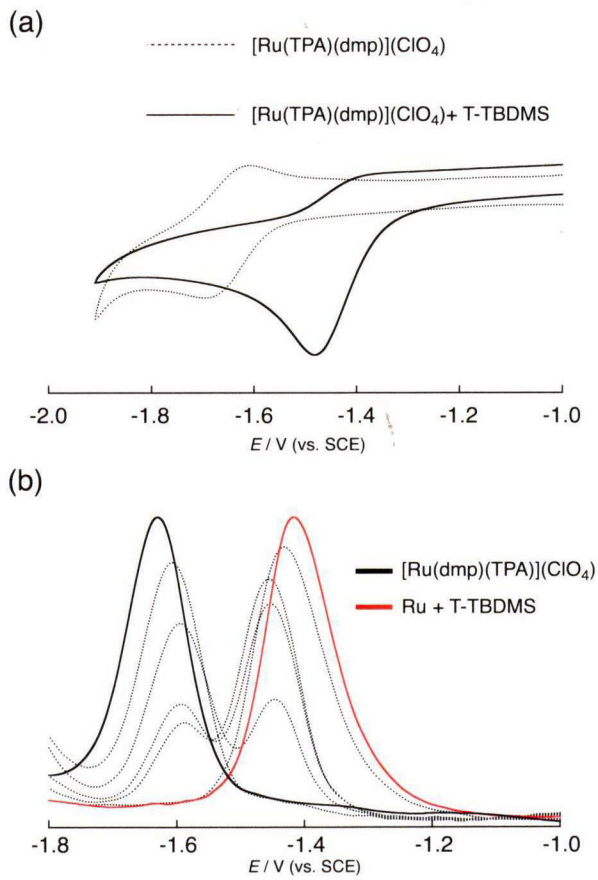

Figure 9. (a) CV traces for **1** (0.84 mM) in the absence of nucleosides (dotted line) and in the presence (solid line) of 3.4 mM of T-TBDMS. (b) DPV traces for **1** in the absence (black solid line) and in the presence of 0.65, 1.3, 1.9, 2.3, 2.7 eq (dotted lines) and 4.0 eq (red solid line) of T-TBDMS in CH_3CN. Measurements were made in the presence of 0.1 M of $TBAPF_6$ as an electrolyte under Ar at room temperature.

As for the addition of C- and A-TBDMS, the one-electron reduction potential exhibited only trivial shifts, at most +0.03 V for C-TBDMS and +0.01 V for A-TBDMS, respectively (Figure 10). These results indicate that cytosine and adenine do not interact significantly with the pterin ligand, regardless of its reduction. Binding constants of the nucleoside derivatives for **1** and redox potentials of the $dmp^{-}/dmp^{\bullet 2-}$ couple are

summarized in Table 5. In comparison with the case of flavins,[6,19] the ΔE_{red} values obtained here for the pterin complex for G- and T-TBDMS are much larger. The author attributes this difference of the hydrogen bonding effects on the redox potentials between pterins and flavins to the positions in the coenzymes to form hydrogen bonding: Flavins have been reported to form hydrogen-bonding adducts at the 2-O, 3-NH, and O-4 positions,[6,17,19] which have little relationship with the PCET process of flavins. In contrast, in the cases of the pterin ligand in **1**, intermolecular hydrogen bonding can be formed at the 8-N position that is involved in the PCET region (5-N, 6-C, 7-C and 8-N) of pterin and forms the strongest hydrogen bonding with a hydrogen donor upon reduction of the pterin ligand in comparison with the 3- and 5-N positions.[13c]

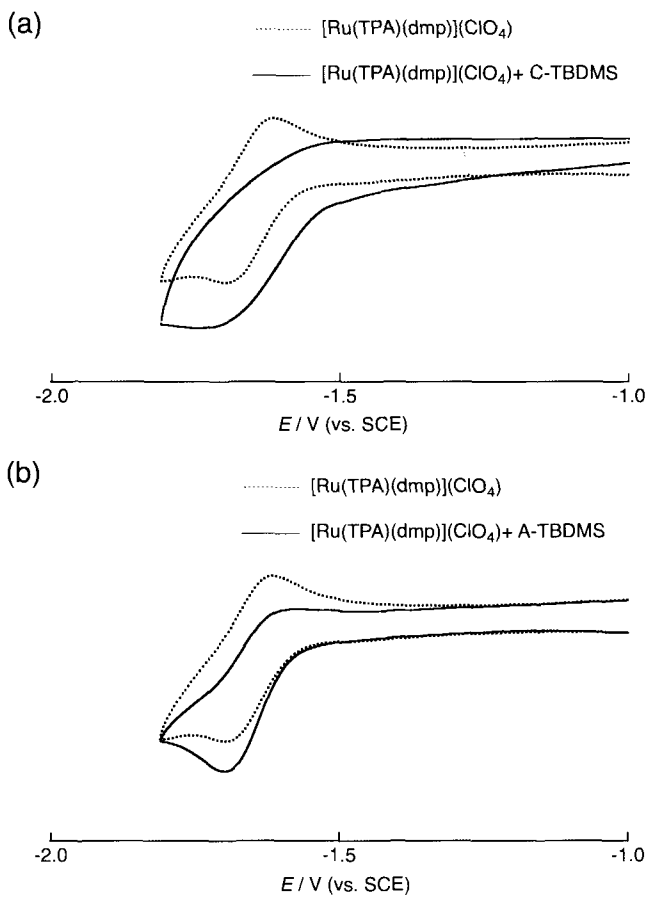

Figure 10. (a) CV traces for **1** (1.2 mM) in the absence of nucleosides (dotted line) in the presence (solid line) of 14 mM of C-TBDMS, and (b) CV traces for **1** (0.81 mM) in the absence of nucleosides (dotted line) in the presence (solid line) of 7.4 mM of A-TBDMS in CH_3CN. CV traces were measured in the presence of 0.1 M of $TBAPF_6$ as an electrolyte under Ar at room temperature.

Table 5. Binding constants of the nucleosides and redox potentials of the $dmp^{-}/dmp^{\bullet 2-}$ couples.

Compound	K_{ox}, M^{-1} [a]	E_{red}, V [b]	ΔE_{red}, V
1	–	−1.63 [c]	–
1–G-TBDMS	1.0×10^3	−1.31	0.32
1–T-TBDMS	$\sim 1 \times 10^2$	−1.42	0.21
1–C-TBDMS	< 10	−1.60	0.03
1–A-TBDMS	<10	−1.62	0.01

[a] Determined by ^{1}H NMR measurements in $CDCl_3/CD_3CN$ (4:1 v/v) at 293 K. [b] Measured relative to $Ag/AgNO_3$ in CH_3CN at 293 K. The potentials (V) were converted to values relative to SCE by adding +0.29 V. The values were obtained by adding 7.7 eq of G-TBDMS, 4.0 eq of T-TBDMS, 12 eq of C-TBDMS and 9.1 eq of A-TBDMS, relative to **1**. [c] Reversible. The value is presented as $E_{1/2}$.

In order to prove the formation of hydrogen bonding between the $dmp^{\bullet 2-}$ ligand and the nucleobases, the author measured ESR spectra of one-electron reduced species of **1** as a probe by means of the chemical reduction of **1** (2.0 mM) with sodium naphthalenide ($Na(naph^{\bullet -})$) in the presence of the nucleosides (20 mM) at 243 K in CH_3CN. The one-electron reduced species of **1** showed a well-resolved ESR signal at g = 1.9991 as shown in Figure 11(a).[13b] Computer simulations of the spectrum allowed us to determine the hyperfine coupling (*hfc*) constants as 4.90 G for 5-N, 4.00 G for 8-N, 0.70 G for 6-CH_3, and 7.70 G for 7-CH_3, respectively, as shown in Figure 11(d). These results indicate that the unpaired electron is delocalized in the PCET region as observed in other related Ru-bound pterin radical species.[13] DFT calculations on the $dmp^{\bullet 2-}$ π-radical dianion were also performed at the B3LYP/6-31G(d) level of theory to estimate the *hfc* constants (Figure 12). ESR spectrum of the reduced species of **1** in the presence of G-TBDMS exhibited a well-resolved ESR signal at g = 1.9990 with hyperfine splitting (Figure 11(b)) and the simulation afforded *hfc* constants as 4.60 G for 5-N, 3.60 G for 8-N, 0.74 G for 6-CH_3 and 7.70 G for 7-CH_3, respectively, as shown in Figure 11(e). The values for 5-N and 8-N became smaller by the addition of G-TBDMS than those of the $dmp^{\bullet 2-}$ π-radical dianion of **1**. This tendency is also confirmed by DFT calculations and is caused by delocalization of an unpaired electron in a wider region: This delocalization can be attained as a result of the intermolecular hydrogen bonding between G-TBDMS and the $dmp^{\bullet 2-}$ π-radical dianion ligand. This indicates that the hydrogen bonding alters the distribution of the unpaired electron as in the case of those for flavins and their derivatives.[19]

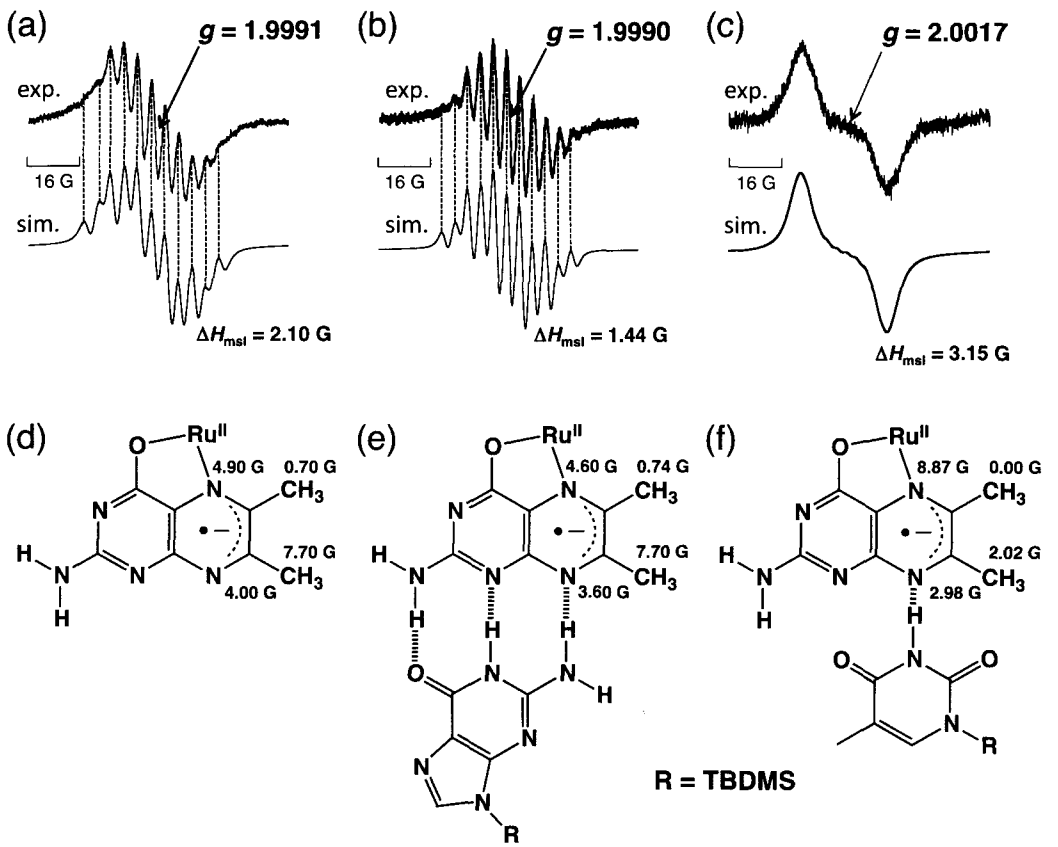

Figure 11. ESR spectra of the reduced species of **1** with their computer simulations (a) and those in the presence of G-TBDMS (b), T-TBDMS (c), in deaerated CH_3CN at 243 K. Estimated *hfc* values with computer simulations are included (d)–(f). ΔH_{msl} denotes the mid-slope line width for the simulation.

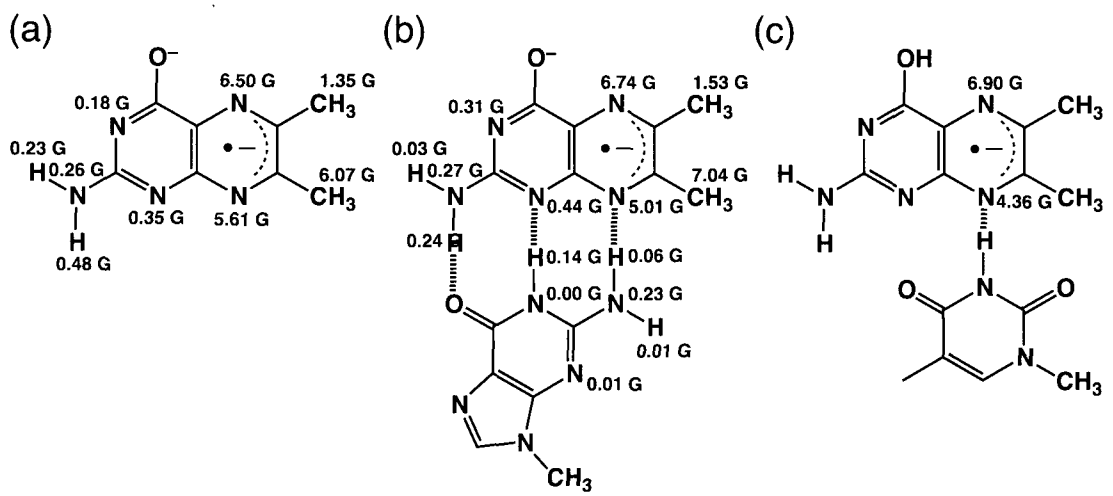

Figure 12. Calculated hyperfine coupling constants of (a) $dmp^{\bullet 2-}$, (b) $dmp^{\bullet 2-}$–Guanine adduct, and (c) $Hdmp^{\bullet -}$–Thymine adduct at the B3LYP/6-31G(d) level of theory.

In the case of T-TBDMS, the ESR spectrum of the reduced species of **1** drastically changed to show an ESR signal at g = 2.0017 as shown in Figure 11(c). Simulation of the spectrum allowed us to estimate the *hfc* constants of 8.87 G for 5-N and 2.98 G for 8-N. Comparison of the *hfc* constants clearly indicates that thymine binds to the $dmp^{\bullet 2-}$ π-radical dianion in a different hydrogen-bonding mode from that of the guanine. The hydrogen bond formation of T-TBDMS is assumed to occur only at the 8–N position of the $dmp^{\bullet 2-}$ ligand, as supported by the fact that a proton shift occurs from 1-N to 8-N in the course of one-electron reduction of protonated $[Ru(TPA)(Hdmp)]^{2+}$, where the proton initially resides at the 1-N position.[13c] Once the dmp^{-} ligand is reduced, the spin density is delocalized onto the N5-C6-C7-N8 region,[13] whereas in the one-electron-reduced species of the protonated complex **1**, the proton goes to the 8-N position to stabilize the radical species.[13c] This suggests that the hydrogen bonding at the 8-N position should be strengthened in the reduced form due to the increase of the negative charge at the 8-N position of the $dmp^{\bullet 2-}$ ligand. Since the pK_a values of the 3-N*H* of guanine and that of thymine have been reported to be 9.2-9.6 and 9.9, respectively,[18] the ΔH of single-point hydrogen bonding at the 3-N*H* should be virtually the same for both the nucleobases in an electrostatic sense. These arguments suggest that the large positive shift of the reduction potential of the dmp^{-} ligand in the presence of T-TBDMS may stem from the change of binding mode: The thymine moiety which binds to the 1-N and 2-NH_2 positions of the dmp^{-} ligand shifts to form a single-point hydrogen bonding to the 8-N position of the $dmp^{\bullet 2-}$ ligand in the one-electron-reduced species of **1** with the imido N-H group of thymine as shown in Figure 13, similar to the proton shift mentioned above.[13c]

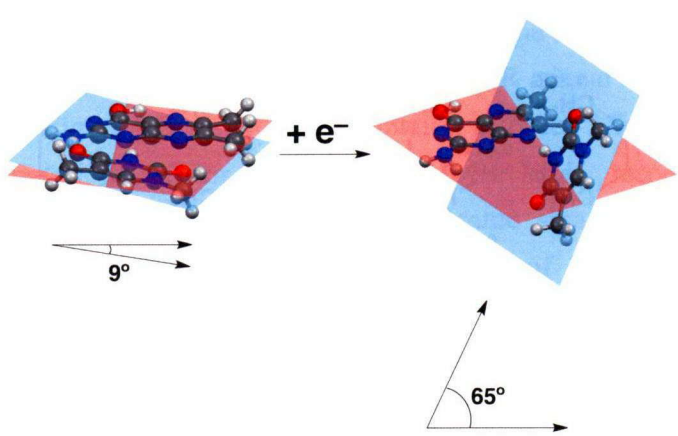

Figure 13. DFT-optimized structures of hydrogen-bonding adducts of Hdmp–1-methylthymine and $Hdmp^{\bullet -}$–1-methylthymine at the B3LYP/6-31G(d) level of theory.

DFT-optimized structure of the one-electron-reduced species of $Hdmp^{\bullet-}$-(1-methylthymine) adduct is depicted in Figure 13 and the dihedral angle between the $Hdmp^{\bullet-}$ ligand and the thymine plane is estimated to be 65°. Thus, the results of DFT calculations also suggest a hydrogen-bond shift of the thymine moiety as shown in Figure 13. The compensation of the attractive interaction (hydrogen bonding) and the electrostatic repulsion between the carbonyl oxygen atoms and the π-electron clouds of the aromatic ring of the pterin ligand caused weaker impact on the redox potential of the pterin ligand, compared to that of the complementarily stabilized guanine adduct.

Summary

In summary, the author has clearly demonstrated the modulation of redox potential of a pterin coenzyme by intermolecular hydrogen bonding for the first time with the aid of the Ru^{II}-TPA coordination environment. The pterin ligand undergoes complementary three-point hydrogen bonding with the guanine derivative, at the 2-NH_2, the 1-N, and the 8-N positions of the dmp^- ligand, as clarified by X-ray crystallography on a complex made of 2-(isobutyrylamide)-6.7-dimethylpterin and 9-isopropylguanine, to show a large anodic shift of the reduction potential of the dmp^- ligand to be +0.32 V. The thymine derivative forms probably two-point intermolecular hydrogen bonding with the dmp^- ligand at the 1-N and 2-NH_2 sites showing a 10-fold smaller binding constant than that of the guanine. The thymidine derivative also induced a fairly large positive shift (+0.21 V) of the reduction potential of the dmp^- ligand. This positive shift is probably derived from a strong single-point hydrogen bonding between the 8-N position of the pterin and the 3-N*H* of the thymine moiety *via* the "proton shift" in the course of the reduction of the pterin ligand. In consequence, the hydrogen bonding toward the 8-N position of pterins, which is involved in the PCET region (5-N, 6-C, 7-C, and 8-N), causes a significant modulation of their redox potentials.

Experimental section

Materials. CH_3CN, CH_2Cl_2, (Wako Pure Chemical Industries) were purified by distillation over CaH_2. Anhydrous *N,N*–dimethylformamide (99.8%, Sigma Aldrich) was kept in a globe box and used without further purification. CH_3OH, $CHCl_3$ (Wako Pure Chemical Industries) were used without further purification. Chloroform-d and acetonitorile-d_3 were purchased from Cambridge Isotope Laboratories, Inc. Guanosine, thymidine, cytidine, and triethylamine were purchased from Wako Pure Chemical

Industries. Adenosine, *tert*-butyldimethylsilyl chloride (TBDMSCl), imidazole, and isobutyric anhydride were purchased from Tokyo Chemical Industries. These reagents were used as received. $TBAPF_6$ (Tokyo Chemical Industries) was recrystallized from water and ethanol (1:1 (v/v)) and then from ethanol. $[Ru(dmp)(TPA)]ClO_4$ (**1**),[20] all TBDMS-derivatives of nucleosides,[21] and 9-isopropylguanine[22] were synthesized according to literature methods.

Apparatus. ^1H NMR spectra were measured on a JNM-EX270 spectrometer. ESR spectra were recorded on a JEOL JEX-REIXE spectrometer. Electrochemical measurements were performed on a BAS CV-50W voltammetric analyzer.

^1H NMR Titration. A mixed solvent of chloroform-*d*/acetonitrile-d_3 (4:1 (v/v)) was used for measurements and chemical shifts were determined relative to an internal standard (TMS). Variable-temperature NMR measurements were made on a sample containing **1** and each nucleoside derivative after incubating for over 3 minutes at a certain temperature. Binding constants were determined by the following equation; $\delta_{obs} =$

$\delta_{[Ru]0}-(\delta_{Ru)0}-\delta_{[NS]})[([Ru]_0+[NS]+(1/K))-\{([Ru]_0+[NS]+(1/K))^2-(4[NS][Ru]_0)\}^{1/2}]/2[Ru]_0$,

where NS denotes nucleosides. Thermodynamic parameters for intermolecular hydrogen bonding, $\Delta H°$, $\Delta S°$ were determined by the following equation: $\ln K = -\Delta H/RT + \Delta S/R$.

ESR Spectroscopy. ESR spectra were recorded at 243 K in CH_3CN and g values were determined relative to an Mn^{2+} marker. $[Ru(TPA)(dmp)](ClO_4)$ (2.0 mM) was reduced by naphthalene radical anion (0.20 M), which was prepared from naphthalene (250 mg) and sodium in dry THF (10 mL).

Electrochemical Measurements. Cyclic voltammetry and differential pulse voltammetry were performed in CH_3CN in the presence of 0.1 M $[(n\text{–butyl})_4N]PF_6$ ($TBAPF_6$) as an electrolyte under Ar at room temperature, with use of a Pt working electrode, $Ag/AgNO_3$ as a reference electrode, and Pt wire as an auxiliary electrode.

DFT Calculations. Density functional theory (DFT) calculations were executed on a 32CPU workstation (PQS, Quantum Cube). Geometry optimizations were carried out using the Becke3LYP functional and 6-31G(d) basis set as implemented in the Gaussian 03 program Revision C.02.[23-25] Graphical outputs of the computational results were generated with the Gauss View software program (ver. 3.09) developed by Semichem, Inc..[26]

X-ray Crystallography. A single crystal of 2-(isobutyrylamide)-6,7-dimethylpterin was obtained by recrystallization from ethanol. A single crystal of the adduct consist of 2-(isobutyrylamide)-6,7-dimethylpterin and 9-isopropylguanine was attained by recrystallization from methanol with vapor diffusion of diethyl ether. All measurements

were performed on a Bruker SMART APEX II ULTRA CCD diffractometer at 120K with graphite-monochromated Mo Kα radiation (λ = 0.71073Å). The structures were solved by direct methods and expanded using Fourier techniques. All non-hydrogen atoms were refined anisotropically including solvents. Refinements were carried out by full-matrix least squares techniques on F^2 with scattering factors[27] and including anomalous dispersion effects.[28] All calculations were performed using the Yadokari-XG crystallographic software package, [29] and structure refinements were made by using *SHELXL 97*.[30]

Synthesis

2-(Isobutyrylamide)-6,7-dimethylpterin.[31] 6,7-dimethylpterin (203 mg, 1.06 mmol) was mixed with triethylamine (1 ml) in neat isobutyric anhydride (2 ml) under Ar. The mixture was heated at 150 °C for 12 h. After cooling down to room temperature, water was poured onto the reaction mixture. The organic layer was extracted with CH_2Cl_2 and then dried on sodium sulfate. The solvent was removed by a rotatory evaporator and the residue was washed with diethyl ether. The yellow-orange product was collected (60.0 mg, 21%). Single crystals of the compound were prepared by recrystallization of the crude product from ethanol for elemental analysis and X-ray crystallography. Elemental analysis (%) calcd. for $C_{12}H_{15.5}N_5O_{2.25}$ ($C_{12}H_{15}N_5O_2$•$0.25H_2O$): C 54.23, H 5.88, N 26.35; found: C 54.50, H 5.71, N 26.18.

References

1 C.–C. Wei, B. R. Crane and D. J. Stuehr, *Chem. Rev.*, 2003, **103**, 2365.

2 a) B. Thöny, G. Auerbach and N. Blau, *Biochem. J.*, 2000, **347**, 1; b) G. Basset, E. P. Quinlivan, M. J. Ziemak, R. Díaz de la Garza, M. Fisher, S. Schiffmann, A. Bacher, J. F. Gregory, III and A. D. Hanson, *Proc. Natl. Acad. Sci., USA*, 2002, **99**, 12489.

3 C.–C. Wei, Z.–Q. Wang,; A. S. Arvai, C. Hemann, R. Hille, E. D. Getzoff and D. J. Stuehr, *Biochemistry*, 2003, **42**, 1969.

4 Z.–Q. Wang, C.–C. Wei, S. Ghosh, A. L. Meade, C. Hemann, R. Hille and D. J. Stuehr, *Biochemistry*, 2001, **40**, 12819.

5 M. Aoyagi, A. S. Arvai, S. Ghosh, D. J. Stuehr, J. A. Tainer and E. D. Getzoff, *Biochemistry*, 2001, **40**, 12826.

6 a) S. Leimkühler, M. M. Wuebbens and K. V. Rajagopalan, *Coord. Chem. Rev.*, 2011, **255**, 1129; b) C.-C. Wei, B. R. Crane and D. J. Stuehr, *Chem. Rev.*, 2003, **103**, 2365.

7 A. C. F. Gorren, A. J. Kungl, K. Schmidt, E. R. Werner and B. Mayer, *Nitric Oxide: Biol. Chem.*, 2001, **5**, 176.

8 For Mo: a) B. Fischer, J. Strähle and M. Viscontini, *Pteridines*, 1992, **3**, 91; b) B. Fischer, H. Schmalle, E. Dubler, A. Schäfer and M. Viscontini, *Inorg. Chem.*, 1995, **34**, 5726; c) B. Fischer, H. W. Schmalle, M. R. Baumgartner and M. Viscontini, *Helv. Chim. Acta.*, 1997, **80**, 103.

9 For Mo: a) S. J. N. Burgmayer, M. R. Arkin, L. Bostick, S. Dempster, K. M. Everett, H. L. Layton, K. E. Paul, C. Rogge and A. L. Rheingold, *J. Am. Chem. Soc.*, 1995, **117**, 5812; b) H. L. Kaufmann, L. Liable-Sands, A. L. Rheingold and S. J. N. Burgmayer, *Inorg. Chem.*, 1999, **38**, 2592; c) H. L. Kaufmann, P. J. Carroll and S. J. N. Burgmayer, *Inorg. Chem.*, 1999, **38**, 2600; d) S. J. N. Burgmayer, H. L. Kaufmann, G. Fortunato, P. Hug and B. Fischer, *Inorg. Chem.*, 1999, **38**, 2607.

10 R. S. Pilato, K. A. Eriksen, M. A. Greaney, E. I. Stiefel, S. Goswami, L. Kilpatrick, T. G. Spiro and E. C. Tayler, *J. Am. Chem. Soc.*, 1991, **113**, 9372.

11 For Cu: a) T. Kohzuma, H. Masuda and O. Yamauchi, *J. Am. Chem. Soc.*, 1989, **111**, 3431; b) A. Odani, H. Masuda, K. Inukai and O. Yamauchi, *J. Am. Chem. Soc.*, 1992, **114**, 6294; c) J. Perkinson, S. Brodie, K. Yoon, K. Mosny, P. J. Carroll, T. V. Morgan and S. J. N. Burgmayer, *Inorg. Chem.*, 1991, **30**, 719; d) M. Mitsumi, J. Toyoda and K. Nakasuji, *Inorg. Chem.*, 1995, **34**, 3367; e) D. –H. Lee, N. N. Murthy, Y. Lin, N. S. Nasir and K. D. Karlin, *Inorg. Chem.*, 1997, **36**, 6328; Other metal ions: Y. Funahashi, Y. Hara, H. Masuda and O. Yamauchi, *Inorg. Chem.*, 1997, **36**, 3869.

12 A. Abelleira, R. D. Galang and M. J. Clarke, *Inorg. Chem.*, 1990, **29**, 633.

13 a) T. Kojima, T. Sakamoto, Y. Matsuda, K. Ohkubo and S. Fukuzumi, *Angew. Chem.*, 2003, **115**, 5101; *Angew. Chem., Int. Ed.*, 2003, **42**, 4951; b) S. Miyazaki, T. Kojima, T. Sakamoto, T. Mastumoto, K. Ohkubo and S. Fukuzumi, *Inorg. Chem.*, 2008, **47**, 333; c) S. Miyazaki, K. Ohkubo, T. Kojima and S. Fukuzumi, *Angew. Chem.*, 2008, **120**, 9815; *Angew. Chem., Int. Ed.*, 2008, **47**, 9669; d) S. Fukuzumi and T. Kojima, *J. Biol. Inorg. Chem.*, 2008, **13**, 321; e) S. Miyazaki, T. Kojima, J. M. Mayer and S. Fukuzumi, *J. Am. Chem. Soc.*, 2009, **131**, 11615.

14 In the ^{1}H NMR spectra of the mixtures of the nucleosides with **1**, the signals derived from the ribose moieties did not show any spectral change from those of the original spectra. Thus, the author concluded that the ribose moiety is not involved in the adduct formation with the pterin ligands.

15 Similar upfield shift in hydrogen bond formation has been reported: S. Goswami, N. K. Das, D. Sen, G. Hazra, J. H. Goh, Y. C. Sing and H.–K. Fun, *New. J. Chem.*, 2011, **35**, 2811.

16 For detail including the numbering scheme (Figure 2(a)) and a view of the crystal packing (Figure 2(b)). Crystallographic data for $C_{22}H_{34}N_{10}O_5$: monoclinic, $P2_1/a$, a = 7.681(3), b = 28.221(12), c = 11.598(5) Å, β = 104.335(6)°, V = 2511.4(18) Å^3, T = 120(2) K, Z = 4, $R1(R_w)$ = 0.0725(0.1724) ($I > 2\sigma(I)$), GOF = 0.997. CCDC 849641 contains the supplementary crystallographic data for this paper. These data can be obtained free of change from The Cambridge Crystallographic Data Centre via www.ccdc.cam.ac.uk/data_ request/cif.

17 A. J. Goodman, E. C. Breinlinger, C. M. McIntosh, L. N. Grimaldi and V. M. Rotello, *Org. Lett.*, 2001, **3**, 1531.

18 V. Verdolino, R. Cammi, B. H. Munk and H. B. Schlegel, *J. Phys. Chem. B*, 2008, **112**, 16860 and references cited therein.

19 S. Miyazaki, K. Ohkubo, T. Kojima and S. Fukuzumi, *Angew. Chem.*, 2007, **119**, 923; *Angew. Chem., Int. Ed.*, 2007, **46**, 905.

20 S. Miyazaki, T. Kojima, T. Sakamoto, T. Mastumoto, K. Ohkubo and S. Fukuzumi, *Inorg. Chem.*, 2008, **47**, 333.

21 A. Gupte and J. K. Buolamwini, *Bioorg. Med. Chem.*, 2007, **15**, 726.

22 S. Fletcher, V. M. Shahani, A. J. Lough and P. T. Gunning, *Tetrahedron*, 2010, **66**, 4621.

23 a) A. D. Becke, *J. Chem. Phys.*, 1993, **98**, 5648; b) C. Lee, W. Yang and R. G. Parr, *Phys. Rev. B*, 1988, **37**, 785.

24 W. J. Hehre, L. Radom, P. v. R. Schleyer and J. A. Pople, *Ab Initio Molecular Orbital Theory*, Wiley, New York, 1986.

25 M. J. Frisch, G. W. Trucks, H. B. Schlegel, G. E. Scuseria, M. A. Robb, J. R. Cheeseman, J. A. Montgomery, J. T. Vreven, K. N. Kudin, J. C. Burant, J. M. Millam, S. S. Iyengar, J. Tomasi, V. Barone, B. Mennucci, M. Cossi, G. Scalmani, N. Rega,; G. A. Petersson, H. Nakatsuji, M. Hada, M. Ehara, K. Toyota, R. Fukuda, J. Hasegawa, M. Ishida, T. Nakajima, Y. Honda, O. Kitao, H. Nakai, M. Klene, X. Li, J. E. Knox, H. P. Hratchian, J. B. Cross, C. Adamo, J. Jaramillo, R. Gomperts, R. E. Stratmann, O. Yazyev, A. J. Austin, R. Cammi, C. Pomelli, J. W. Ochterski, P. Y. Ayala, K. Morokuma, G. A. Voth, P. Salvador, J. J. Dannenberg, V. G. Zakrzewski, S. Dapprich, A. D. Daniels, M. C. Strain, O. Farkas, D. K. Malick,; A. D. Rabuck, K. Raghavachari, J. B. Foresman, J. V. Ortiz, Q. Cui, A. G. Baboul, S. Clifford, J. Cioslowski, B. B. Stefanov, G. Liu, A. Liashenko, P. Piskorz, I. Komaromi, R. L. Martin, D. J. Fox, T. Keith, M. A. Al-Laham, C. Y. Peng, A.

Nanayakkara, M. Challacombe, P. M. W. Gill, B. Johnson, W. Chen, M. W. Wong, C. Gonzalez and J. A. Pople, *Gaussian 03, Revision C.02,*, Gaussian, Inc., Wallingford CT, 2004.

26 R. Dennington II, T. Keith, J. Millam, K. Eppinnett, W. L. Hovell and R. Gilliland, Semichem, Inc., Shawnee Mission, KS, 2003.

27 D. C. Creagh and W. J. McAuley, *International Tables for X-ray Crystallography*, A. J. C. Wilson, Ed. Kluwer Academic Publisher, Boston, 1992, vol. **C**, Table 4.2.6.8 and 6.1.1.4.

28 J.A. Ibers and W.C. Hamilton, Dispersion corrections and crystal structure refinements. *Acta Cryst.*, 1964, **17**, 781.

29 *Yadokari-XG 2009*: Crystal Structure Analysis Package; modified by T. Nemoto, 2009, based on version 2007.5.12 (written by K. Wakita, C. Kabuto, S. Akine, T. Nemoto, E. Kwon). Release of software (Yadokari-XG 2009) for crystal structure analyses: *J. Cryst. Soc. Jpn.*, 2009, **51**, 218.

30 G. M. Sheldrick, *Acta Cryst.*, 2008, **A64**, 112.

31 D. H. Lee, N. N. Murthy, Y. Lin, N. S. Nasir and K. D. Karlin, *Inorg. Chem.*, 1997, **36**, 6328.

Chapter 3

A Tetranuclear Iridium(III) Complex Having a Flavin Analog as Bridging Ligands in Different Coordination Modes and Exchangeable Anion Encapsulation in a Supramolecular Cage

Abstract

A novel tetranuclear Ir(III) complex involving unprecedented coordination modes of alloxazine formed a closed π-space by intermolecular hydrogen bonding and the counter anions encapsulated in the space could be exchanged via self-assembly.

Introduction

Discrete multinuclear transition metal complexes have been constructed by organized accumulation of mononuclear units with use of heteroaromatic compounds as bridging ligands.[1] Those multinuclear complexes have been demonstrated to form closed inner space for inclusion of electrically neutral guest molecules.[2] To our knowledge, however, no example has been reported on construction of supramolecular assembly consisting of multinuclear metal complexes linked by non-covalent interactions to form a discrete functional space.

Heteroaromatic coenzymes, including flavins and pterins, have been known to coordinate to metal ions to form metal complexes.[3-5] Since those heteroaromatic coenzymes have several potential metal binding sites, more than two metal ions can be expected to bind to those coenzymes acting as bridging ligands. A number of mononuclear metal-coenzyme complexes have been reported to demonstrate mainly their structures and redox behavior, however, their ability acting as bridging ligands to form multinuclear metal complexes has never been demonstrated. In addition to multinucleating ability of the heteroaromatic coenzymes and their analogs as bridging ligands, it should be recognized that they have several hydrogen bonding sites.[6] Their hydrogen bonding ability has been applied to construction of supramolecular structures via self-assembly in organic chemistry.[7] However, the demonstration of discrete supramolecular structure by virtue of hydrogen bonding has yet to be explored to construct a closed π space.

Among those heteroaromatic coenzymes, flavin and its analogs have been revealed to form a five-membered chelate ring by the coordination of the 4-oxygen and the 5-nitrogen in the flavin skeleton.[5] Recently, the author has demonstrated that alloxazine (H_2Allo), which is a flavin analog, binds to a Ru(II) complex by the coordination of the 1- and 10-nitrogens to form an unusual four-membered chelate ring.[8] The discovery of this novel coordination mode has opened a way to make alloxazine act as a bridging ligand together with the traditional 4, 5-chelation.

The author reports herein the preparation and crystal structure of a novel tetranuclear iridium(III) complex bridged by three alloxazines that show two different types of bridging modes. The tetranuclear Ir(III)-alloxazine complex possesses a cavity and dimerizes to form a closed cage by intermolecular hydrogen bonding to include exchangeable anions into the cage.

Results and discussion

Synthetic procedure of the tetranuclear Ir(III)-alloxazine complex is summarized in Scheme 1. After removing chloride anions from $[Ir(Cp^*)Cl_2]_2$ by using $AgPF_6$ in CH_3CN and filtering AgCl off, the filtrate was dried up and dissolved into CH_3OH. To the solution, H_2Allo was added under N_2 and the mixture was stirred at room temperature. The purification and isolation of a mononuclear precursor, $[Ir(Cp^*)Cl(H_2Allo)]PF_6$ (**A**), was made by washing the crude product with $CHCl_3$ and the complex was obtained in 33% yield. After washing with $CHCl_3$, the ^1H NMR signal of the product, (**A**), in acetone-d_6 indicated that the compound **A** contained one kind of the Cp* ligand (Figure 1). In the ESI-MS spectrum in acetone, **A** showed a peak cluster assigned to $[Ir(Cl)(Cp^*)(H_2allo)]^+$ (*m/z* = 577.1) (Figure 2). In the IR measurement of **A** in a KBr pellet, the stretching vibration of one of C=O bonds in the alloxazine ligand shifted to a small wave number (1709 to 1600 cm^{-1}) by the metalation (Figure 3). To attain the information of the number of protons attaching to allxaozine, UV-Vis titration was conducted by adding a base (Figure 4). As the result, the spectral change occurred in two steps with two distinct isosbestic points. Thus it was revealed that the alloxazine

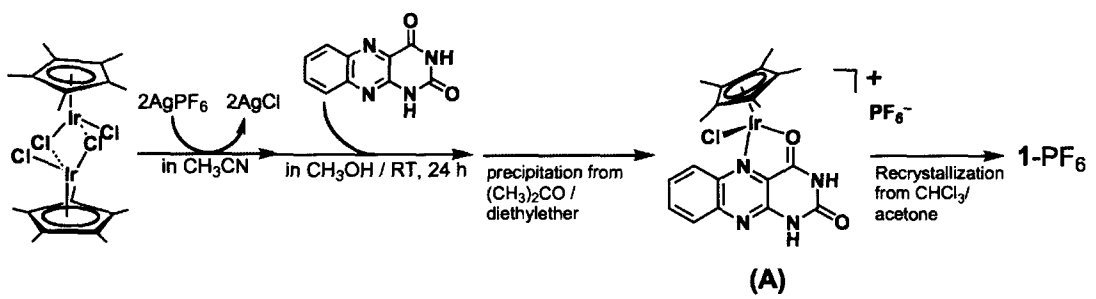

Scheme 1. Synthetic procedure of **1**-PF_6.

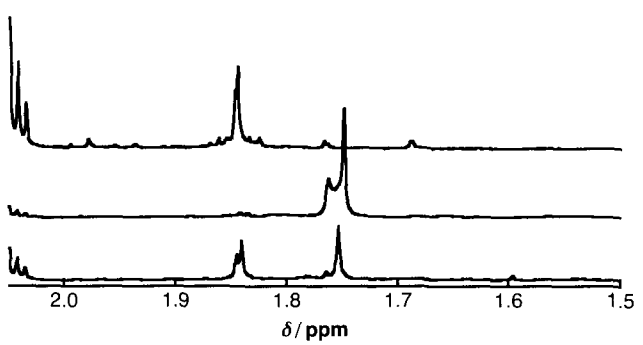

Figure 1. ^1H NMR spectrum in acetone-d_6 at RT: The crude product mixture after synthesis (lower), and the filtrate (middle) and the residue (**A**) (upper) obtained by washing $CHCl_3$.

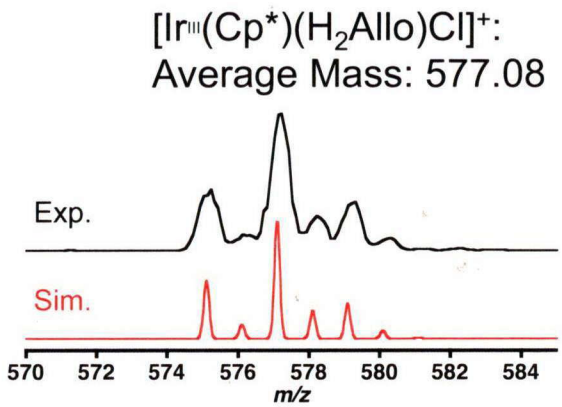

Figure 2. ESI-MS spectrum of (**A**) in acetone.

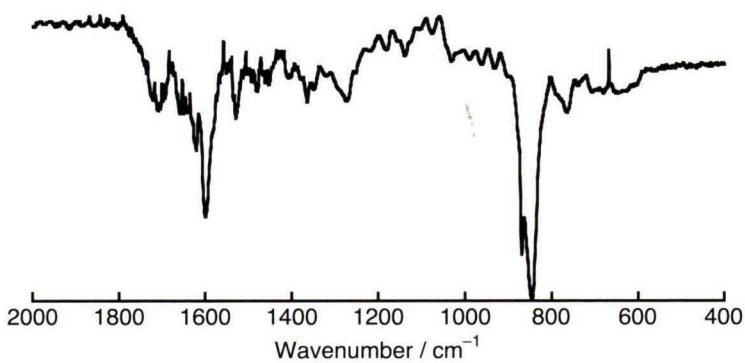

Figure 3. IR spectrum of (**A**) in a KBr pellet at room temperature.

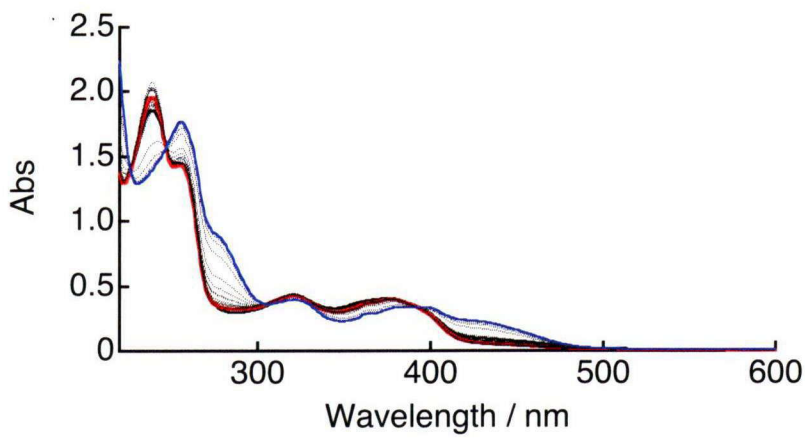

Figure 4. UV-titration of (A) (20 μM) by adding tetra-*n*-butylammonium hydroxide (TBAOH) in CH_3OH at room temperature. The red line is the spectrum after adding 2 eq of TBAOH and the blue line is the spectrum after adding 30 eq of TBAOH.

ligand in **A** should have two dissociable protons.

Recrystallization of the precursor **A** from acetone with vapor diffusion of $CHCl_3$ gave red crystals of the tetranuclear Ir(III)-alloxazine complex, $[Ir_4(Allo)(Cp^*)_4(Hallo)_2Cl_2](PF_6)_2$ (**1**-PF_6). In the ^1H NMR measurements in acetone-d_6, one singlet was observed for **A** at 1.84 ppm and, in contrast, four singlet signals were detected for **1**-PF_6 at 1.27, 1.46, 1.69, and 1.98 ppm, indicating the existence of four inequivalent Cp* moieties (Figure 5).

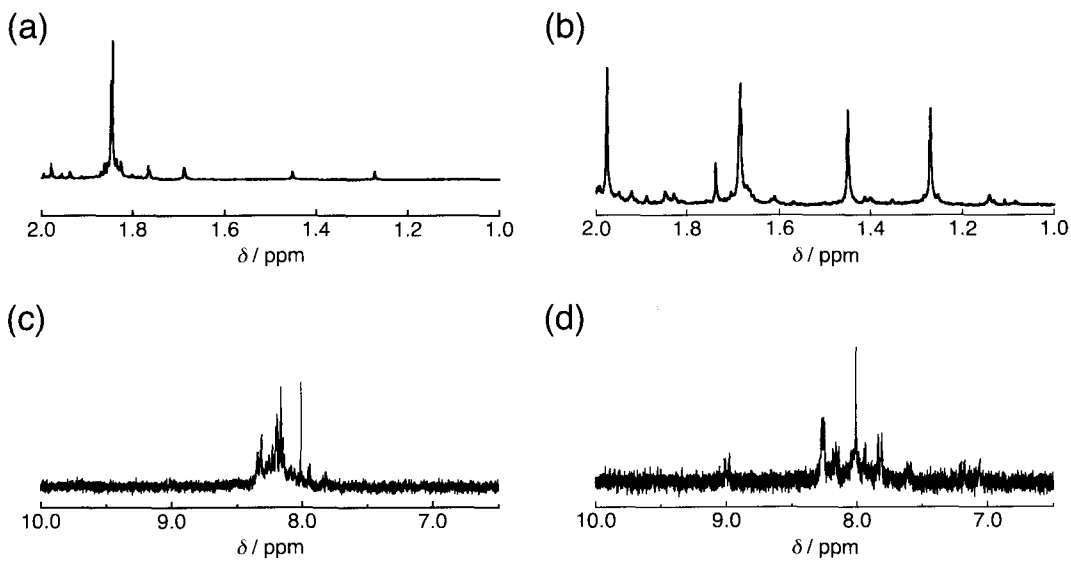

Figure 5. ^1H NMR spectrum of (**A**) (the Cp* part (a) and the alloxazine part (c)) and that of the tetranuclear iridium complex obtained by recrystallization of **A** (the Cp* part (b) and the alloxazine part (d)) in acetone at room temperature.

The tetranuclear Ir(III) complex **1**-PF_6 was crystallized in the monoclinic space group of *C*2/*c*.[9] The crystal structure of the cation moiety of **1**-PF_6 is depicted in Figure 6(a) with thermal ellipsoids at the 50% probability level. Selected bond lengths are listed in the figure caption. The four Ir(III)-Cp* units including two terminal and two hinge moieties are seen to be linked by three alloxazine ligands to form a U-shaped structure. The most striking feature of this complex is two different bridging modes of the alloxazine ligands. The two hinge [Ir(Cp*)] units are linked by di-deprotonated dianion, $Allo^{2-}$, via the 4,5-bidenntate coordination mode for Ir2 and the 1,10-bidentate mode for Ir4. In this case the $Allo^{2-}$ ligand is in a μ:η^2,η^2-fashion. The two alloxazine ligands are deprotonated to be a monoanion, $Hallo^-$, to bind to the terminal [Ir(Cp*)Cl] (Ir1 and Ir3) unit via the 4,5-bidentate mode and to the hinge [Ir(Cp*)] unit (Ir2 or Ir4)

via the 3-monodentate mode. In this case, the Hallo$^-$ ligand is in a μ:η^1,η^2-fashion. In the crystal, one of the counter PF_6^- anions was included in the U-shaped cavity and the

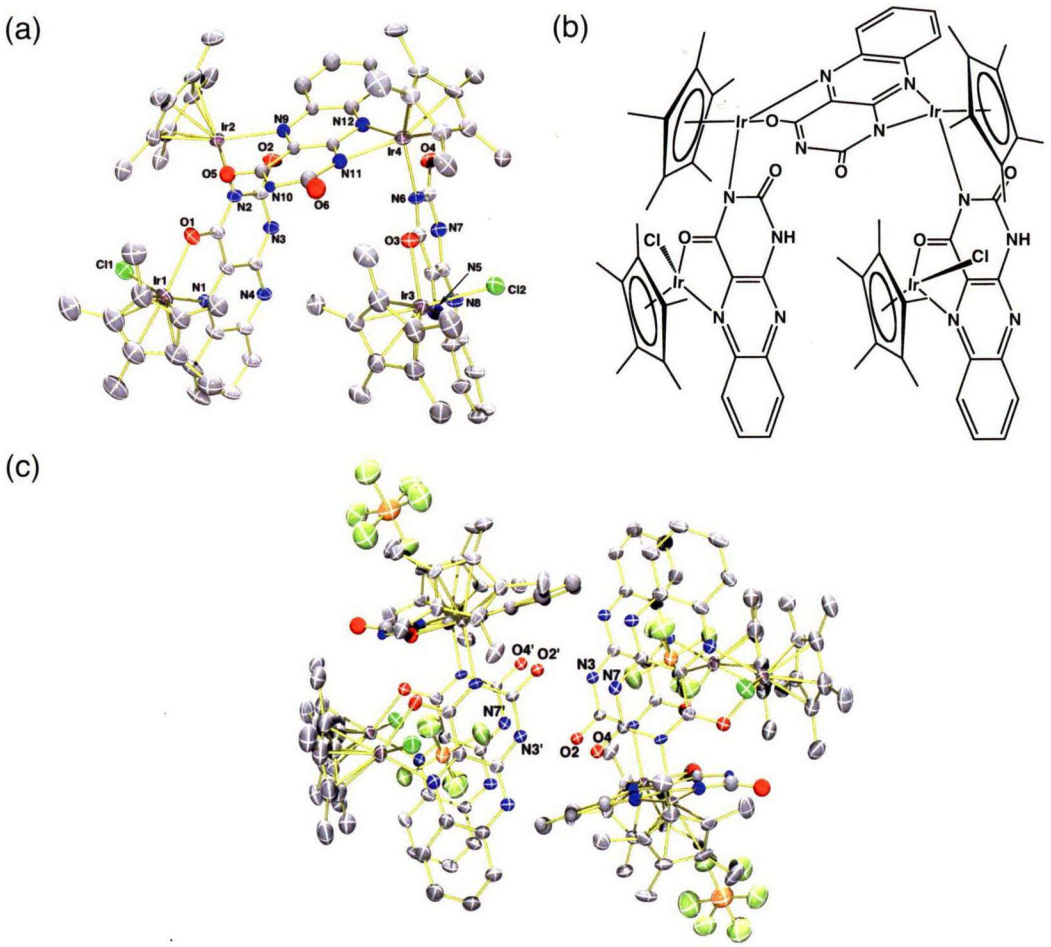

Figure 6. a) Crystal structure of the cation moiety of **1**-PF_6. Light gray carbon, blue nitrogen, red oxygen, light green chlorine, purple iridium. Hydrogen atoms are omitted for clarity. Selected bond lengths (Å) and angles (deg): Ir1-Cl1 2.375(3), Ir1-O1 2.155(7), Ir1-N1 2.119(9), Ir2-N2 2.121(7), Ir2-O5 2.224(7), Ir2-N9 2.284(5), Ir3-Cl2 2.387(3), Ir3-O3 2.154(7), Ir3-N5 2.119(8), Ir4-N6 2.140(7), Ir4-N11 2.135(6), Ir4-N12 2.157(6); O1-Ir1-N1 77.0(3), O5-Ir2-N9 72.70(15), O3-Ir3-N5 76.8(3), N11-Ir4-N12 65.51(13). b) A schematic description of the tetranuclear structure. c) A dimeric structure in the crystal. Two PF_6^- anions are encapsulated in the cage. Phosphorus orange, fluorine yellow green.

other was located outside of the cavity, just above the μ:η^2,η^2-Allo^{2-} bridging ligand (Figure 6(c)). Moreover, the two of the adjacent tetranuclear complexes form intermolecular hydrogen bonds for O2•••N7' (2.808 Å) and N3•••O4' (2.804 Å), resulting in supramolecular dimerization to form a closed cage including two PF_6^- anions as shown in Figure 6(c). The inner space is surrounded by six alloxazine molecules to be a π-space and the size of the space can be estimated to be 9 × 8 × 17 Å^3. It is noteworthy that the anion encapsulation of **1** does not involve hydrogen bonding as observed anion binding systems reported so far.[10]

The author also examined the exchange of confined counter anions in the cavity. The single crystals of **1**-PF_6 were dissolved into methanol and 20-fold excess amount of [(*n*-butyl)$_4$N]ClO_4 was added to the solution. Crystallization was made from an acetone solution with vapor diffusion of $CHCl_3$ to obtain again red crystals. This result indicates that PF_6^- ions in **1**-PF_6 are completely replaced by ClO_4^- ions. X-ray crystallographic analysis revealed the crystal structure of a ClO_4^--included tetranuclear Ir(III)-alloxazine complex as shown in Figure 7 with thermal ellipsoids at the 50% probability level.[9] The complex, [Ir$_4$(Allo)(Hallo)$_2$-(Cp*)$_4$Cl$_2$](ClO_4)$_2$ (**1**-ClO_4), exhibited the same structure as that of **1**-PF_6 in the tetragonal space group of $I4_1/a$, which was different from that of **1**-PF_6. Thus, the author can conclude that the confined anion species can be exchanged without losing the tetranuclear structural motif.

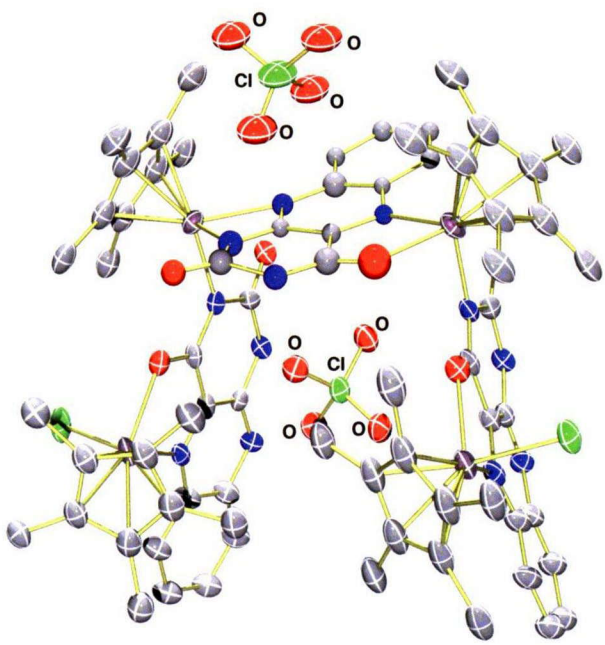

Figure 7. Crystal structure of **1**-ClO_4. Purple iridium, green chlorine, red oxygen, blue nitrogen, grey carbon.

Table 1. Crystallographic Data for **1**-PF_6 and **1**-ClO_4

	1-PF_6	**1**-ClO_4
formula	$C_{74.5}H_{82.5}Cl_{15.5}F_{12}Ir_4N_{12}O_8P_2$	$C_{73.5}H_{77.5}Cl_{14.5}Ir_4N_{12}O_{12}$
fw	2882.38	2635.94
crystal system	monoclinic	tetragonal
space group	*C*2/*c*	$I4_1/a$
a, Å	31.4226(7)	27.1659(9)
b, Å	24.4702(5)	27.1659(9)
c, Å	34.0543(8)	60.542(1)
β, deg	122.6940(7)	
V, Å^3	22036.3(8)	44679(2)
Z	8	16
d_{calc}, g cm^{-1}	1.737	1.567
T, °C	−150	−150
no. of observn	25019	20165
no. of variants	1048	852
*R*1 ($I > 2\sigma(I)$)[a]	0.0778	0.1078
wR[b,c]	0.2292	0.3517
GOF	10.58	1.346
CCDC no.	726570	729384

[a] $R1 = \Sigma \, ||F_o| - |F_c|| \, / \, \Sigma \, |F_o|$. [b] $Rw = [\Sigma(w(F_o^2 - F_c^2)^2) \, / \, \Sigma w(F_o^2)^2]^{1/2}$. [c] $w = 1 \, / \, [\sigma^2(F_o^2) + (0.0500 \cdot P)^2 + 30.0000 \cdot P$, where $P = (\mathrm{Max}(F_o^2, 0) + 2F_c^2) \, / \, 3$.

The infrared spectrum of the crystals exhibited a strong absorption due to the Cl-O stretching mode of ClO_4^- at ~1100 cm^{-1} with overlap of signals derived from the alloxazine units and no peak assigned to that of P-F bond in PF_6^- at 845 cm^{-1} (Figure 8).

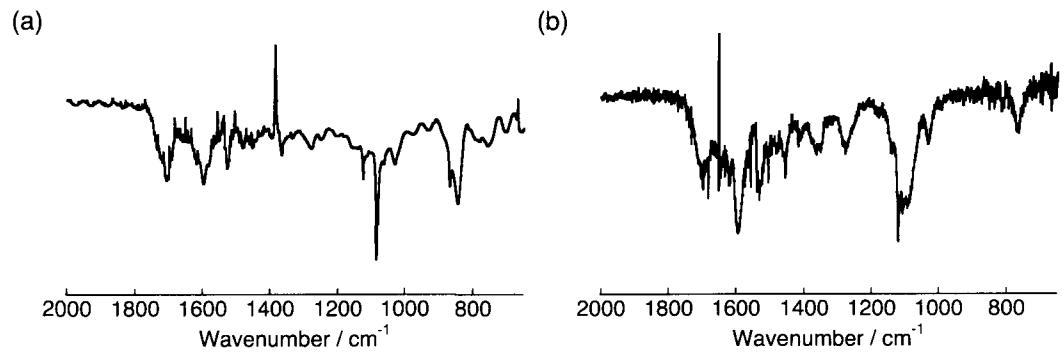

Figure 8. IR spectra of **1**-PF_6 (a) and **1**-ClO_4 (b) measured in KBr pellets at room temperature.

In order to shed some lights on the exchange mechanism for the confined anions, the author examined the solution behavior of **1**-PF_6 in acetone by spectroscopic methods. The author observed the fragmentation of the tetranuclear form in acetone by ^1H NMR and ESI-MS spectroscopies. The ESI-MS spectroscopic measurements allowed us to observe peak clusters which were assignable to those of $[Ir(Cp^*)Cl]^+$ (362.9), $[Ir(Cp^*)(HAllo)]^+$ (540.6), $[\{Ir(Cp^*)\}_2(Allo)\text{-}Cl]^+$ (902.5), $[\{Ir(Cp^*)\}_2(Hallo)_2Cl]^+$ (1116.7), $[\{Ir(Cp^*)\}_3(Allo)\text{-}(Hallo)Cl_2]^+$ (1478.6), and $[\{Ir(Cp^*)\}_4(Allo)_2(Hallo)Cl_2]^+$ ($[M\text{-}H^+]^+$, 2018.2), just after dissolving the crystals of **1**-PF_6 into acetone (Figure 9).

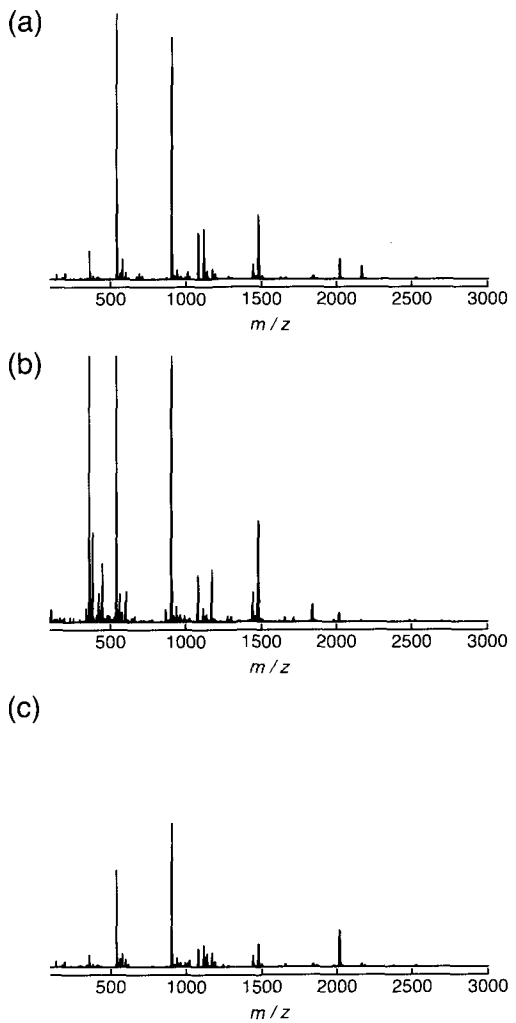

Figure 9. ESI-MS spectra of **1**-PF_6 just after dissolving into acetone (a), 24h later after dissolving crystals of **1**-PF_6 into acetone (b), and recrystallized sample of **1**-PF_6 just after dissolving into acetone.

After 24h, the peak cluster due to the $[M\text{-}H^+]^+$ ion disappeared, however, other peaks were still observed with increased intensity for the peaks attributed to $[Ir(Cp^*)Cl]^+$. Finally, the author could recover the same ESI-MS spectrum as that of the original **1**-PF_6 for the recrystallized sample from the same acetone solution with vapor diffusion of $CHCl_3$. Thus, the author concludes that the PF_6^- counter anion in the cavity of the tetranuclear unit can be exchanged via fragmentation and self-organization (Scheme 2).

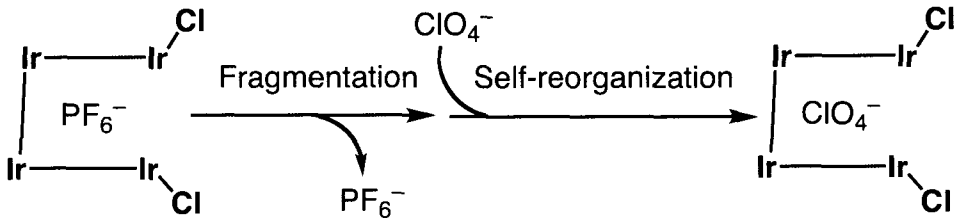

Scheme 2. Exchange mechanism of a confined counter anion in the U-shaped tetranuclear unit.

Summary

In summary, the author prepared a novel tetranuclear motif based on Ir(III)-Cp* units with use of alloxazine, a flavin analog, as a bridging ligand. The tetranuclear Ir(III) complex involves unprecedented coordination modes of alloxazine to link the Ir(III) centers to give rise to a U-shaped structure with a cavity for inclusion of a counter anion. The alloxazine ligands also undergo intermolecular hydrogen bonding to form a supramolecular dimeric structure with a closed π-space that can encapsulate two of counter anions. The confined anions can be exchanged by self-reorganization through the fragmentation process to release the originally entrapped anions. The findings described here have provided a strategy for the construction of integrated metal-coenzyme complexes and their new functionality involving exchangeable anion encapsulation via self-reorganization.

Experimental section

Materials and Methods. $CHCl_3$, CH_3OH, acetone, 1,2–diethylether (Wako Pure Chemical Industries), 1,2,3,4,5-pentamethylcyclopentadiene (KANATO CHEMICAL Co., Inc.) were used without further purification. Acetone–d_6 were purchased from Cambridge Isotope Laboratories, Inc. IrH_2Cl_4 was purchased from Tanaka Kikinzoku.

CH_3CN (Wako Pure Chemical Industries) was purified by distilled over CaH_2. Alloxazine was synthesized according to a literature method.[11]

Apparatus. ^1H NMR spectra were measured on a JEOL JMN–AL 300 spectrometer. UV–vis absorption spectra were recorded on a Hewlett–Packard HP8453 diode array spectrophotometer at room temperature. ESI–MS spectra were measured on a Perkin–Elmer API–150 EX spectrometer. Infrared spectra were recorded on Thermo Nicolet Nexus 870 FT–IR spectrometer.

X–ray Crystallography. All X–ray measurement were made on a Rigaku/MSC Mercury CCD diffractometer with graphite–monochromated Mo K*a* radiation (*l* = 0.71075 Å) at –150 °C and the data were processed using *CrystalClear* program (Rigaku Corp.).[12]

For both **1**-PF_6 and **1**-ClO_4, the structures were solved by direct methods (SIR 97 and SHELXS 97)[13] and refined by full-matrix least-squares method on F^2 by using *CrystalStructure* program package.[14] All non-hydrogen atoms were refined anisotropically. Crystallographic data are summarized in Table 1. For **1**-ClO_4, one of the ligands, bridged between Ir2 and Ir4, could be resolved with two disordered moieties, which were treated as rigid groups. The atoms in the disordered portions were heavily superimposed, so that they were refined isotropically. All the chloroforms were disordered with site occupancy of 0.5.

Synthesis

1-PF_6. To a suspension of $[IrCl_2(Cp^*)]_2$ (161 mg, 0.20 mmol) in acetonitrile (20 ml), was added $AgPF_6$ (103 mg, 0.41 mmol). After 30 min of stirring at RT, the white precipitate of AgCl was filtered off through a Celite pad and yellow powder was obtained by removing acetonitrile. After dissolving the yellow powder into methanol (30 ml), alloxazine (87.8 mg, 0.41 mmol) was added to the solution under Ar. The mixture was stirred for 24 h at RT and then the solvent was removed by a rotary evaporator. The residue was dissolved in a small volume of acetone and the solution was filtered and then orange powder precipitated by adding a large amount of diethyl ether to the filtrate. The orange powder was stirred overnight in chloroform. After that the orange precipitate of $[Ir(Cp^*)(Hallo)Cl]PF_6$ (**A**) was collected by filtration, washed with chloroform and then dried in vacuo (yield: 33%). Elemental analysis (%) calcd for $C_{20.5}H_{21.5}O_2N_4IrCl_{2.5}PF_6$(**A**·0.5($CHCl_3$)): C 31.50, H 2.77, N 7.17; found: C 31.80, H 2.94, N 6.62.

The precursor complex **A** was dissolved into acetone and vapor diffusion of $CHCl_3$ into the solution gave crude crystalline **1**-PF_6, which was contaminated by alloxazine.

This crude product was dissolved into acetone and the solution was filtered to remove alloxazine. To the solution, $CHCl_3$ vapor was diffused again to obtain red single crystals of **1**-PF_6. Elemental analysis (%) calcd for $C_{73}H_{81}N_{12}O_8Cl_{11}P_2F_{12}Ir_4$ (**1**-PF_6•3$CHCl_3$•2H_2O): C 32.43, H 3.02, N 6.22; found: C 32.40, H 2.97, N 6.30. Absorption maxima in acetone (λ_{max}, nm (ε, M^{-1} cm^{-1})): 358 (2.4×10^4), 400 (2.4×10^4), 455 and 535 (shoulder).

1-ClO_4. The single crystals of **1**-PF_6 were dissolved into methanol and 20-fold excess amount of [(*n*-butyl)$_4$N]ClO_4 was added to the solution. Crystallization was made from an acetone solution with vapor diffusion of $CHCl_3$ to obtain again red crystals. Elemental analysis (%) calcd for $C_{72.5}H_{76.5}N_{12}O_{14}Cl_{11.5}Ir_4$ (**1**-ClO_4•2.5$CHCl_3$): C 34.60, H 3.06, N 6.68; found: C 34.60, H 3.16, N 6.89.

References

1 a) M. Tominaga, K. Suzuki, M. Kawano, T. Kusukawa, T. Ozeki, S. Sakamoto, K. Yamaguchi and M. Fujita, *Angew. Chem., Int. Ed.,* 2004, **43**, 5621; b) M. Fujita, J. Yazaki and K. Ogura, *J. Am. Chem. Soc.,* 1990, **112**, 5645.

2 a) Y. Yamauchi, M. Yoshizawa and M. Fujita, *J. Am. Chem. Soc.*, 2008, **130**, 5832; b) S. Sato, J. Iida, K. Suzuki, M. Kawano, T. Ozeki and M. Fujita, *Science*, 2006, **313**, 1273; c) P. J. Steel, *Acc. Chem. Res.*, 2005, **38**, 243; d) S. Hiraoka, K. Harano, M. Shiro and M. Shionoya, *Angew. Chem., Int. Ed.*, 2005, **44**, 2727; e) K. Nakabayashi, M. Kawano and M. Fujita, *Angew. Chem., Int. Ed.*, 2005, **44**, 5322; f) S. Tashiro, M. Tominaga, M. Kawano, B. Therrien, T. Ozeki and M. Fujita, *J. Am. Chem. Soc.*, 2005, **127**, 4546; g) A. H. Mahmoudkhani, A. P. Côté and G. K. H. Shimizu, *Chem. Commun.,* 2004, 2678.

3 a) W. Kaim, B. Schwederski, O. Heilmann and F. M. Hornung, *Coord. Chem. Rev.*, 1999, **182**, 323; b) S. J. N. Burgmayer, *Struct. Bonding.*, 1998, **92**, 67.

4 Pterins: a) T. Kohzuma, H. Masuda and O. Yamauchi, *J. Am. Chem. Soc.*, 1989, **111**, 3431; b) J. Perkinson, S. Brodie, K. Mosny, P. J. Carroll, T. V. Morgan and S. J. N. Burgmayer, *Inorg. Chem.*, 1991, **30**, 719; c) A. Odani, H. Masuda, K. Inukai and O. Yamauchi, *J. Am. Chem. Soc.,* 1992, **114**, 6294; d) A. Abelleira, R. D. Galang and M. J. Clarke, *Inorg. Chem.,* 1990, **29**, 633; e) C. Bessenbacher, C. Vogler and W. Kaim, *Inorg. Chem.,* 1989, **28**, 4645; f) T. Kojima, T. Sakamoto, K. Ohkubo, S. Fukuzumi and Y. Matsuda, *Angew. Chem., Int. Ed.*, 2003, **42**, 4951; g) S. Miyazaki, T. Kojima, T. Sakamoto, T. Matsumoto, K. Ohkubo and S. Fukuzumi, *Inorg. Chem.*, 2008, **47**, 333; h) S. Miyazaki, K. Ohkubo, T. Kojima and S. Fukuzumi, *Angew. Chem., Int. Ed.*, 2008, **47**, 9669.

5 Flavins: a) M. J. Clarke, M. G. Dowling, A. R. Garafalo and T. F. Brennan, *J. Biol. Chem.*, 1980, **255**, 3472; b) F. M. Hornung, O. Heilmann, W. Kaim, S. Zalis and J. Fiedler, *Inorg. Chem.*, 2000, **39**, 4052; c) O. Heilmann, F. M. Hornung, W. Kaim and J. Fiedler, *J. Chem. Soc., Faraday Trans.*, 1996, **92**, 4233; d) M. G. Dowling and M. J. Clarke, *Inorg. Chim. Acta.*, 1983, **78**, 153; e) M. J. Clarke and M. G. Dowling, *Inorg. Chem.*, 1981, **20**, 3506; f) S. Fukuzumi and T. Kojima, *J. Bioinog. Chem.*, 2008, **13**, 321.

6 a) A. Niemz and V. M. Rotello, *Acc. Chem. Res.*, 1999, **32**, 44; b) E. Breinlinger, A. Niemz and V. M. Rotello, *J. Am. Chem. Soc.*, 1995, **117**, 5379; c) A. Niemz and V. M. Rotello, *J. Mol. Recog.*, 1996, **9**, 158; d) A. Niemz and V. M. Rotello, *J. Am. Chem. Soc.*, 1997, **119**, 6833.

7 a) Y. Kamikawa, M. Nishii and T. Kato, *Chem.–Eur. J.*, 2004, **10**, 5942; b) T. Kato, T. Matsuoka, M. Nishii, Y. Kamikawa, K. Kanie, T. Nishimura, E. Yashima and S. Ujiie, *Angew. Chem., Int. Ed.*, 2004, **43**, 1969.

8 a) S. Miyazaki, K. Ohkubo, T. Kojima and S. Fukuzumi, *Angew. Chem., Int. Ed.*, 2007, **46**, 905; b) S. Miyazaki, T. Kojima and S. Fukuzumi, *J. Am. Chem. Soc.*, 2008, **130**, 1556.

9 a) Crystal data for **1**-PF_6: monoclinic, *C*2/*c*, (No. 15), a = 31.4226(7), b = 24.4702(5), c = 34.0543(8) Å, b = 122.6940(7)°, V = 22036.3(8) Å^3, Z = 8, $R1(R_w)$ = 0.078(0.229) ($I > 2\sigma(I)$), GOF = 1.06; b) Crystal data for **1**-ClO_4: tetragonal, $I4_1/a$, (No. 88), $a = b$ = 27.1659(9), c = 60.5418(11) Å, V = 44679(2) Å^3, Z = 16, $R1(R_w)$ = 0.104(0.340) ($I > 2\sigma(I)$), GOF = 1.30. CCDC-726570 (**1**-PF_6) and CCDC-729384 (**1**-ClO_4) contain the supplementary crystallographic data for this paper. These data can be obtained free of charge from The Cambridge Crystallographic Data Centre via www.ccdc.cam.ac.uk/data_request/cif.

10 a) M. P. Wintergerst, T. G. Levitskaia, B. A. Moyer, J. L. Sessler and L. H. Delmau, *J. Am. Chem. Soc.*, 2008, **130**, 4129; b) J. Pérez, L. Riera, *Chem. Soc. Rev.*, 2008, **37**, 2658; c) P. D. Beer and P. A. Gale, *Angew. Chem., Int. Ed.*, 2001, **40**, 486; d) J. L. Sessler and J. M. Davis, *Acc. Chem. Res.*, 2001, **34**, 989.

11 H. G. Petering and G. J. van Giessen, *J. Org. Chem.*, 1961, **26**, 2818.

12 *CrystalClear 1.3.5* SP2: Rigaku,1998–2003

13 G. M. Sheldrick, *SIR 97* and *SHELX 97, Programs for Crystal Structure Refinement*; University of Göttingen, Göttingen, Germany, 1997.

14 *CrystalStructure 3.8.2*: Crystal Structure Analysis Package, Rigaku and Rigaku/MSC, The Woodlands, TX, 2000-2008.

Chapter 4

A Triangular Prismatic Hexanuclear Iridium(III) Complex Bridged by Flavin Analogues Showing Reversible Six-Electron Redox Processes

Abstract

$[Ir_6(alloCl_2^{2-})_3(Cp^*)_6(OH)_3](PF_6)_3$ (complex 1) which has a novel coordination mode was synthesized and characterized the crystal structure by X-ray analysis. The complex indicated the reversible six-electron redox process on alloxazine ligands in the organic solvent; an alloxazine can be reduced by two-electron. First reduction processes on each of three alloxazine ligands in 1 to $[Ir^{III}{}_6Cp^*{}_6(\mu\text{-}alloCl_2^{\bullet 3-})_3(OH)_3]$ occurred at very near reduction potentials, such as one-step reduction process, -0.65 V (vs $Fc^{0/+}$). And also second reduction processes on each of three alloxazine ligands in 1 were recorded in almost same reduction potential, -0.78 V (vs $Fc^{0/+}$), and the multi-electron reduced form, $[Ir^{III}{}_6Cp^*{}_6(\mu\text{-}alloCl_2^{4-})_3(OH)_3]^{3-}$, was obtained. This *organic metal* in solution could act as an electron pool due to the reversibility of the redox process; by the UV-Vis measurement, the reduction process of 1 was traced with cobaltocene, and the oxidation process of reduced form was underwent with *p*-chloranil. The radical anion of alloxazine derivative was detected by the EPR measurement.

Introduction

In nature, multi-electron redox reactions are found in important biological processes including water oxidation at the oxygen evolving complex in photosystem II[1] and nitrogen fixation by nitrogenase.[2] In the former case, proton-coupled four-electron oxidation of water to afford dioxygen is performed at a tetranuclear manganese-oxo cluster.[3] In the latter, proton-coupled six-electron reduction of dinitrogen is conducted at the iron-molybdenum-cofactor, which is an iron-sulfur cluster with one molybdenum centre, to form ammonia.[4] In each case, the multinulclear metal cluster manipulates the multi-electron redox reaction as the redox-active site. Synthetic metal clusters having bridging ligands have also demonstrated reversible multi-electron redox processes, in which mixed-valence species are often involved.[5] In those metal clusters, redox processes usually occur stepwise due to strong interactions among metal centers.[5] Redox reactions of the bridging ligands in metal clusters, however, have not yet to be much explored.[6]

Organic molecules often exhibit ill-reversible redox behaviour due to their large structural change in the course of the redox processes. For example, heteroaromatic coenzymes such as flavins[7] and pterins[8] mainly manipulate two-electron processes, although they show irreversible redox behaviour *in vitro*. The metal coordination of the coenzymes mentioned above makes their redox processes reversible by stabilization of radical intermediates involved in the redox processes.[9-11] In spite of their rich redox chemistry, the redox-active heteroaromatic coenzymes have not been applied as bridging ligands to form metal clusters exhibiting multi-electron redox processes.

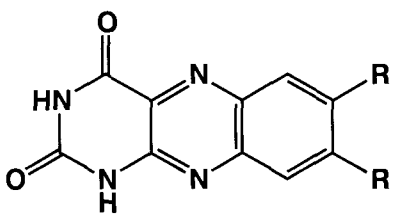

R = H : Alloxazine (H_2allo)
R = Cl: 7,8-dichloroalloxazine ($H_2alloCl_2$)

Figure 1. Structures of alloxazine derivatives.

As a strategy to converge redox-active heteroaromatic coenzymes, the author adopted alloxazines (Figure 1) as flavin analogues performing stepwise two-electron redox processes and the stable and redox-innocent iridium(III)-Cp* unit (Cp* =

pentamethylcyclopentadienyl anion) as a platform to form Ir(III)-alloxazine complexes. The author has reported that alloxazine forms a tetranuclear Ir(III) complex, in which alloxazine (H_2allo) acts as a bridging ligand, however, the tetranuclear complex having allo^{2-} as bridging ligands is unstable to undergo fragmentation in solution.[12] The instability of the tetranuclear complex has precluded to examine the redox process in solution. Therefore, in this work, the author has employed 7,8-dichloroalloxazine ($H_2alloCl_2$) as a bridging ligand to attain a stable multinuclear Ir(III)-Cp* complex on the basis of its better π-accepting character, i.e. the lower LUMO level, than H_2allo to enhance π-back bonding from the Ir(III) centre (Figure 2). The author reports herein the synthesis, characterization, and redox behaviour of a unique hexanuclear prismatic Ir(III) complex having three deprotonated $H_2alloCl_2$, $alloCl_2^{2-}$, as bridging ligands. The complex exhibits excellent stability in solution, making it possible to examine the multi-electron redox processes.

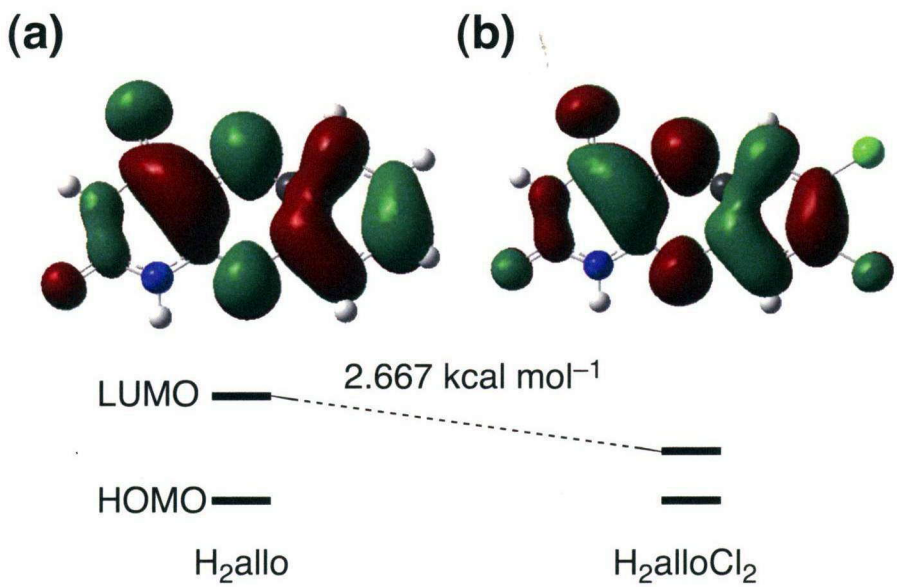

Figure 2. LUMO orbitals of H_2allo (a) and $H_2alloCl_2$ obtained by DFT calculations at the B3LYP/6-31G level of theory. The energy level of LUMO ($H_2alloCl_2$) was lower than that of LUMO (H_2allo) by 2.667 kcal mol^{-1}.

Result and discussion

A novel hexanuclear Ir(III) complex was synthesized by the procedure described in Scheme 1. After the removal of the chloride ligands of a dinuclear bis-μ-chloro Ir(III) complex, $[Ir(Cp^*)Cl_2]_2$, by $AgPF_6$ in methanol, $H_2alloCl_2$ was added to the solution

under Ar. The mixture was stirred for 16 h at reflux. After cooling to room temperature, the reaction mixture was filtered and orange powder precipitated by adding a large amount of diethyl ether to the filtrate. The orange precipitate was recrystallized from 2-propanol to purify, and finally, the red crystal of **1** was obtained in 12% yield.

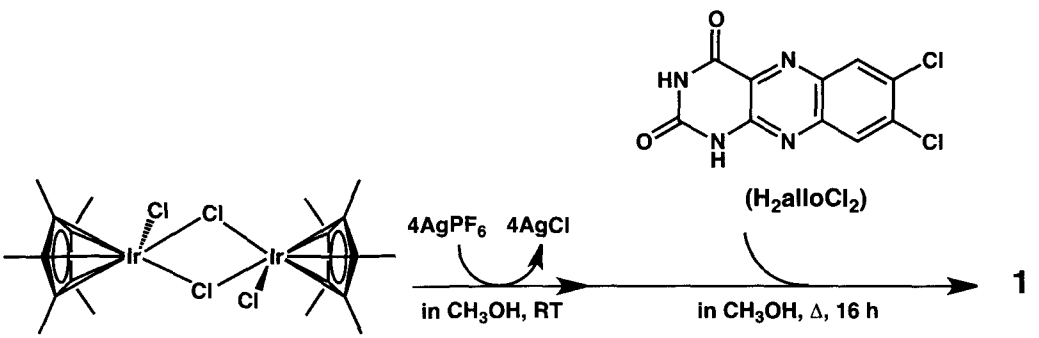

Scheme 1. Synthetic procedure of **1**.

The crystal structure of $[Ir_6(alloCl_2)_3(Cp^*)_6(OH)_3](PF_6)_3$ (**1**) is shown in Figure 3.[13] The crystal system was trigonal and the space group was *R3c*. As can be seen in the Figure 3(a), the hexanuclear complex shows a three-fold symmetric structure. In Figure 3(b), the structure of the $Ir_6(alloCl_2)_3$ core is presented by omitting the Cp* ligands and PF_6^- counter anions for clarity. Each alloxazine ligand coordinates to three Ir(III) ions in a μ_3-η^1:η^2:η^2-fashion. The complex includes a triangle-pole π-space surrounded by alloxazine ligands, and the maximum distance between the alloxazine ligands is 3.5 Å. This indicates that there are intramolecular π-π interactions to stabilize the structure.[14] Two protons at 1–N*H* and 3–N*H* of $H_2alloCl_2$ are deprotonated to be a dianion and replaced by Ir(III) ions. The bond lengths for the Ir1 centre having the monodentate N1 nitrogen (labeled as N3) of $alloCl_2^{2-}$ and a five-membered chelate ring involving N4 (labeled as N1) and O5 (labeled as O1) positions were determined to be 2.16(4) (Ir1-N3), 2.17(3) (Ir1-N1), and 2.14(4) Å (Ir1-O1), respectively. As for the Ir2 centre having a four-membered chelate ring consisting of the N3 (labeled as N2) and O2 (labeled as O2) positions of the alloxazine ligand, the bond lengths of Ir1-N2 and Ir2-O2 were determined to be 1.98(3) and 2.22(4) Å with the bond angle of O2-Ir2-N2 to be 60.6(12)°, respectively. In addition, the complex **1** contains three OH^- ligands: The bond distance of Ir-OH (Ir-O3 in Figure 3(a)) was 2.13(4) Å. The three OH^- ligands form strong intramolecular hydrogen bonding, with the distance of 2.66 Å, which also contributes to stabilize the hexanuclear prismatic structure of **1**.

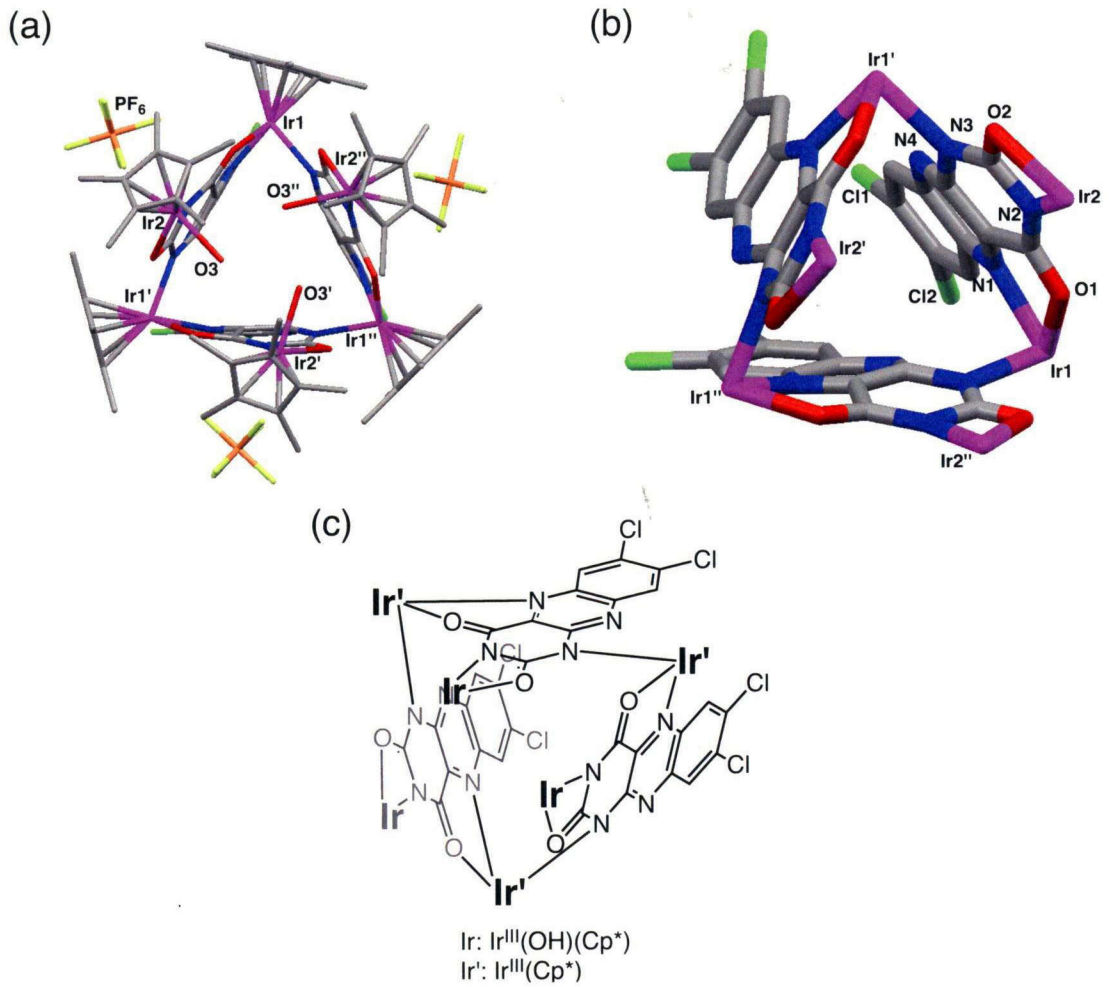

Figure 3. Stick description of crystal structure of **1**. (a) A view of the hexanuclear structure from the three-fold axis. (b) A view of the $\{Ir_6(alloCl_2)_3\}$ core; the Cp* ligands and the OH ligands on the Ir2 centers are omitted for clarity. (c) A schematic description of the hexanuclear core structure of **1**.

Table 1. X-ray crystallographic data for **1**•PF_6.

formula	$C_{90}H_{99}Cl_6F_{18}Ir_6N_{12}O_9P_3$
fw	3293.78
crystal system	trigonal
space group	*R*3*c*
T (K)	123
a (Å)	16.0783(6)
c (Å)	74.528(6)
V (Å^3)	16685.1(15)
Z	6
no. of reflections measured	31593
no. of observations	2214
no. of parameters refined	211
$R1$ [a]	0.0965
R_W [b,c]	0.2415 ($I > 2.0\sigma(I)$)
GOF	1.092
CCDC no.	888985

[a] $R1 = \Sigma \, ||Fo| - |Fc|| \, / \, \Sigma \, |Fo|$. [b] $Rw = [\, \Sigma \, (w \, (F_0^2 - F_c^2)^2) \, / \, \Sigma \, w(F_0^2)^2]^{1/2}$. [c] $w = 1 \, / \, [\sigma^2(F_0^2) + (0.1361P)^2 + 1691.4005P]$, where $P = (\mathrm{Max}(F_0^2, 0) + 2F_c^2) \, / \, 3$

Table 2. Selected bond lengths (Å) and angles (deg) of **1**

Ir1 – O1	2.14(4)	N1 – Ir1 – O1	72.5(11)
Ir1 – N1	2.17(3)	N1 –Ir1 – N3	87.1(14)
Ir2 – N2	1.98(3)	O1– Ir1 – N3	82.7(13)
Ir2 – O2	2.22(4)	Ir1 – O1 – C12	119 (3)
Ir2 – O3	2.13(4)	Ir1 – N1 – C11	111.7(17)
Ir1 – N3	2.16(2)	Ir1 – N3 – C13	118.1(18)
O1 – C12	1.23(4)	Ir1 – N3 – C14	121 (2)
N1 – C11	1.35(4)	O1 – C12 – C11	116 (3)
N1 – C20	1.35(4)	N1 – C11 – C12	116(2)
N2 – C12	1.39(5)	N2 – Ir2 – O2	60.6(12)
N2 – C13	1.39(4)	N2 – Ir2 – O3	91.0(13)
O2 – C13	1.10(5)	Ir2 – N2 – C13	92.3(19)
N3 – C13	1.39(5)	Ir2 – O2 – C13	89(3)
N3 – C14	1.39(5)	O2 – C13 – N2	118(3)
N4 – C14	1.35(4)	O2 – C13 – N3	122(3)
N4 – C15	1.35(4)		
C11 – C12	1.39(5)		

The stabilization of the hexanuclear structure of **1** in organic solvents was confirmed by diffusion-ordered NMR spectroscopy (DOSY) measurements in CD_2Cl_2. The diffusion coefficient of **1** estimated from the DOSY spectrum (Figure 4) was 7.6 – 7.7 x 10^{-10} m^2 s^{-1}. On the basis of the result, the excluded volume of the molecule was calculated to be 1.4 x 10^3 $Å^3$. According to the crystal structure, the radius of **1** is 7.2 Å, and the excluded volume is calculated to be *ca.* 1.5 x 10^3 $Å^3$. The good agreement between the excluded volume obtained from DOSY experiment and that estimated from the crystal structure indicates that the hexanuclear structure should be stable and maintained in solution. In addition, the ^1H NMR spectrum of **1** was intact (Figure 5), in sharp contrast to that of the tetranuclear Ir(III) complex reported before.[12] These results

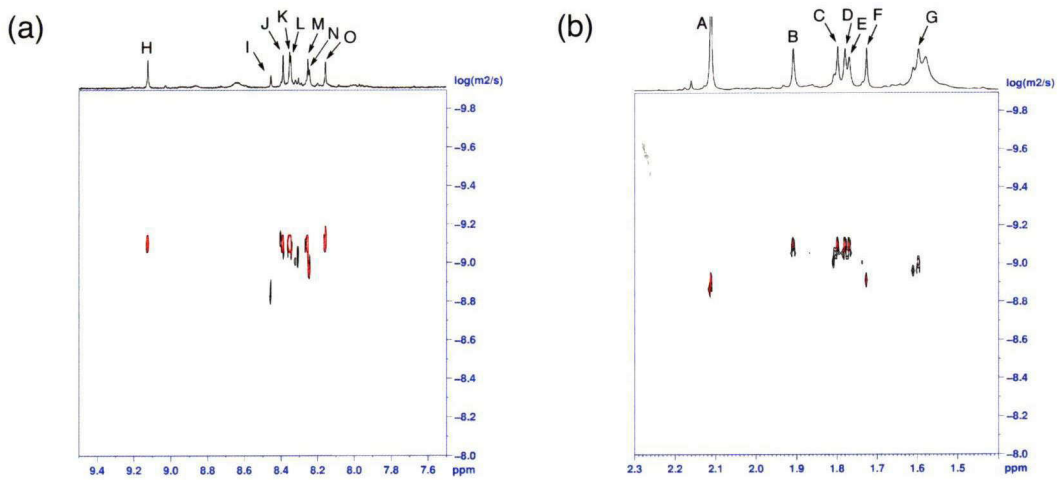

Figure 4. DOSY spectra of **1** (2.8 mM) at room temperature in CD_2Cl_2 after 48 h since making sample: (a) Low magnetic field; (b) high magnetic field.

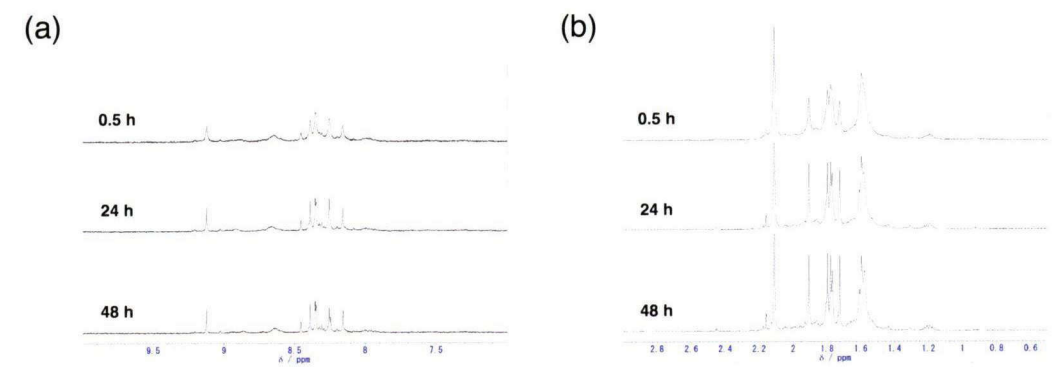

Figure 5. ^1H NMR spectra of **1** (2.8 mM) at room temperature in CD_2Cl_2 after 0.5 h, 24 h and 48 h: (a) Low magnetic field; (b) high magnetic field.

allow us to conclude that **1** is stable in solution and thus the redox behavior of the hexanuclear Ir(III) complex having three redox-active alloxazine ligands can be discussed by electrochemical and spectroscopic measurements.

ESI-MS measurements also support the stability of the hexanuclear structure in methanol solution to observe the peak cluster assigned to $[\{Ir(Cp^*)\}_6(alloCl_2)_3(CH_3O)_3]^{3+}$ (m/z = 967.1) as shown in Figure 6.

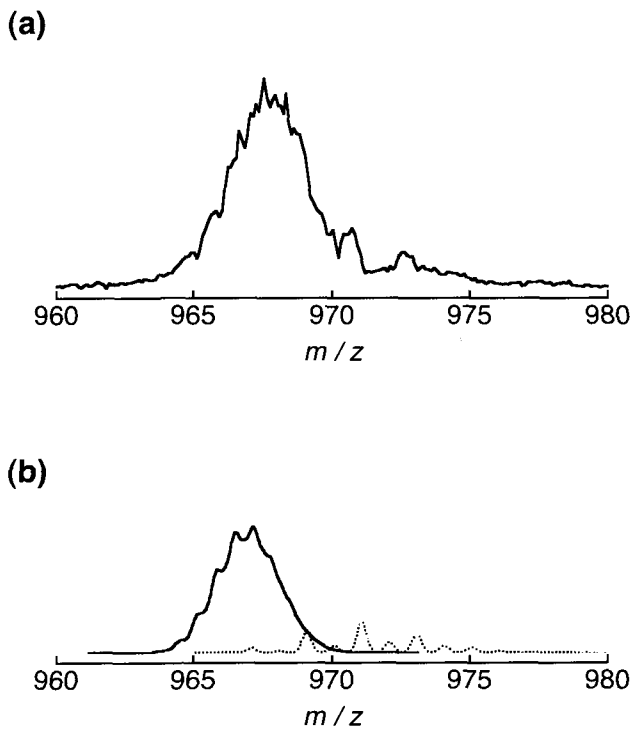

Figure 6. (a) ESI-MS spectrum of **1** in CH_3OH at room temperature. (b) Calculated mass number of $[\{Ir(Cp^*)\}_6(alloCl_2)_3(CH_3O)_3]^{3+}$ (black line) and $[\{Ir(Cp^*)\}_2(alloCl_2)Cl]^{+}$ (dotted line).

The traces of cyclic voltammograms of **1** and $H_2alloCl_2$ in CH_3CN are presented in Figure 7. The first reduction potential of the iridium complex was determined to be –0.65 V (vs. ferrocene/ferrocenium (Fc/Fc^+)), and the process is assigned as the reduction of the alloxazine ligand ($alloCl_2^{2-}/alloCl_2^{\bullet 3-}$) by EPR measurements (shown in Figure 10). Owing to the interaction with three Ir(III) ions, the reduction potential of the alloxazine ligand was positively shifted by +0.52 V in comparison with that (–1.17 V) of uncoordinated $H_2alloCl_2$ (dotted line in Figure 7).[15] The second reduction potential of **1** was determined to be –0.78 V (vs. Fc/Fc^+).[15] The reduction processes of **1** exhibited

improved reversibility in comparison with those of uncoordinated $H_2alloCl_2$: Peak separations are 0.12 V in the first reduction and 0.08 V in the second reduction. The two-step reduction of **1** indicates that the three $alloCl_2^{2-}$ ligands are simultaneously reduced in each step to form $[Ir^{III}{}_6Cp^*{}_6(\mu\text{-}alloCl_2^{\bullet 3-})_3(OH)_3]$ and $[Ir^{III}{}_6Cp^*{}_6(\mu\text{-}alloCl_2^{4-})_3(OH)_3]^{3-}$, respectively. Thus, each redox process can be ascribed to a three-electron process. In the reduction processes, the Ir(III) centre is redox-innocent, since the Ir(III) centre would undergo two-electron reduction to afford a diamagnetic Ir(I) centre in a square-planar geometry by losing some ligands. This is inconsistent with EPR spectral change in the course of the reduction as discussed below.

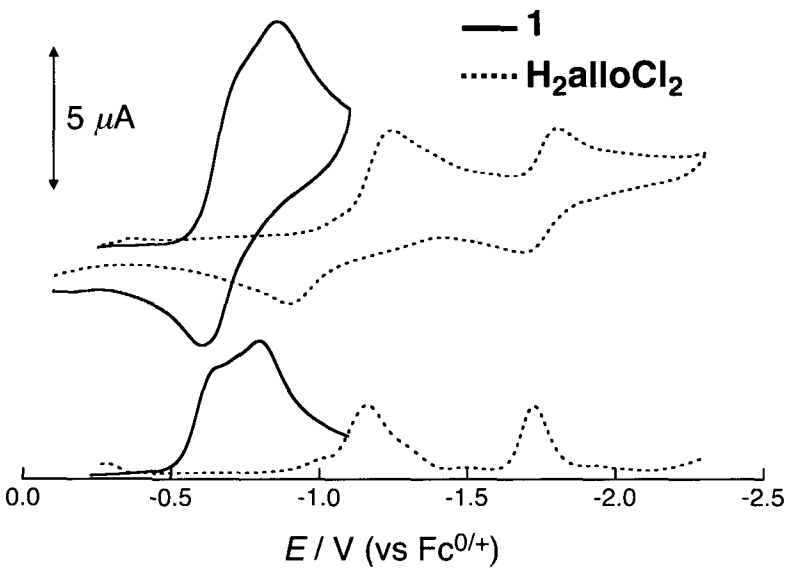

Figure 7. Cyclic (upper) and differential pulse (lower) voltammograms of **1** and $H_2alloCl_2$. Conditions: (black line) **1** (1 mM), (broken line) $H_2alloCl_2$ (1 mM) in the presence of $TBAPF_6$ (0.1 M) in CH_3CN under Ar at room temperature using Pt as working and counter electrodes, and $Ag/AgNO_3$ as a reference electrode.

UV-vis absorption spectral change in the course of the reduction of **1** with cobaltocene ($CoCp_2$) is shown in Figure 8. The spectral change continued until adding 6 equivalents of $CoCp_2$, indicating that three two-electron accepter ligands (the $alloCl_2^{2-}$ ligands) in **1** were fully reduced to reserve six electrons in one molecule. It should be noted that the spectral change was reversible: The original spectrum of **1** was recovered by oxidation with *p*-chloranil (Figure 9). The increase of the absorbance at 648 nm (LMCT) is enhanced after the addition of three equivalents of $CoCp_2$, as shown in Fig. 5(b). This result suggests that the spectral change in the first reduction step of the

alloCl^{2-} ligands is smaller than that for the second reduction step of the ligands. The spectral change also indicates that the three alloxazine ligands are reduced by cobaltocene independently and three radical anions are produced ([Ir_6(alloCl$_2^{2-}$)$_3$(Cp*)$_6$(OH)$_3$]$^{3+}$/[Ir_6(alloCl$_2^{\bullet 3-}$)$_3$-(Cp*)$_6$(OH)$_3$]). After the first independent one-electron reduction, the three one-electron-reduced alloxazine (alloCl$_2^{\bullet 3-}$) ligands undergo another simultaneous one-electron reduction to afford alloCl$_2^{4-}$. Thus, it is concluded that the hexanuclear Ir(III)-alloxazine complex **1** can accept six electrons reversibly at higher potential than -1 V.

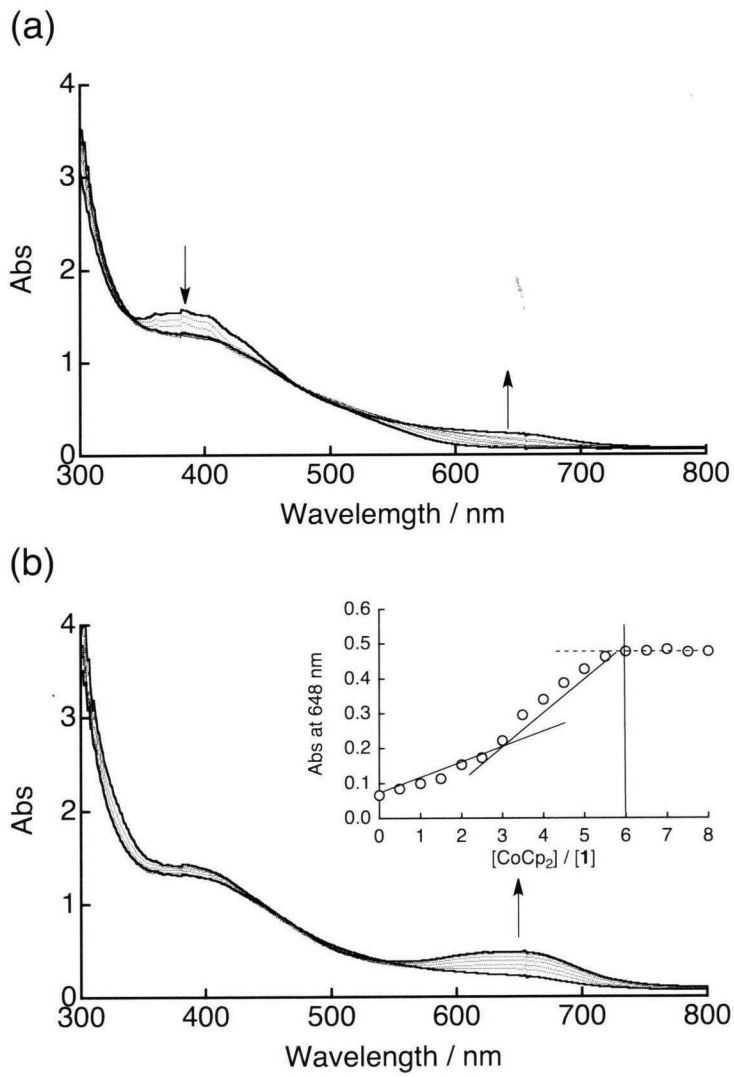

Figure 8. Absorption spectral change in the reduction of **1** with cobaltocene in CH_3CN at room temperature. Inset: The titration curve based on the absorbance change at 648 nm relative to the concentration of cobaltocene: (a) 0 – 3eq of $CoCp_2$; (b) 4 - 8eq of $CoCp_2$.

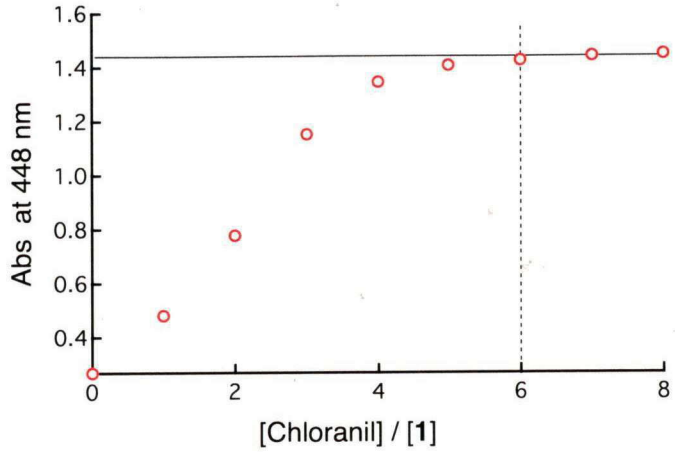

Figure 9. UV-vis titration with *p*-chloranil for the six-electron reduced species of **1** formed by cobaltocene in CH_3CN (see Figure 8). The reoxidation process was monitored by the absorption at 448 nm due to the radical anion of *p*-chloranil.

EPR measurements for the reduced species of **1** formed by the reduction with $CoCp_2$ were carried out in CH_3CN at 100 K. Upon addition of 1 equivalent of $CoCp_2$, an EPR signal was observed at g = 1.9977 without showing any hyperfine structure as shown in Figure 10. The signal was assigned to an Ir(III)-coordinated radical anion of

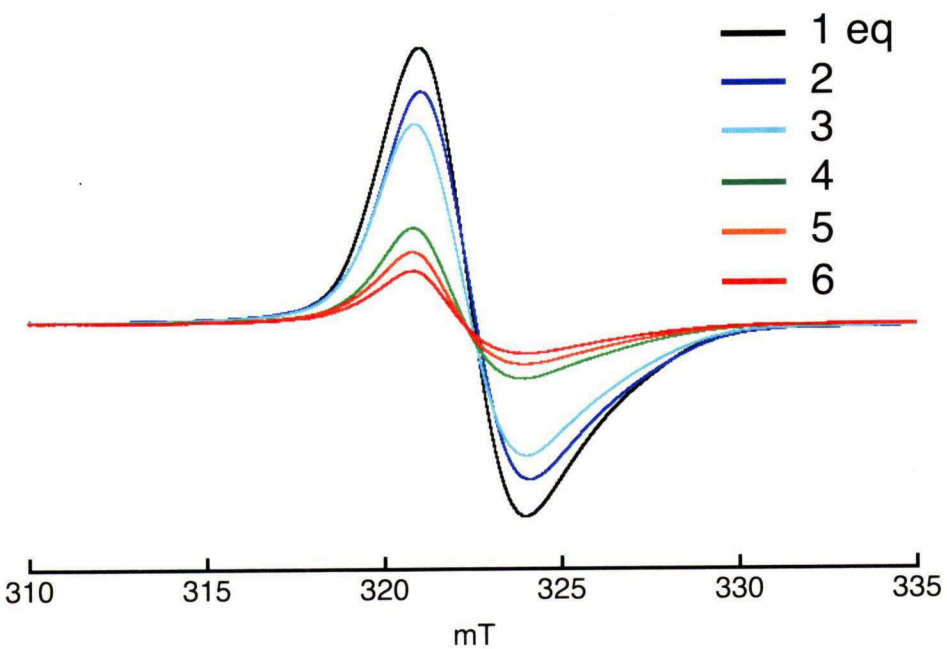

Figure 10. EPR spectral change observed in the course of the reduction of **1** (1 mM) with cobaltocene in acetonitrile under N_2 at 100 K.

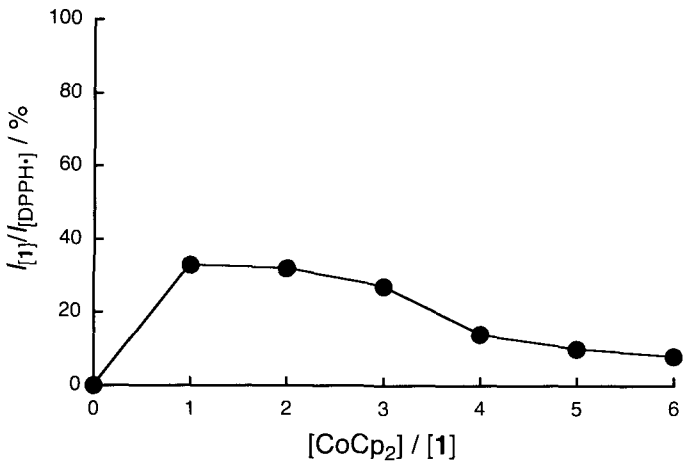

Figure 11. Change of spin concentration of reduced species of **1** relative to the ratio of [$CoCp_2$]/[**1**]. The spin concentration was represented by the percentage of double integration of the signals due to the reduced species of **1** relative to that of the same concentration of DPPH (2,2-diphenyl-1-picrylhydrazyl).

the alloxazine ligand. The signal is not merely due to the simply one-electron reduced species of **1**, but also one or two or three $alloCl_2^{2-}$ of the three $alloCl_2^{2-}$, which can be reduced independently, since the three alloxazine ligands in **1** show the same redox potential as described above.[16] In addition, the alloxazine ligands exhibit intermolecular π-π interactions as indicated by the crystal structure, and thus some magnetic coupling may operate among the alloxazine radical anions through space. The second equivalent of $CoCp_2$ slightly decreased the EPR signal intensity at the same *g* value, however, the spin concentration was little altered as shown by the peak integration in Figure 11.[16] In the third electron injection, the spin concentration was almost the same as those observed in addition of the first and second equivalents of $CoCp_2$. It is suggested that the unpaired electrons are coupled antiferromagnetically, not ferromagnetically, to reduce the EPR signal intensity in the two- and three-electron reduced species of **1** due to the close contact among the $alloCl_2^{2-}$ ligands.[17]

In order to elucidate the little spin concentration change in the course of the three-electron reduction of **1**, disproportionation of the two-electron reduced complex can be considered to give the one-electron and three-electron reduced species upon the addition of the second equivalent $CoCp_2$ as depicted in Figure 12. The driving force of the disproportionation should be neutralization of the molecular charge. The third equivalent of the reductant affords the three-electron reduced species involving the three $alloCl_2^{\bullet 3-}$ ligands.

In the four-, five-, and six-electron reduction steps, the alloxazine radical anions ($alloCl_2^{\bullet 3-}$) are further reduced to two-electron-reduced diamagnetic alloxazine anions ($alloCl_2^{4-}$). In this process, the $alloCl_2^{\bullet 3-}$ showed a different g value (1.9992) from that (1.9977) of the first three-electron reduction process because of the interaction with $alloCl_2^{4-}$ in place of $alloCl_2^{\bullet 3-}$.

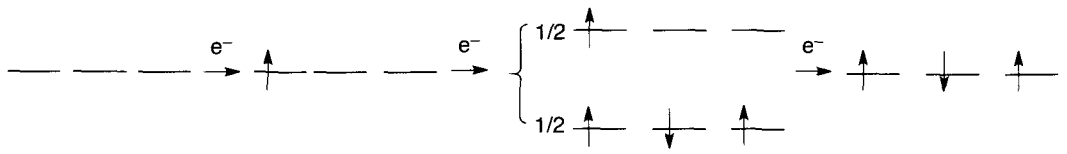

Figure 12. Schematic description of unpaired electron occupancy of π^* orbitals of the $alloCl_2^{2-}$ ligands of **1** in the course of the first three-electron reduction.

Summary

The author has synthesized an organometallic Ir(III) hexanuclear prismatic complex with alloxazine derivatives as redox-non-innocent bridging ligands. In sharp contrast to the previously reported tetranuclear Ir(III)-alloxazine complex, the complex **1** exhibited excellent stability in solution without fragmentation. The stability allows us to observe the reversible multi-electron redox processes at the bridging ligands to give a six-electron reduced species of **1** in solution. The strategy to converge redox-active organic molecules into one multinuclear metal complex as bridging ligands would provide new functionality of integrated metal complexes as ligand-centered multi-electron redox systems.

Experimental section

Material and Method

CH_3CN (Wako Pure Chemical Industries) was purified by distillation over CaH_2. CH_3OH (Wako Pure Chemical Industries) was used without further purification. Iridium(III) trichloride was purchased from Tanaka Holdings Co., Ltd.. Alloxane, 4,5-dichloro-1,2-phenylenediamine, 1,2,3,4,5-pentamethylcyclo-pentadiene were purchased from Tokyo Chemical Industries. Silver hexafluorophosphate was purchased from Sigma-Aldrich. These reagents were used as received. $TBAPF_6$ (Tokyo Chemical Industries) was recrystallized from water and ethanol (1:1 (v/v)) and then from ethanol.

$[IrCl_2(Cp^*)]_2$[18] and 7,8-dichloro-alloxazine[19] were prepared according to literature methods.

Apparatus. UV–vis absorption spectra were recorded on a Hewlett-Packard HP8453 diode array spectrophotometer. ESI-MS spectra were measured on a Perkin-Elmer API-150 EX spectrometer. Electrochemical measurements were performed on a BAS CV-50W. EPR spectra were recorded on a JEOL JEX-REIXE spectrometer. All the measurements were carried out at room temperature.

Electrochemical Measurements. Cyclic voltammetry and differential pulse voltammetry were performed in CH_3CN in the presence of 0.1 M $[(n\text{–butyl})_4N]PF_6$ ($TBAPF_6$) as an electrolyte under Ar at room temperature, with use of a Pt electrode as a working electrode, $Ag/AgNO_3$ as a reference electrode, and a Pt wire as an auxiliary electrode.

UV-vis Absorption Spectroscopy. UV-vis absorption spectra were measured at RT in CH_3CN (3 ml) under Ar. The concentration of hexanuclear iridium complex was 46 μM. CH_3CN was degassed by freeze-pump-thaw cycling and was filled with Ar. The reduction of **1** by cobaltocene (99%) was followed by UV-vis spectroscopy in CH_3CN at room temperature.

EPR Spectroscopy. EPR spectra of reduced species of **1** (1 mM) with sequential addition of cobaltocene were recorded in CH_3CN (300 μl) at room temperature and the g values were determined relative to an Mn^{2+} marker.

DFT Calculations. Density functional theory (DFT) calculations were made on a 32CPU workstation (PQS, Quantum Cube). Geometry optimizations were carried out using the Becke3LYP functional and the 6-31G(d) basis set as implemented in the Gaussian 03 program Revision C.02.[20-22] Graphical outputs of the computational results were generated with the Gauss View software program (ver. 3.09) developed by Semichem, Inc.[23]

X-ray Crystallography. The single crystal of **1** was obtained by recrystallization from 2-propanol. X–ray diffraction data were collected on a Rigaku R-AXIS RAPID imaging plate diffractometer with graphite–monochromated Cu Kα radiation (λ = 1.54187 Å) at –150°C. The data were processed using *PROCESS–AUTO* program (Rigaku Corp.).[24] For the hexanuclear iridium(III) complex, the structure was solved by direct methods (SHELXS 97)[25] and refined by full-matrix least-squares method on F^2 [26] by using *CrystalStructure 4.0.1* program package (Rigaku Corp.).[27] The six-membered rings of $alloCl_2^{2-}$ and the Cp* groups were treated as rigid groups, and the latter groups were refined isotropically. The hydrogen atom of OH^- coordinated to Ir ion could not be located. After successive trials, solvent-accessible voids of 1870 $Å^3$ in all (calculated by SQUEEZE) were left unfilled, in which heavily disordered solvent molecules were

supposed to be contained. The last refinement was performed using the reflection data modified by SQUEEZE. Crystallographic data are summarized in Table 1. The selected bond lengths (Å) and angles (deg) are listed in Table 2.

Synthesis

Complex 1. To a suspension of $[IrCl_2(Cp^*)]_2$ (83.6 mg, 0.105 mmol) was added to the solution of $AgPF_6$ (113.5 mg, 0.449 mmol) and methanol (10 ml). After 15 min of stirring at room temperature, the white precipitate of AgCl was filtered off through a Celite pad. The filtrate was concentrated to a small volume and 7,8-dichloroalloxazine (29.7 mg, 0.105 mmol) was added to the solution under Ar. The mixture was refluxed for 16 h and then the solution was cooled down to room temperature. After the solvent was removed, the residue was dissolved in acetonitrile. The solution was filtered through a Celite pad and then the filtrate was dried up by a rotary evaporator. The residue was dissolved in acetone and a large amount of diethyl ether was added to obtain orange precipitate. Recrystallization of the precipitate from 2-propanol afforded red crystals of **1** (40.0 mg 12%). Elemental analysis (%): Found. C 33.06, H 3.03, N 5.53; Calcd. for $C_{92}H_{102}N_{13}O_9Ir_6P_3F_{18}Cl_6$ (1•CH_3CN) C 33.14, H 3.08, N 5.46. ESI-MS in CH_3OH: m/z = 967.1 ($[\{Ir(Cp^*)\}_6(alloCl_2)_3\text{-}(CH_3O)_3]^{3+}$).

References

1 a) Y. Umena, K. Kawakami, J.-R. Shen and N. Kamiya, *Nature*, 2011, **473**, 55; b) H. Dau and I. Zaharieva, *Acc. Chem. Res.*, 2009, **42**, 1861; c) J. Barber, *Inorg. Chem.*, 2008, **47**, 1700.

2 O. Einsle, F. A. Tezcan, S. L. A. Andrade, B. Schmid, M. Yoshida, J. B. Howard and D. C. Rees, *Science*, 2002, **297**, 1696.

3 a) M. Haumann, P. Liebisch, C. Müller, M. Barra, M. Grabolle and H. Dau, *Science*, 2005, **310**, 1019; b) J. P. McEvoy and G. W. Brudvig, *Chem. Rev.*, 2006, **106**, 4455.

4 a) D. Lukoyanov, Z.-Y. Yang, B. M. Barney, D. R. Dean, L. C. Seefeldt and B. M. Hoffman, *Proc. Natl. Acad. Sci., USA*, 2012, **109**, 5583; b) B. K. Burgess and D. J. Lowe, *Chem. Rev.*, 1996, **96**, 2983.

5 a) J. A. Baumann, D. J. Salmon, S. T. Wilson and T. J. Meyer, *Inorg. Chem.*, 1978, **17**, 3342; b) K. Ota, H. Sasaki, T. Matsui, T. Hamaguchi, T. Yamaguchi, T. Ito, H. Kido and C. P. Kubiak, *Inorg. Chem.*, 1999, **38**, 4070; c) H. E. Toma, K. Araki, A.

D. P. Alexiou, S. Nikolaou and S. Dovidauskas, *Coord. Chem. Rev.*, 2001, **219-221**, 187.

6 a) S. Bivaud, J.-Y. Balandier, M. Chas, M. Allain, S. Goeb and M. Sallé, *J. Am. Chem. Soc.*, 2012, **134**, 11968; b) S. Kar, B. Sarkar, S. Ghumaan, D. Janardanan, J. van Slageren, J. Fiedler, V. G. Puranik, R. B. Sunoj, W. Kaim and G. K. Lahiri, *Chem.–Eur. J.*, 2005, **11**, 4901; c) N. Fujita, K. Biradha, M. Fujita, S. Sakamoto and K. Yamaguchi, *Angew. Chem., Int. Ed.*, 2001, **40**, 1718.

7 a) T. C. Bruice, *Acc. Chem. Res.*, 1980, **13**, 256; b) A. Niemz, J. Imbriglio and V. M. Rotello, *J. Am. Chem. Soc.*, 1997, **119**, 887; c) A. Niemz and V. M. Rotello, *Acc. Chem. Res.*, 1999, **32**, 44.

8 a) C.-C. Wei, B. R. Crane, D. J. Stuehr, *Chem. Rev.*, 2003, **103**, 2365; b) R. Raghavan and G. Dryhurst, *J. Electroanal. Chem.*, 1981, **129**, 189.

9 a) W. Kaim, B. Schwederski, O. Heilmann and F. M. Hornung, *Coord. Chem. Rev.*, 1999, **182**, 323; b) S. Fukuzumi and T. Kojima, *J. Biol. Inorg. Chem.*, 2008, **13**, 321.

10 Flavin-metal complexes: a) M. J. Clarke, M. G. Dowling, A. R. Garafalo and T. F. Brennan, *J. Biol. Chem.*, 1980, **255**, 3472; b) M. J. Clarke and M. G. Dowling, *Inorg. Chem.*, 1981, **20**, 3506; c) M. G. Dowling and M. J. Clarke, *Inorg. Chim. Acta*, 1983, **78**, 153; d) F. M. Hornung, O. Heilmann, W. Kaim, S. Zalis and J. Fiedler, *Inorg. Chem.*, 2000, **39**, 4052; e) O. Heilmann, F. M. Hornung, J. Fiedler and W. Kaim, *J. Organomet. Chem.*, 1999, **589**, 2; f) S. Miyazaki, K. Ohkubo, T. Kojima and S. Fukuzumi, *Angew. Chem., Int. Ed.*, 2007, **46**, 905.

11 Pterin-metal complexes: a) A. Abelleira, R. D. Galang and M. J. Clarke, *Inorg. Chem.*, 1990, **29**, 633; b) T. Kojima, T. Sakamoto, Y. Matsuda, K. Ohkubo and S. Fukuzumi, *Angew. Chem.*, 2003, **115**, 5101; *Angew. Chem., Int. Ed.*, 2003, **42**, 4951; c) S. Miyazaki, T. Kojima, T. Sakamoto, T. Matsumoto, K. Ohkubo and S. Fukuzumi, *Inorg. Chem.*, 2008, **47**, 333; d) S. Miyazaki, K. Ohkubo, T. Kojima and S. Fukuzumi, *Angew. Chem.*, 2008, **120**, 9815; *Angew. Chem., Int. Ed.*, 2008, **47**, 9669; e) S. Miyazaki, T. Kojima, J. M. Mayer and S. Fukuzumi, *J. Am. Chem. Soc.*, 2009, **131**, 11615; f) P. Basu and S. J. N. Burgmayer, *Coord. Chem. Rev.*, 2011, **255**, 1016; g) Y. Inui, S. Miyazaki, K. Ohkubo, S. Fukuzumi and T. Kojima, *Angew. Chem., Int. Ed.*, 2012, **51**, 4623.

12 T. Kojima, Y. Inui, S. Miyazaki, M. Shiro and S. Fukuzumi, *Chem. Commun.*, 2009, 6643.

13 Crystallographic data for **1**: Trigonal, *R*3*c* (#161), a = 16.0783(6) Å, c = 74.528(6) Å, V = 16685.1(15) Å^3, Z = 6, T = 123 K, $R1(R_w)$ = 0.0965(0.2415) ($I > 2\sigma(I)$), GOF = 1.092. CCDC 888985 contains the supplementary crystallographic data for

this paper. These data can be obtained free of change from The Cambridge Crystallographic Data Centre via www.ccdc.cam.ac.uk/data_ request/cif.

14 C. A. Hunter and J. K. M. Sanders, *J. Am. Chem. Soc.*, 1990, **112**, 5525.

15 Addition of "proton sponge" gave rise to no change of the potentials of the first and second reduction processes. Thus, the possibility of protonation of the reduced species of **1** was excluded.

16 The first equivalent $CoCp_2$ can afford three species, (1,0,0), (1,1,0) and (1,1,1), in which the number in parentheses indicate the number of electrons accepted by each $alloCl_2^{2-}$ ligand in **1**. The second equivalent $CoCp_2$ can afford the same species in a different population. In addition, the alloxazine radicals can interact antiferromagnetically due to the close contact as observed in the crystal structure. Therefore, the equivalents of $CoCp_2$ do not simply reflect the number of the alloxazine radicals formed, and thus, the peak intensity does not simply correlate to the amounts of $CoCp_2$ and the radicals in **1**.

17 These facts advocate that the hexanuclear structure is maintained in the course of the reduction in the solution, because the fragmentation of the hexanuclear structure to give species with one alloxazine ligand should lead to the monotonous increase in the signal intensity up to the addition of the three equivalents of $CoCp_2$ relative to **1**.

18 R. G. Ball, W. A. G. Graham, D. M. Heinekey, J. K. Hoyano, A. D. McMaster, B. M. Mattson and S. T. Michel, *Inorg. Chem.*, 1990, **29**, 2023.

19 H. G. Petering and G, J. v. Giessen, *J. Org. Chem.*, 1961, **26**, 2818.

20 a) A. D. Becke, *J. Chem. Phys.*, 1993, **98**, 5648; b) C. Lee, W. Yang and R. G. Parr, *Phys. Rev. B*, 1988, **37**, 785.

21 W. J. Hehre, L. Radom, P. v. R. Schleyer and J. A. Pople, *Ab Initio Molecular Orbital Theory*, Wiley, New York, 1986.

22 M. J. Frisch, G. W. Trucks, H. B. Schlegel, G. E. Scuseria, M. A. Robb, J. R. Cheeseman, J. A. Montgomery, J. T. Vreven, K. N. Kudin, J. C. Burant, J. M. Millam, S. S. Iyengar, J. Tomasi, V. Barone, B. Mennucci, M. Cossi, G. Scalmani, N. Rega,; G. A. Petersson, H. Nakatsuji, M. Hada, M. Ehara, K. Toyota, R. Fukuda, J. Hasegawa, M. Ishida, T. Nakajima, Y. Honda, O. Kitao, H. Nakai, M. Klene, X. Li, J. E. Knox, H. P. Hratchian, J. B. Cross, C. Adamo, J. Jaramillo, R. Gomperts, R. E. Stratmann, O. Yazyev, A. J. Austin, R. Cammi, C. Pomelli, J. W. Ochterski, P. Y. Ayala, K. Morokuma, G. A. Voth, P. Salvador, J. J. Dannenberg, V. G. Zakrzewski, S. Dapprich, A. D. Daniels, M. C. Strain, O. Farkas, D. K. Malick,; A. D. Rabuck, K. Raghavachari, J. B. Foresman, J. V. Ortiz, Q. Cui, A. G. Baboul, S. Clifford, J. Cioslowski, B. B. Stefanov, G. Liu, A. Liashenko, P. Piskorz, I.

Komaromi, R. L. Martin, D. J. Fox, T. Keith, M. A. Al-Laham, C. Y. Peng, A. Nanayakkara, M. Challacombe, P. M. W. Gill, B. Johnson, W. Chen, M. W. Wong, C. Gonzalez and J. A. Pople, *Gaussian 03, Revision C.02,*, Gaussian, Inc., Wallingford CT, 2004.

23 R. Dennington II, T. Keith, J. Millam, K. Eppinnett, W. L. Hovell and R. Gilliland, Semichem, Inc., Shawnee Mission, KS, 2003.

24 *CrystalClear 1.3.5* SP2: Rigaku,1998–2003

25 G. M. Sheldrick, *Acta Cryst.*, 2008, **A64**, 112.

26 D. C. Creagh and W. J. McAuley, *International Tables for X-ray Crystallography*, A. J. C. Wilson, Ed. Kluwer Academic Publisher, Boston, 1992, vol. **C**, Table 4.2.6.8 and 6.1.1.4

27 *Yadokari-XG 2009*: Crystal Structure Analysis Package; modified by T. Nemoto, 2009, based on version 2007.5.12 (written by K. Wakita, C. Kabuto, S. Akine, T. Nemoto, E. Kwon). Release of software (Yadokari-XG 2009) for crystal structure analyses: *J. Cryst. Soc. Jpn.* 2009, **51**, 218.

Concluding Remarks

In this thesis, the author described crystal structures of metal-containing assemblies of *N*-heteroaromatics as ligands. Thermodynamic analysis of formation behaviors of assemblies and elucidation of the impact of the formation of supramolecular assemblies by non-covalent interactions gave us important information in relevance to biologically important phenomena. As component of assemblies, the *N*-heteroaromatics form various non-covalent interactions with molecules or ions by using their π-conjugated ring, hydrogen-bonding sites, and coordination sites. Metal ions occasionally act as template cations to form well-organized structures and improve the reversibility of the redox behavior of redox-active heteroaromatics. Results and findings in this work are summarized as follow.

(1) The main purpose of the direct observation of the interaction between a G-quartet and porphyrins was achieved by producing the stable G-quartet without bulky peripheral functional groups. Crystal structures of G-quartets with Na^+ and Ca^{2+} as templates and without template cations were obtained and the formation behavior of G-quartet structures with Na^+ and Ca^{2+} was analyzed on the basis of the thermodynamic analysis. The author elucidated that the electrostatic interactions is the most important factor to stabilize the G-quartet structures and the Lewis acidity of template cations inversely affected on the enthalpy of the formation of the G-quartet. It was clarified that the adduct of the G-quartet and a porphyrin is formed by J-type π-π stacking. It was suggested that the driving force of the adduct formation is the electrostatic interaction between an anionic porphyrin ligand and the cationic G-quartet. The assembly of the G-quartet and a porphyrin changed the structural motif depending on temperatures.

(2) The effect of hydrogen bonding on the redox behavior of the pterin ligand was investigated using nucleobases in organic solvents. The first reduction potential of pterin ligand was demonstrated to show large positive shift by the three-point complementary hydrogen binding with a guanosine derivative. Binding constants of nucleosides to the Ru(II)-bound pterin was determined and the thermodynamic parameters of the formation of the supramolecular assemblies were analyzed on the basis of van't Hoff plots. The crystal structure of the adduct of the pterin derivative and a guanine derivative was determined to demonstrate the three-point hydrogen bonding in the adduct. In the presence of thymidine, the formation behavior of

adduct of the pterin ligand and the thymidine derivative was suggested to be different according to the redox state of the pterin ligand: The thymidine binds to the oxidized form in a two-point mode and to the reduced form in a single-point mode with the N-8 position.

(3) The author synthesized and characterized a novel tetranuclear iridium(III) complex with alloxazine as a functional bridging ligand in various coordination modes. The novel tetranuclear iridium(III) complex was demonstrated to form a supramolecular structure having a cavity, in which two of counter anions were included, through intermolecular hydrogen bonding. The counter anion could be exchanged to another counter anion via self-reorganization in the course of crystallization.

(4) A dichlorinated alloxazine derivative was revealed to act as a bridging ligand to stabilize a hexanuclear prismatic iridium(III) complex in solutions due to enhanced π-back bonding from the Ir(III) center to the lowered π^* orbital of the alloxazine ligand. The stable hexanuclear iridium(III) complex allowed us to observe the redox behavior of the three bridging alloxazine ligands in the integrated metal complex. Two-step three-electron reduction processes of the alloxazine ligands were reversible and the potentials were higher over -0.5 V than those of the corresponding uncoordinated neutral alloxazine. Thus, it was revealed that six-electron reduction in total occurred in one molecule due to the integration of the alloxazine ligands. The integration of functional ligands as bridging ligands into one multinuclear metal complex provides possibility to access new redox functions of those complexes.

Assemblies regulated by non-covalent interactions demonstrate characteristic structures and properties *in vivo* as well as *in vitro*. The self-organization is absolutely imperative for life. Throughout this thesis, the author has demonstrated the elegance of the optimized environment and structural design of biological systems through the compounds prepared in this work. The author believes that the fundamental insights into assemblies of bioactive heteroaromatics via self-organization can provide the development of enhanced understanding biological reactions and the application of biological phenomena to develop functional molecular and supramolecular assemblies.

list of Publications

(1) "A tetranuclear iridium(III) complex having a flavin analogue as a bridging ligand in different coordination modes and exchangeable anion encapsulation in a supramolecular cage"
Takahiko Kojima, Yuji Inui, Soushi Miyazaki, Motoo Shiro and Shunichi Fukuzumi, *Chem. Commun.*, 2009, 6643.

(2) "Regulation of Redox Potential of a Pterin Derivative Bound to a Ruthenium(II) Complex by Intermolecular Hydrogen Bonding with Nucleobases"
Yuji Inui, Soushi Miyazaki, Kei Ohkubo, Shunichi Fukuzumi and Takahiko Kojima, *Angew. Chem., Int. Ed.*, 2012, **51**, 4623.

(3) "A triangular prismatic hexanuclear iridium(III) complex bridged by flavin analogues showing reversible redox processes"
Yuji Inui, Motoo Shiro, Takahiro Kusukawa, Shunichi Fukuzumi and Takahiko Kojima, *Dalton Trans.*, 2013, **42**, 2773.

(4) "Quartet formation of a guanine derivative with an isopropyl group: Crystal structures of "naked" G-quartets and thermodynamics of G-quartet formation"
Yuji Inui, Motoo Shiro, Shunichi Fukuzumi and Takahiko Kojima, *Org. Biomol. Chem.*, 2013, **11**, 758.

(5) "Formation of a supramolecular assembly between a Na^+-templated G-quartet and a Ni(II)-porphyrin complex"
Yuji Inui, Shunichi Fukuzumi and Takahiko Kojima, 2013, doi: 10.1039/C3DT330 34F

Supplementary Publication

(6) "Pure red electrophosphorescence from polymer light-emitting diodes doped with highly emissive bis-cyclometalated iridium(III) complexes"
Hidetaka Tsujimoto, Shigeyuki Yagi, Hotaka Asuka, Yuji Inui, Shigeru Ikawa, Takeshi Maeda, Hiroyuki Nakazumi and Yoshiaki Sakurai, *J. Organomet. Chem.*, 2010, **695**, 1972.

Acknowledgement

The author would like to express his gratitude to Professor Shunichi Fukuzumi and Professor Takahiko Kojima for their kind guidance, invaluable suggestions and encouragement throughout this study.

The author desires to express his sincere thanks to Dr. Yusuke Yamada, Dr. Tomoyoshi Suenobu, Dr. Kei Ohkubo, Dr. Tomoya Ishizuka and Dr. Hiroaki Kotani for their valuable suggestions.

The author is deeply grateful to Dr. Motoo Shiro (Rigaku Corp.) for his expertise in crystal structure determination, Prof. Takahiro Kusukawa (Kyoto Institute of Technology) for his help to obtain DOSY spectra, and Dr. Soushi Miyazaki (Osaka University) for his valuable suggestions and kind collaboration.

Thanks are also given to all members of the Fukuzumi's group in Osaka University and the Kojima's group in University of Tsukuba for their kind help, teaching and friendship.

The author acknowledgement financial support from the Global COE programs "Global Education and Research Center for Bio-Environmental Chemistry".

Finally, the author would like to express his appreciation for continuous encouragement and assistant given by my family and my friends.

Yuji Inui

Department of Material and Life Science
Division of Advanced Science and Biotechnology
Graduate School of Engineering, Osaka University
ALCA, JAPAN Science and Technology Agency

Osaka Japan
January 2013